AFRL-RY-HS-TR-2011-0012

DIRECTION OF ARRIVAL (DOA) ESTIMATION AND MULTI-USER INTERFERENCE IN A TWO- RADAR SYSTEM

M. Rangaswamy

AFRL/RYHE
80 Scott Drive
Hanscom AFB, MA 01731

M. Greco and F.Gini

University of Pisa, Italy

30 September 2009

Final Report

APPROVED FOR PUBLIC RELEASE; DISTRIBUTION UNLIMITED

AIR FORCE RESEARCH LABORATORY
Sensors Directorate
Electromagnetics Technology Division
80 Scott Drive
Hanscom AFB MA 01731-2909

NOTICE AND SIGNATURE PAGE

Distribution: Unlimited, Statement A

NOTICE

AFRL-RY-HS-TR-2011-0012 HAS BEEN REVIEWED AND IS APPROVED FOR PUBLICATION IN ACCORDANCE WITH ASSIGNED DISTRIBUTION STATEMENT.

Muralidhar Rangaswamy

MURALIDHAR RANGASWAMY
Electronics Engineer
Electromagnetic Scattering Branch

Bertus Weijers

BERTUS WEIJERS
Branch Chief
Electromagnetic Scattering Branch

Robert V. McGahan

ROBERT V. McGAHAN
Technical Communication Advisor
Electromagnetics Technology Division

REPORT DOCUMENTATION PAGE	*Form Approved OMB No. 0704-0188*

The public reporting burden for this collection of information is estimated to average 1 hour per response, including the time for reviewing instructions, searching existing data sources, gathering and maintaining the data needed, and completing and reviewing the collection of information. Send comments regarding this burden estimate or any other aspect of this collection of information, including suggestions for reducing the burden, to Department of Defense, Washington Headquarters Services, Directorate for Information Operations and Reports (0704-0188), 1215 Jefferson Davis Highway, Suite 1204, Arlington, VA 22202-4302. Respondents should be aware that notwithstanding any other provision of law, no person shall be subject to any penalty for failing to comply with a collection of information if it does not display a currently valid OMB control number.

PLEASE DO NOT RETURN YOUR FORM TO THE ABOVE ADDRESS.

1. REPORT DATE *(DD-MM-YYYY)*	**2. REPORT TYPE**	**3. DATES COVERED** *(From - To)*
30-09-2009	FINAL REPORT	1 OCT 2005-30 SEPT 2009

4. TITLE AND SUBTITLE
DIRECTION OF ARRIVAL (DOA) ESTIMATION AND MULTI-USER INTERFERENCE IN A TWO- RADAR SYSTEM

5a. CONTRACT NUMBER
N/A

5b. GRANT NUMBER
N/A

5c. PROGRAM ELEMENT NUMBER
61102F

6. AUTHOR(S)
M. RANGASWAMY (1), M. GRECO, AND F.GINI (2)

5d. PROJECT NUMBER
2311

5e. TASK NUMBER
HE

5f. WORK UNIT NUMBER
02

7. PERFORMING ORGANIZATION NAME(S) AND ADDRESS(ES)
(1) ELECTROMAGNETIC SCATTERING BRANCH, AFRL/RYHE
80 SCOTT DRIVE HANSCOM AFB, MA 01731-2909
(2) UNIVERSITY OF PISA, ITALY

8. PERFORMING ORGANIZATION REPORT NUMBER
N/A

9. SPONSORING/MONITORING AGENCY NAME(S) AND ADDRESS(ES)
AIR FORCE RESEARCH LABORATORY SENSORS DIRECTORATE
AFRL/RYHE 80 SCOTT DRIVE HANSCOM AFB, MA 01731-2909

10. SPONSOR/MONITOR'S ACRONYM(S)
AFRL/RYHE

11. SPONSOR/MONITOR'S REPORT NUMBER(S)
AFRL-RY-HS-TR-2011-0012

12. DISTRIBUTION/AVAILABILITY STATEMENT
DISTRIBUTION A. APPROVED FOR PUBLIC RELEASE; DISTRIBUTION UNLIMITED. APPROVED BY 88 ABW/PA WPAFB-08-5134

13. SUPPLEMENTARY NOTES
N/A

14. ABSTRACT
Multistatic radars utilize multiple transmitter and receiver sites to provide several different monostatic and bistatic channels of observation. Multistatic passive and active radar systems can offer many advantages in terms of coverage and accuracy in the estimation of target signal parameters. Unfortunately, their performances are heavily sensitive to the position of receivers and transmitters with respect to the position of the target. It is well know that geometry factors play an important role in the shape of the ambiguity function (AF) which is often used to measure the possible global resolution and large error properties of the target parameters estimates. In this work we exploit the relation between the ambiguity function and the Cramer-Rao lower bound (CRLB) to calculate the bistatic CRLBs of target range and velocity and so obtaining a local measure of the estimation a ccuracy of these parameters. We also propose an algorithm for choosing in a multistatic scenario, along the trajectory of the tracked target, the pair transmitter-receiver with the best asymptotic performance calculated in terms of CRLB on estimation accuracy.

15. SUBJECT TERMS
CramérRao lower bound, ambiguity function, bistatic radar, multistatic radar

16. SECURITY CLASSIFICATION OF: a. REPORT	b. ABSTRACT	c. THIS PAGE	**17. LIMITATION OF ABSTRACT**	**18. NUMBER OF PAGES**	**19a. NAME OF RESPONSIBLE PERSON**
U	U	U	UU	90	MURALIDHAR RANGASWAMY
					19b. TELEPHONE NUMBER *(Include area code)*

Reset

Blank Page

List of Figures Page

ABSTRACT

Multistatic radars utilize multiple transmitter and receiver sites to provide several different monostatic and bistatic channels of observation. Multistatic passive and active radar systems can offer many advantages in terms of coverage and accuracy in the estimation of target signal parameters. Unfortunately, their performances are heavily sensitive to the position of receivers and transmitters with respect to the position of the target. It is well know that geometry factors play an important role in the shape of the ambiguity function (AF) which is often used to measure the possible global resolution and large error properties of the target parameters estimates. In this work we exploit the relation between the ambiguity function and the Cramer-Rao lower bound (CRLB) to calculate the bistatic CRLBs of target range and velocity and so obtaining a local measure of the estimation accuracy of these parameters. We also propose an algorithm for choosing in a multistatic scenario, along the trajectory of the tracked target, the pair transmitter-receiver with the best asymptotic performance calculated in terms of CRLB on estimation accuracy.

Keywords: *CramérRao lower bound, ambiguity function, bistatic radar, multistatic radar*

1 INTRODUCTION

In active radar a known waveform is transmitted, and the signal reflected from the target of interest is used to estimate its parameters. Typically the received signal is a scaled, delayed and Doppler-shifted version of the transmitted signal. In monostatic configuration, estimation of the time delay and Doppler shift directly provides information on range and velocity of the target. This is possible also in the case of bistatic radar configuration, even if the relation between measured or estimated time delay and Doppler frequency, and target distance and velocity is not linear [Tsa97]. To measure the possible global resolution and large error properties of the target parameters estimates, the ambiguity function (AF) is often used both in mono and in multistatic scenarios.

In this technical report, after calculating the bistatic ambiguity function (BAF) for a burst of linear frequency modulated (LFM) pulses, we exploit the relation between the AF and the Cramér-Rao lower bound (CRLB) to calculate the bistatic CRLBs of target range and velocity. The bistatic CRLBs provide a local measure of the estimation accuracy of these parameters. Moreover, we compare monostatic and bistatic CRLBs as a function of the number of integrated pulses, target direction of arrival (DOA), and bistatic baseline length.

The information gained through the calculation of the bistatic CRLBs can be used in a multistatic radar system for the choice of the optimum transmit-receive pair. As known, a multistatic radar system utilizes multiple transmitter and receiver sites to provide several different monostatic and bistatic channels of observation, leading to an increase in the information on a particular area of surveillance. The performance of each bistatic channel heavily depends upon the geometry of the scenario and the position of the target with respect to each receiver and transmitter. In this work we approach the problem of optimally selecting the transmitter-receiver (TX-RX) pair based upon the CRLB for the bistatic geometry of each TX-RX pair. The optimal pair is defined as that exhibiting the lowest bistatic CRLB for the target velocity or range. These results can be used for the dynamical selection of the TX-RX signals for the tracking of a radar target moving along a trajectory in a multistatic scenario.

2 THE AMBIGUITY FUNCTION

The bistatic geometry is pictorially drawn in Figure 1. The positions of the transmitters receivers, and target are generic. Considering an ordinary Cartesian grid, the TX is located at point *T*, whose coordinates are $\left(x_T, y_T\right)$, the RX is located at point *R* in $\left(x_R, y_R\right)$ and the target is located at point B, whose coordinates are (x, y). The triangle formed by the transmitter, the receiver, and the target is called the **bistatic triangle**.

As shown in Figure 1, the sides of the bistatic triangle are R_T, R_R, and L, where R_T is the range from the transmitter to the target, R_R is the range from the receiver to the target and L is the baseline between the transmitter and the receiver. The internal angles of the bistatic triangle, that without lack of generality are assumed to be positive, are α, β, and γ. In particular, the bistatic angle β is the angle at the apex of the bistatic triangle, at the vertex which represents the target. Assuming that the coordinates of the transmitter, receiver, and target are known, it is possible to calculate all the parameters of the bistatic triangle. θ_T and θ_R are the look angle of the transmitter and the look angle of the receiver, respectively, they are measured positive clockwise from the vector normal to the baseline pointing forward the target.

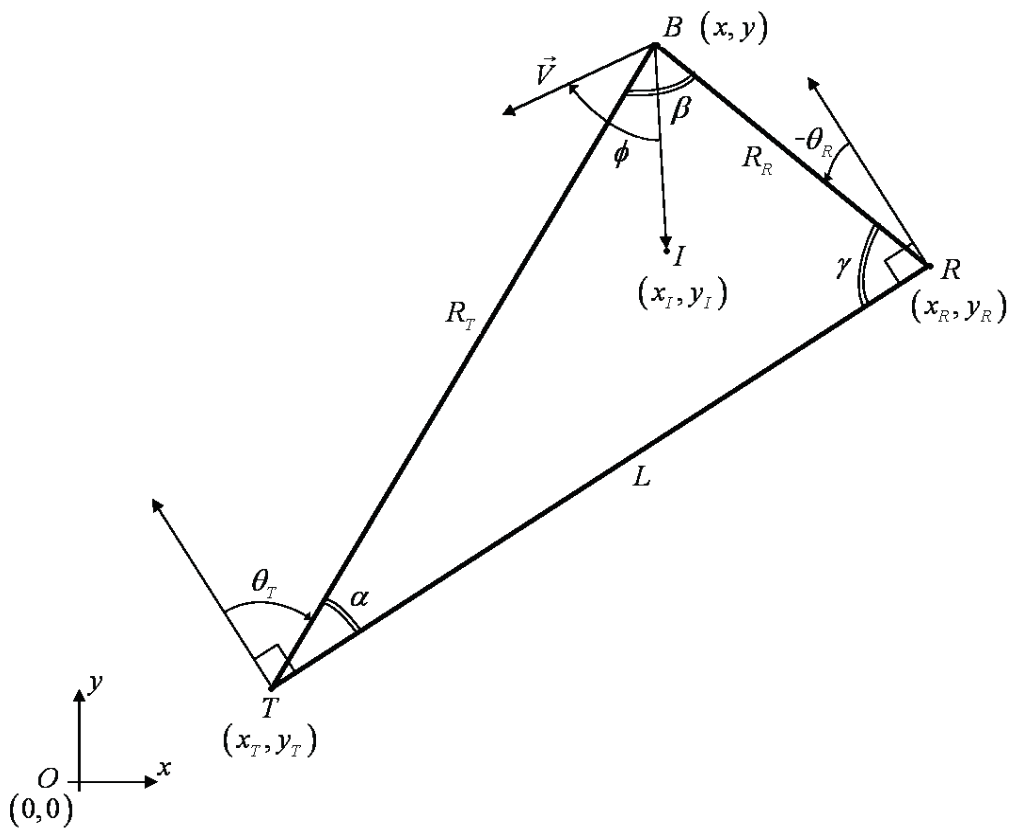

Fig. 1 – Bistatic geometry.

From Fig.1, we have that $\theta_T = 90° - \alpha$, $\theta_R = \gamma - 90°$, $\beta = 180° - \alpha - \beta = \theta_T - \theta_R$, and $R_T{}^2 = R_R{}^2 + L^2 - 2R_R L \sin\theta_R$, which gives the range from transmitter to target R_T, as a function of the range from receiver to target R_R and the look angle of the receiver θ_R.

In Figure 1 we plot also the target velocity vector $\vec{V}$; ϕ is the angle between the target velocity vector and the bistatic bisector, which is measured in a positive clockwise direction from the bisector. In particular, the bistatic bisector is represented by the vector $\overrightarrow{BI}$, where I is the in-center of the bistatic triangle, whose coordinates are (x_I, y_I).

The coordinates of the incenter can be easily obtained as

$$(x_I, y_I) = \frac{L}{L+R_R+R_T}(x, y) + \frac{R_R}{L+R_R+R_T}(x_T, y_T) + \frac{R_T}{L+R_R+R_T}(x_R, y_R).$$

In the bistatic geometry, an important parameter is the radial velocity V_a, which is the target velocity component along the bistatic bisector. From the observation of Figure 1, we obtain $V_a = \vec{V} \cdot \overrightarrow{BI} \big/ \left|\overrightarrow{BI}\right| = \left|\vec{V}\right| \cos\phi$. The bistatic radar geometry can be completely specified in terms of any three of the five parameters, θ_T, θ_R, L, R_R, and R_T. In this technical report we will use θ_R, L, and R_R.

We suppose that the radar transmits a sequence of **linear frequency modulated** (LFM) pulses or chirps. The complex envelope of the transmitted unitary power signal is then given by:

$$u(t) = \frac{1}{\sqrt{N}} \sum_{n=0}^{N-1} u_1(t - nT_R), \tag{1}$$

where

$$u_1(t) = \begin{cases} \frac{1}{\sqrt{T}} \exp\left(j\pi k t^2\right) & 0 \le t \le T \\ 0 & elsewhere \end{cases} \tag{2}$$

N is the number of sub-pulses for each transmitted burst, T_R is the burst repetition time and T is the duration of each pulse, with $T<T_R/2$. Moreover, $kT^2 = BT$ is the effective time-bandwidth product of the signal and B is the total frequency deviation.

As known, the ambiguity function (AF) represents the time response of a filter matched to a nominal signal, when the signal is received with a delay τ_a and a Doppler shift ν_a relative to the nominal values τ_H and ν_H expected by the filter. Then, the AF definition is [Tsa97]:

$$\left|X\left(\tau_H,\tau_a,\nu_H,\nu_a\right)\right| = \left|\int_{-\infty}^{+\infty} u(t-\tau_a)u^*\left(t-\tau_H\right)\exp\left(-j2\pi\left(\nu_H-\nu_a\right)t\right)dt\right| \tag{3}$$

where $u(t)$ is the complex envelope of the signal, τ_a and ν_a are the actual delay and Doppler frequency of the radar target respectively and τ_H and ν_H are the hypothesized delay and frequency. In the monostatic case there is a linear relation between τ_a and ν_a and the range position R_a and radial velocity V_a of the target, $\tau_a = 2R_a/c$ and $\nu_a = -2V_a f_C/c$. Similar relations hold for τ_H and ν_H. Clearly, $\left|X\left(\tau_H,\tau_a,\nu_H,\nu_a\right)\right|$ is maximum for $\tau_a = \tau_H$ and $\nu_a = \nu_H$.

Based upon the definition (3) we can calculate the monostatic AF for the signal $u(t)$ in (1) and (2) as [Lev04]:

$$X\left(\tau,\nu\right) = \begin{cases} \dfrac{1}{N}\displaystyle\sum_{p=-(N-1)}^{(N-1)} \exp\left[j\pi\nu(N-1+p)T_R\right]\left(1-\dfrac{\left|\tau-pT_R\right|}{T}\right)\cdot \\ \cdot\dfrac{\sin\left[\pi T\left(\nu-k\left(\tau-pT_R\right)\right)\left(1-\left|\tau-pT_R\right|/T\right)\right]}{\pi T\left(\nu-k\left(\tau-pT_R\right)\right)\left(1-\left|\tau-pT_R\right|/T\right)}\dfrac{\sin\left[\pi\nu\left(N-|p|\right)T_R\right]}{\sin\left(\pi\nu T_R\right)} & for\left|\tau-pT_R\right|<T \\ 0 & elsewhere \end{cases} \tag{4}$$

where we set $\tau = \tau_H - \tau_a$ and $\nu = \nu_H - \nu_a$.

If we limit the delay to the mainlobe area, namely to $|\tau| \le T$ (p=0), eqs. (3) and (4) reduce to:

$$\left|X(\tau,\nu)\right| = \left(1-\frac{|\tau|}{T}\right)\left|\frac{\sin\left[\pi T(\nu-k\tau)\left(1-|\tau|/T\right)\right]}{\pi T(\nu-k\tau)\left(1-|\tau|/T\right)}\right|\left|\frac{\sin\left[\pi\nu N T_R\right]}{N\sin\left(\pi\nu T_R\right)}\right| \quad \text{for } |\tau|<T. \tag{5}$$

The AF exhibits its maximum in $\tau=0$ and $\nu=0$. The AF of eq. (4) is plotted in Fig. 2 for BT=20, T_R=1 s, T=0.1 s and N=8.

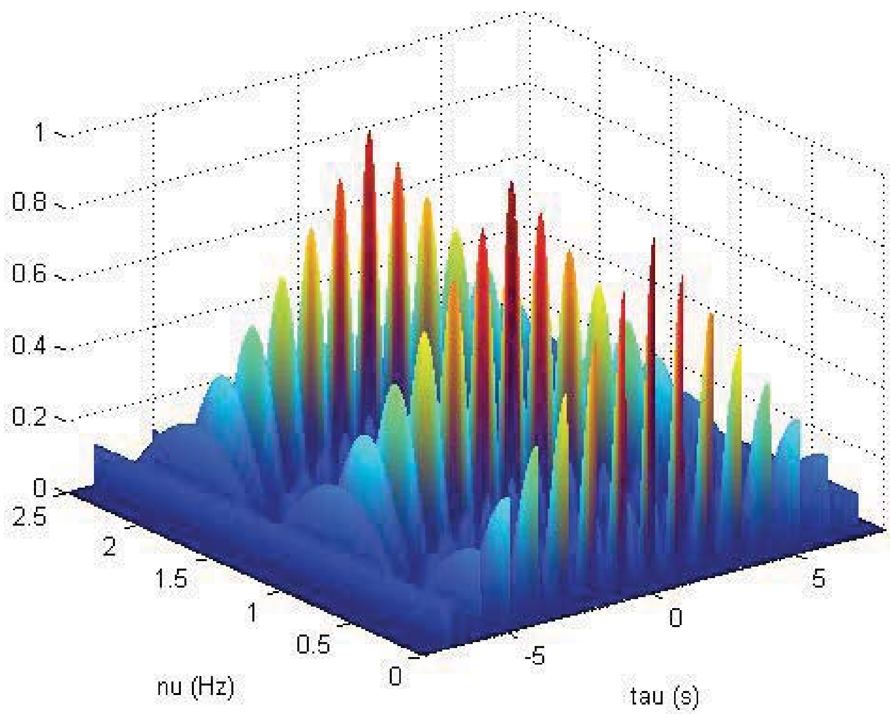

Fig. 2 – Monostatic AF for burst of chirps, BT=20, T_R=1 s, T=0.1 s and N=8.

To refer eqs. (4) and (5) to the bistatic geometry of Fig.1 and to obtain the expression of the bistatic AF, we must replace in (4)-(5) the relations [Tsa97]:

$$\tau_H(R_R,\theta_R,L) = \frac{R_R + \sqrt{R_R^2 + L^2 + 2R_R L\sin\theta_R}}{c} \tag{6}$$

and

$$\nu_H(R_R, V\cos\phi, \theta_R, L) = 2\frac{f_c}{c}V\cos\phi\sqrt{\frac{1}{2}+\frac{R_R + L\sin\theta_R}{2\sqrt{R_R^2 + L^2 + 2R_R L\sin\theta_R}}}\,. \qquad (7)$$

The plots of eq. (4) are reported in Figures 3-7 for different values of *BT* and T_R in the bistatic plane R_R-V_B with $V_B = V\cos\phi$ with V_a=600 m/s, R_a=60 Km. For low values of *BT* the shape of the bistatic ambiguity function heavily depends on the target angle θ_R, as evident comparing Figs.3-4 to Fig.5. For some particular values of θ_R as $\theta_R \simeq \pi/2$, the range resolution is very poor (see Fig. 5c). For high values of *BT* the ambiguity function seems to be less dependent on θ_R, as apparent in Figs. 6 and 7.

For completing the analysis in Figs. 8-10 the slices of AF are plotted for *N*=1, 2 and 32 showing that for increasing *N* the range resolution improves but many peaks appear in the bistatic AF shape.

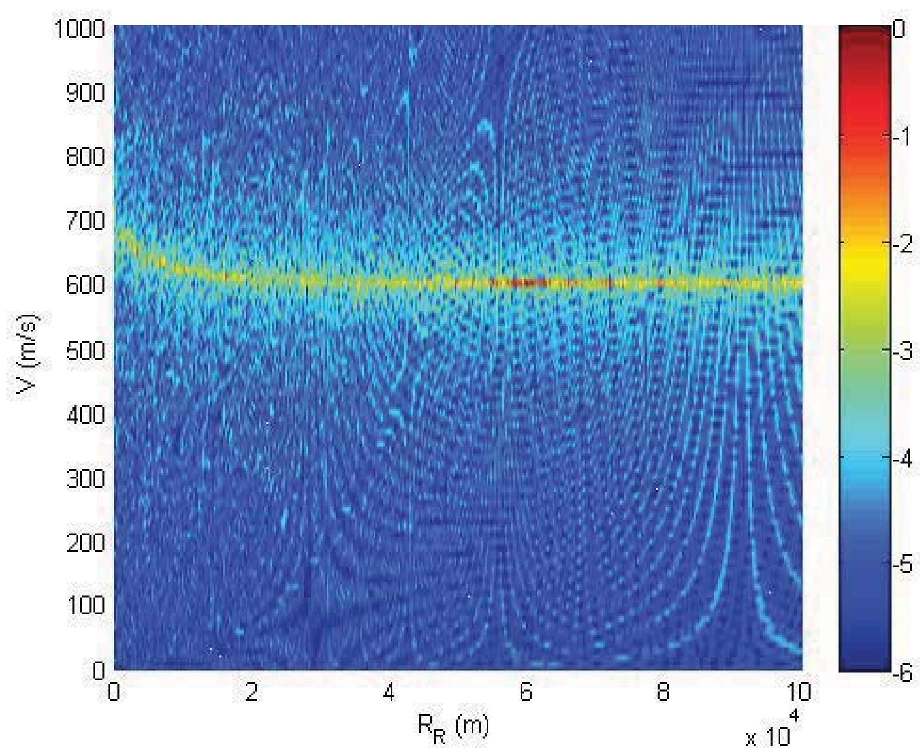

Fig. 3a – Logarithm of the bistatic AF, *BT*=20, T_R=1s, *T*=0.1s, *N*=8, $\theta_R = \pi/6$, V_a=600m/s, R_a=60Km

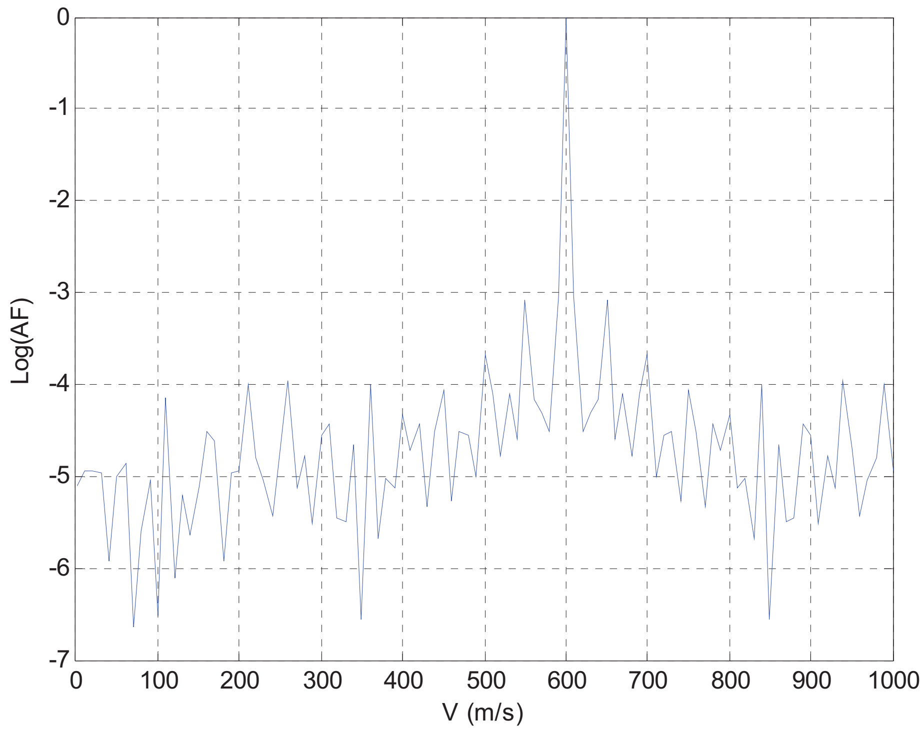

Fig. 3b – Logarithm of the bistatic AF, R_R=60Km, BT=20, T_R=1s, T=0.1s, N=8, $\theta_R = \pi/6$, V_a=600m/s, R_a=60Km

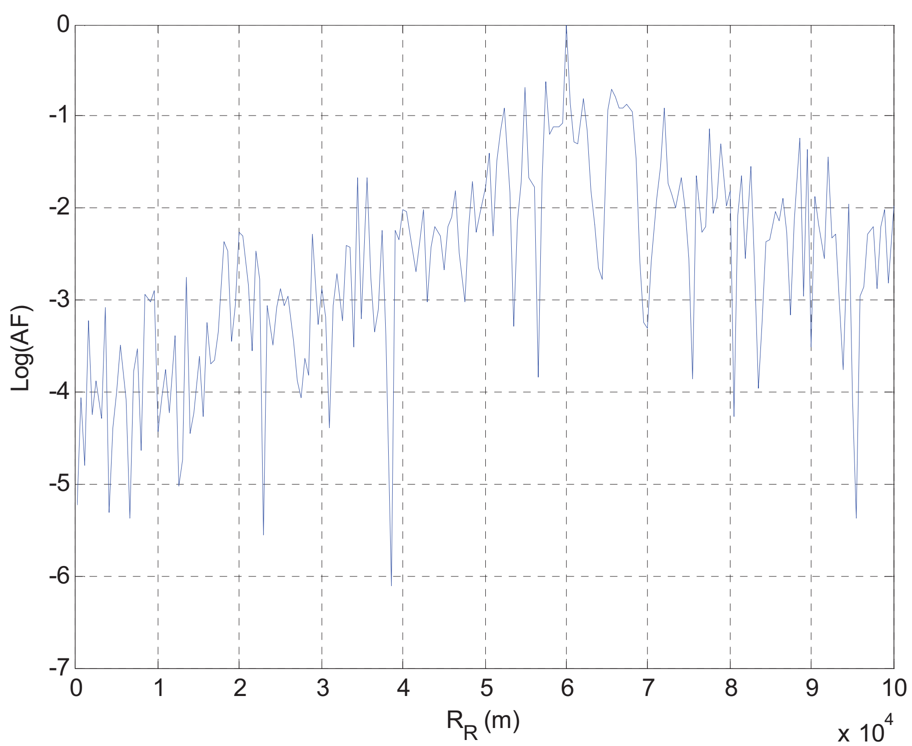

Fig. 3c – Logarithm of the bistatic AF, V=V_a, BT=20, T_R=1s, T=0.1s, N=8, $\theta_R = \pi/6$, V_a=600m/s, R_a=60Km

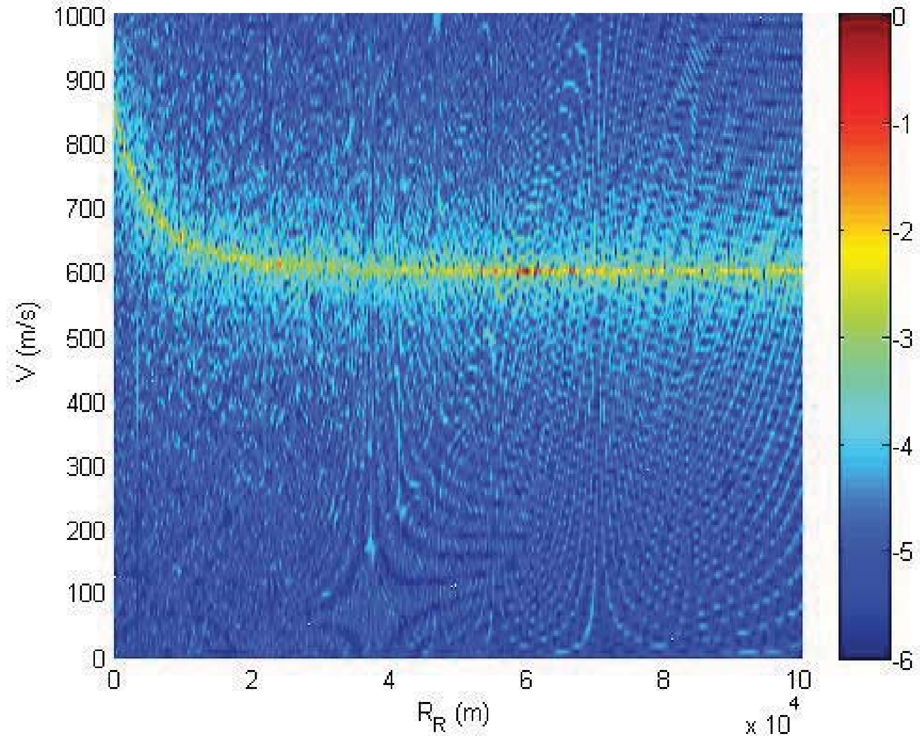

Fig. 4a – Logarithm of the bistatic AF, BT=20, T_R=1s, T=0.1s, N=8, $\theta_R = \pi$, V_a=600m/s, R_a=60Km

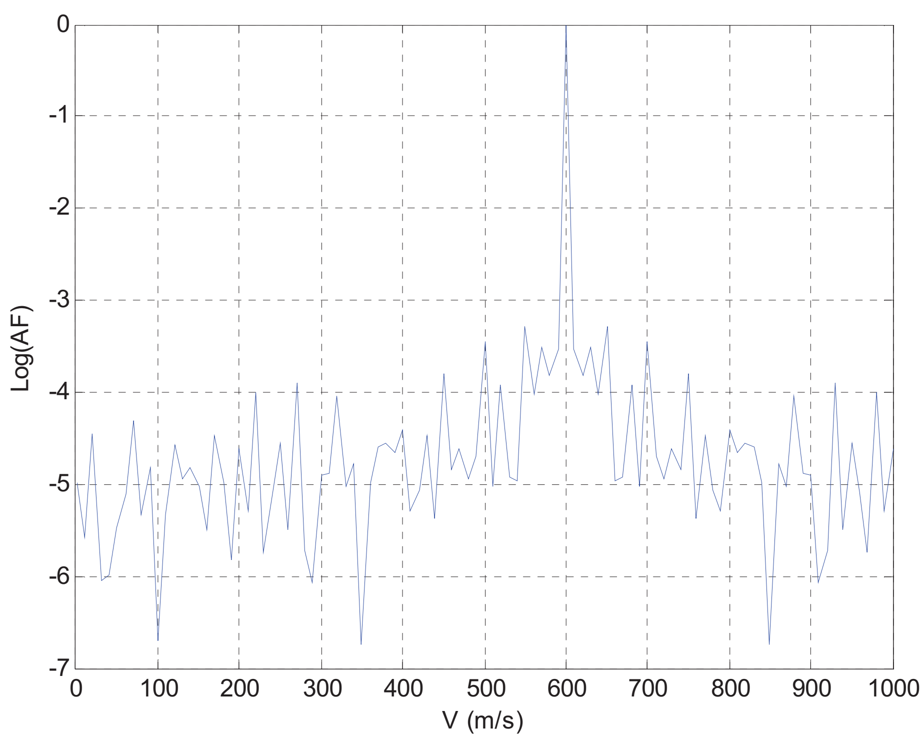

Fig. 4b – Logarithm of the bistatic AF, BT=20, T_R=1s, T=0.1s, N=8, $\theta_R = \pi$, V_a=600m/s, R_a=60Km

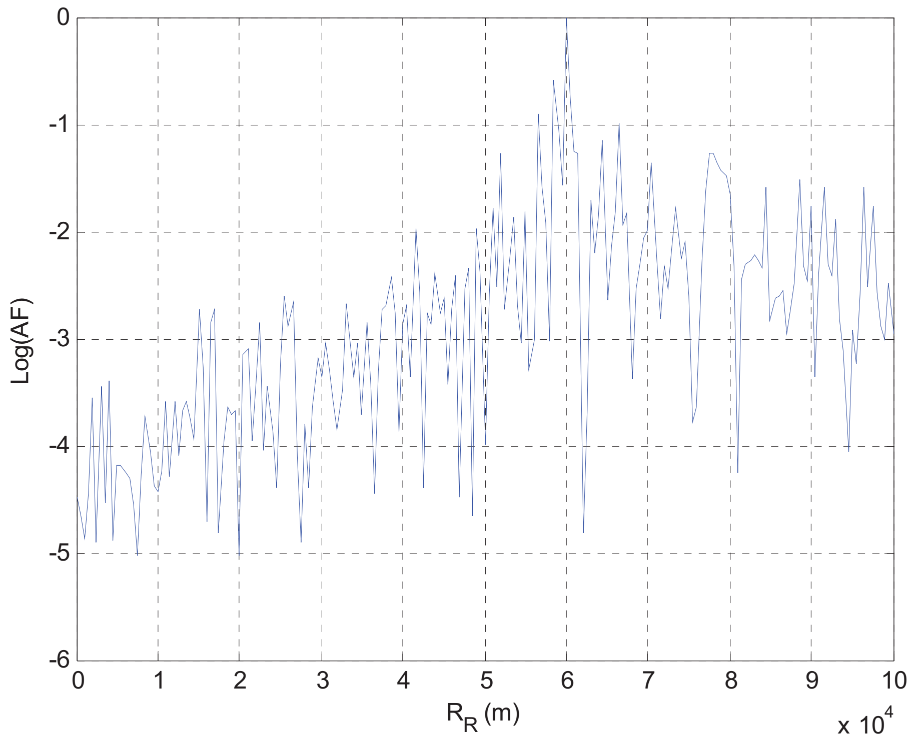

Fig. 4c – Logarithm of the bistatic AF, BT=20, T_R=1s, T=0.1s, N=8, $\theta_R = \pi$, V_a=600m/s, R_a=60Km

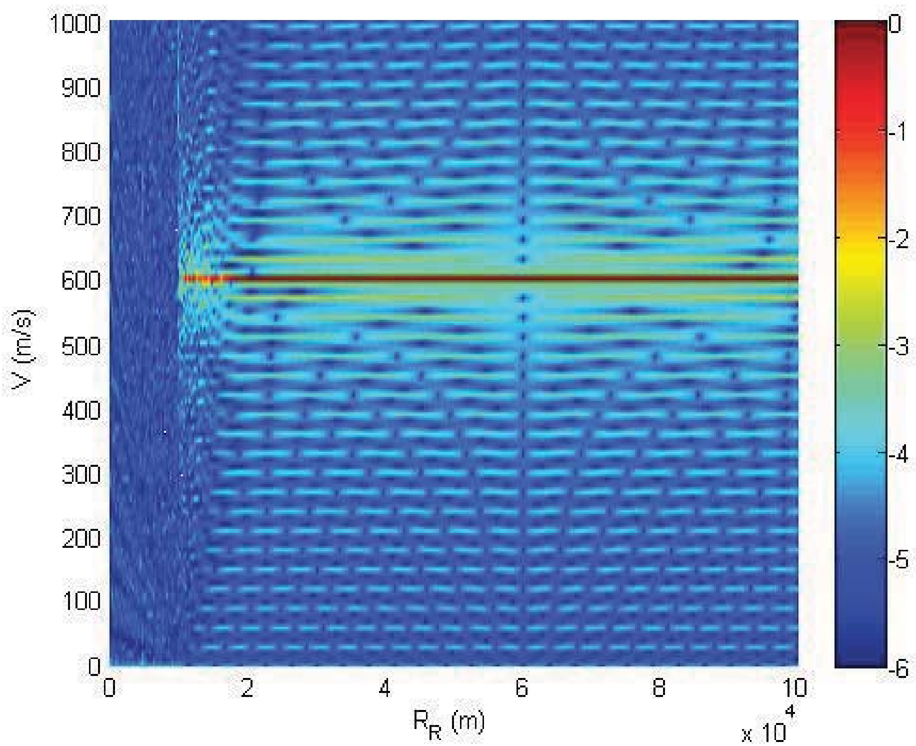

Fig. 5a – Logarithm of the bistatic AF, BT=20, T_R=1s, T=0.1s, N=8, $\theta_R = -0.499\pi$, V_a=600m/s, R_a=60Km

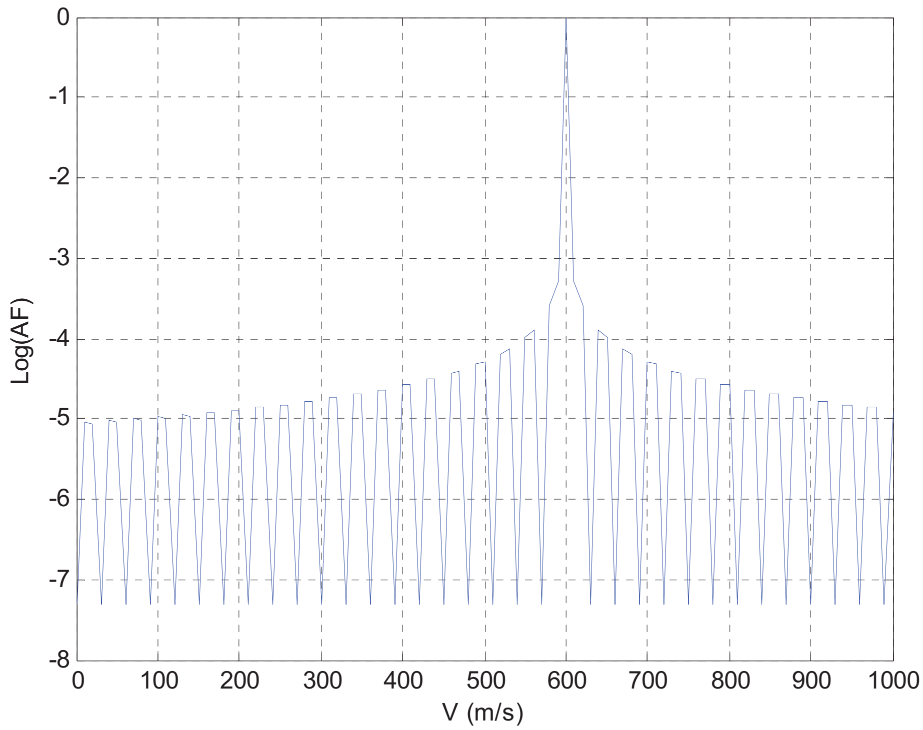

Fig. 5b – Logarithm of the bistatic AF, BT=20, T_R=1s, T=0.1s, N=8, $\theta_R = -0.499\pi$, V_a=600m/s, R_a=60Km

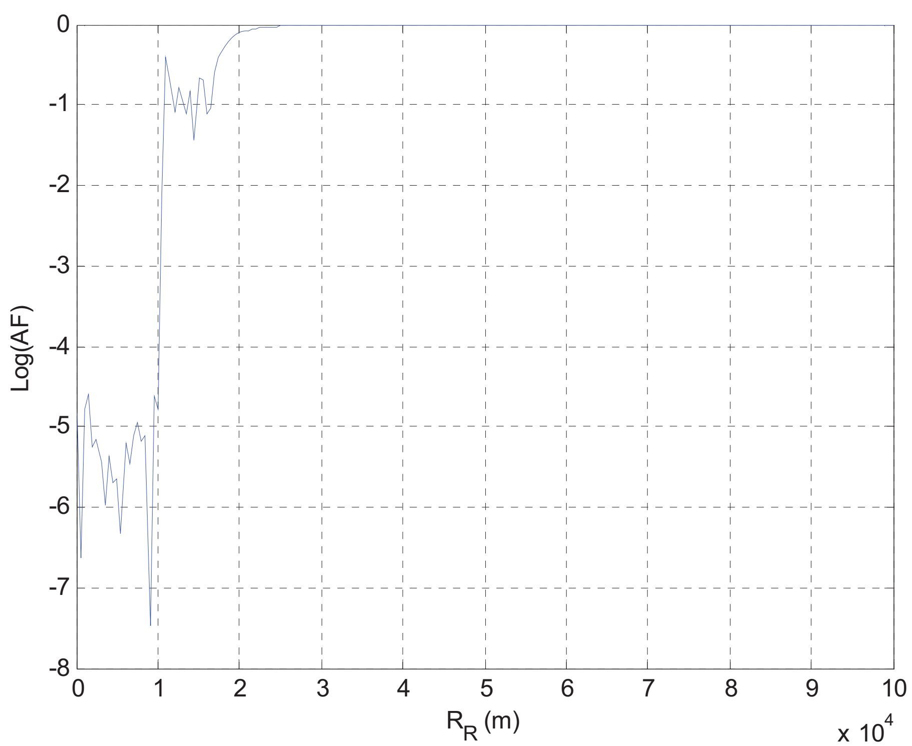

Fig. 5c – Logarithm of the bistatic AF, BT=20, T_R=1s, T=0.1s, N=8, $\theta_R = -0.499\pi$, V_a=600m/s, R_a=60Km

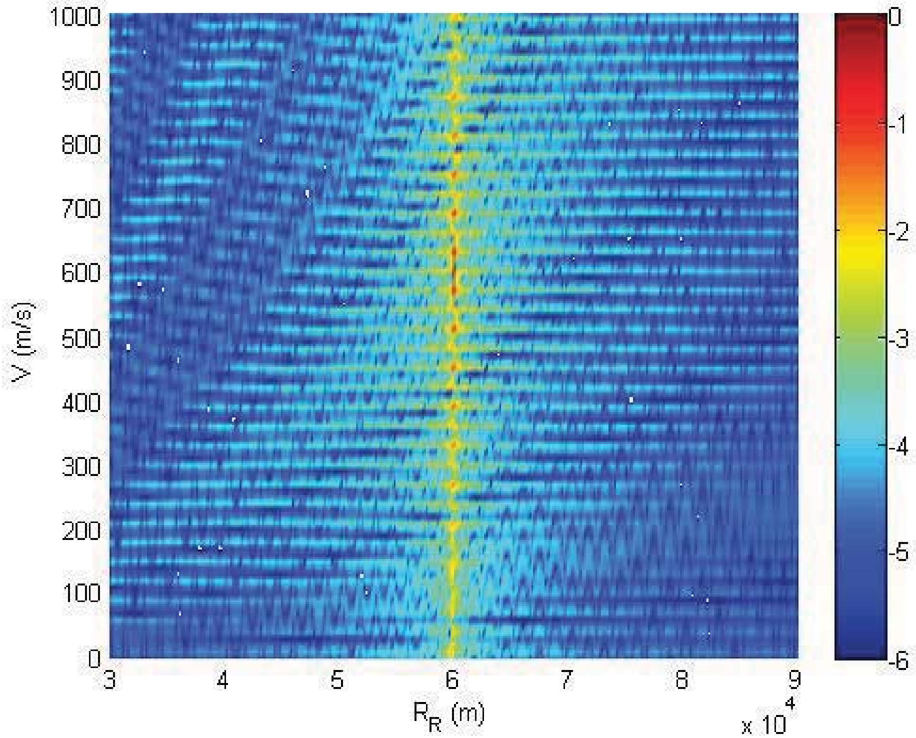

Fig. 6a – Log of the bistatic AF, BT=2500, T_R=1ms, T=250µs, N=8, $\theta_R = \pi$, V_a=600m/s, R_a=60Km

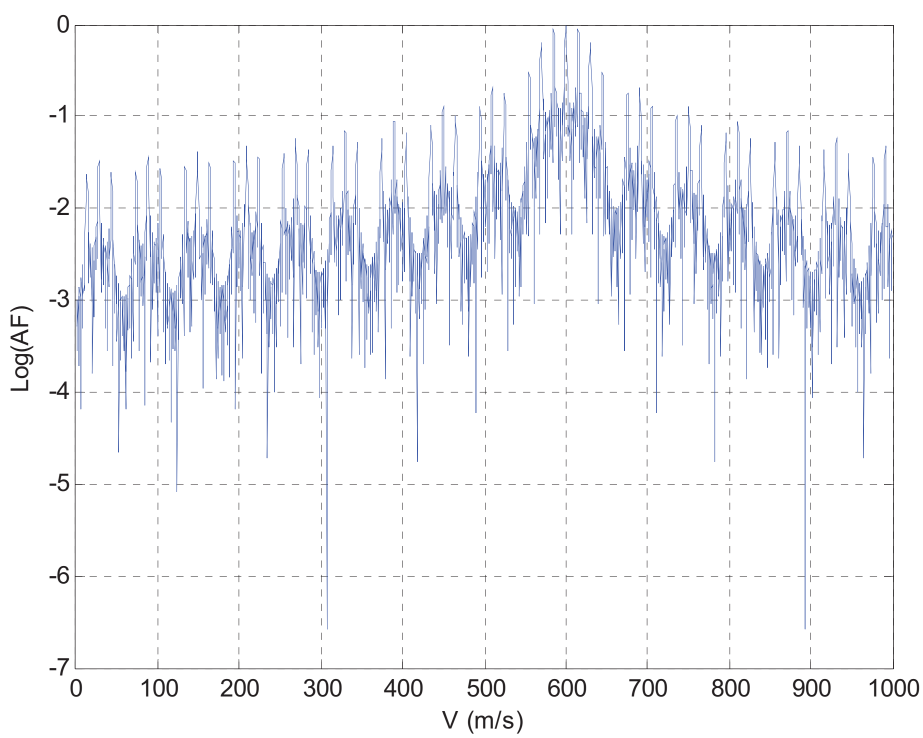

Fig. 6b – Log of the bistatic AF, BT=2500, T_R=1ms, T=250µs, N=8, $\theta_R = \pi$, V_a=600m/s, R_a=60Km

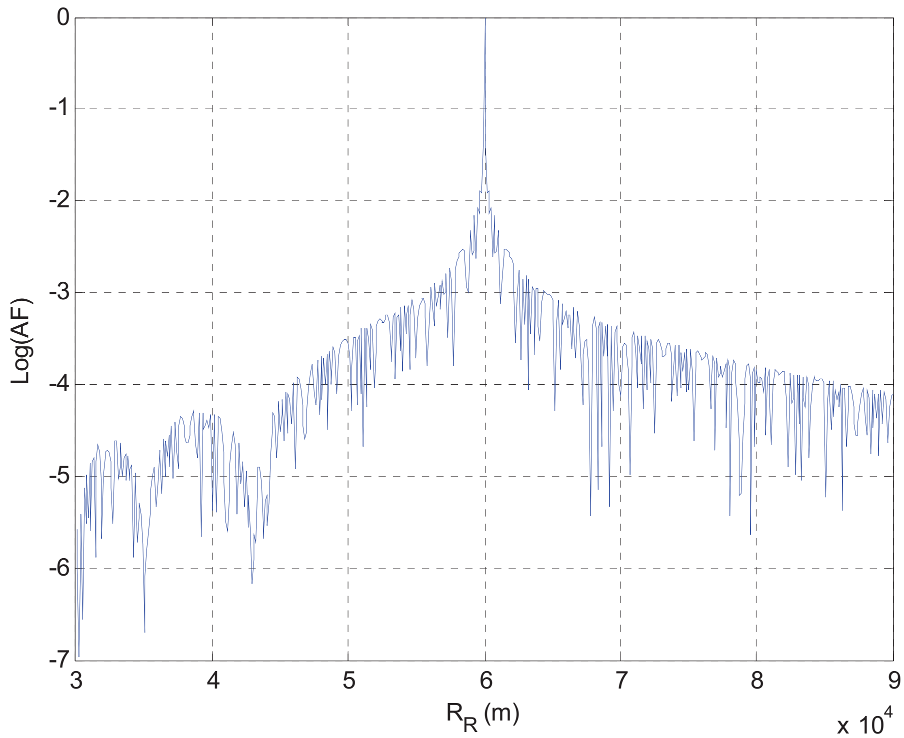

Fig. 6c – Log of the bistatic AF, BT=2500, T_R=1ms, T=250μs, N=8, $\theta_R = \pi$, V_a=600m/s, R_a=60Km

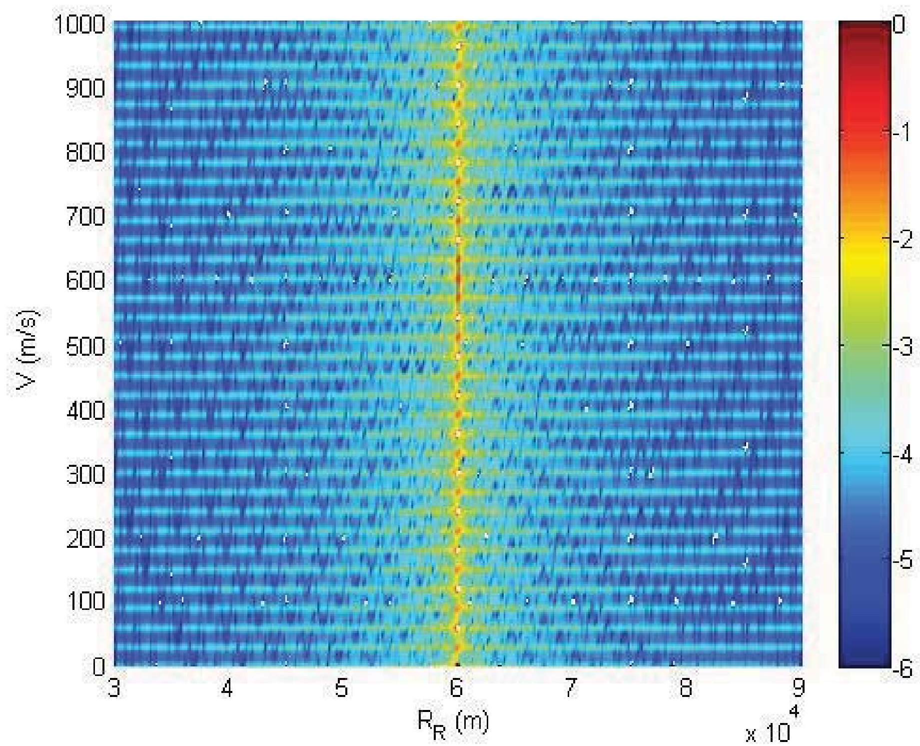

Fig. 7a – Log of the bistatic AF, BT=2500, T_R=1ms, T=250μs, N=8, $\theta_R = -0.499\pi$, V_a=600m/s, R_a=60Km

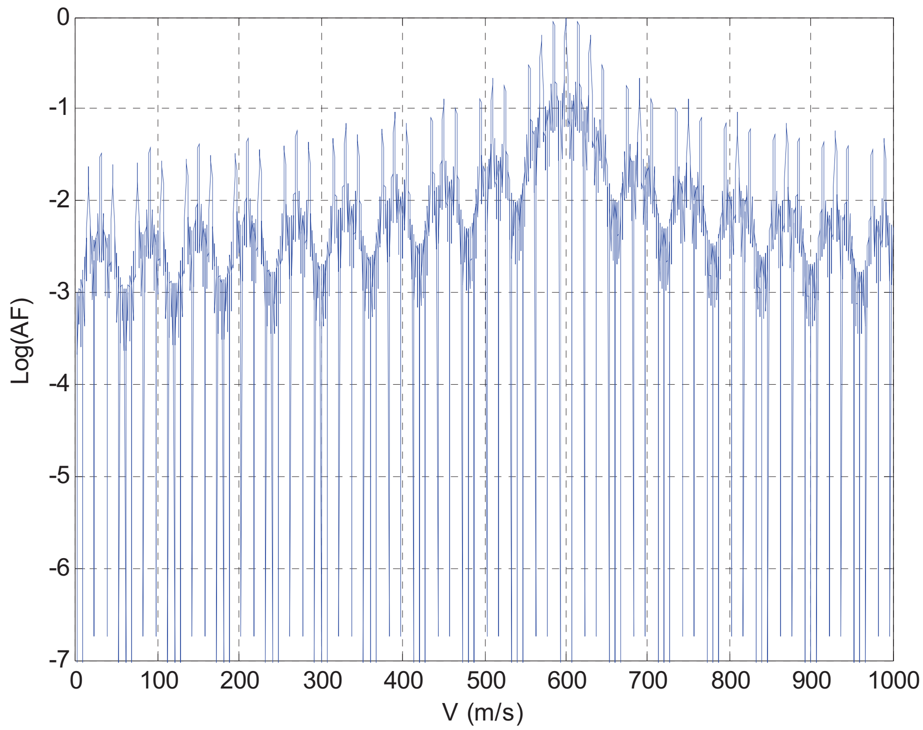

Fig. 7b – Log of the bistatic AF, BT=2500, T_R=1ms, T=250μs, N=8, $\theta_R = -0.499\pi$, V_a=600m/s, R_a=60Km

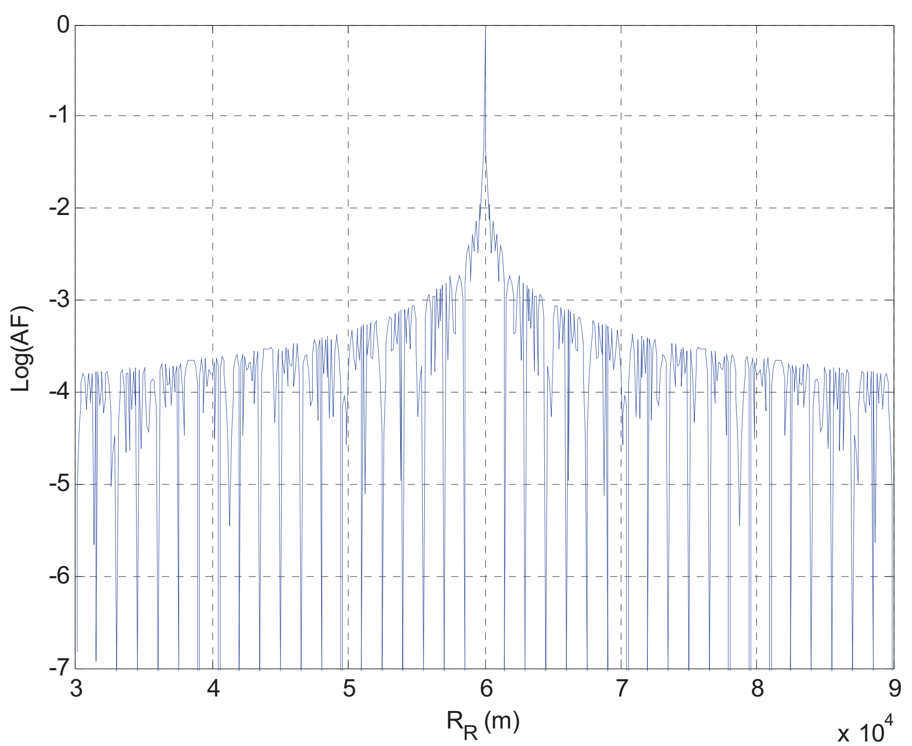

Fig. 7c – Log of the bistatic AF, BT=2500, T_R=1ms, T=250μs, N=8, $\theta_R = -0.499\pi$, V_a=600m/s, R_a=60Km

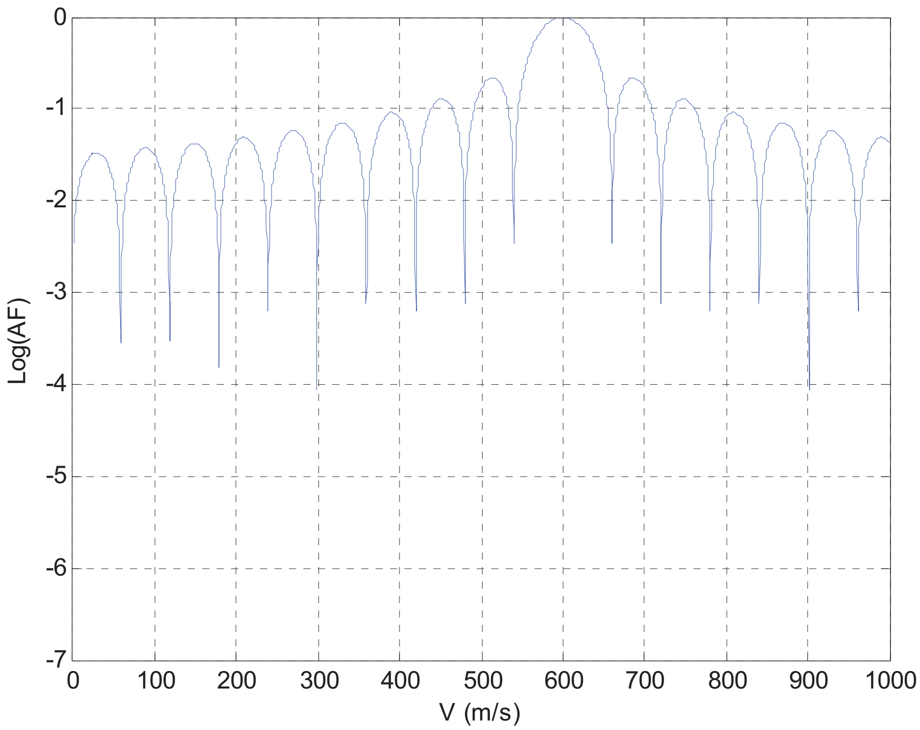

Fig. 8 – Log of the bistatic AF, BT=2500, T_R=1ms, T=250µs, N=1, $\theta_R \approx -\pi/2$, V_a=600m/s, R_a=60Km

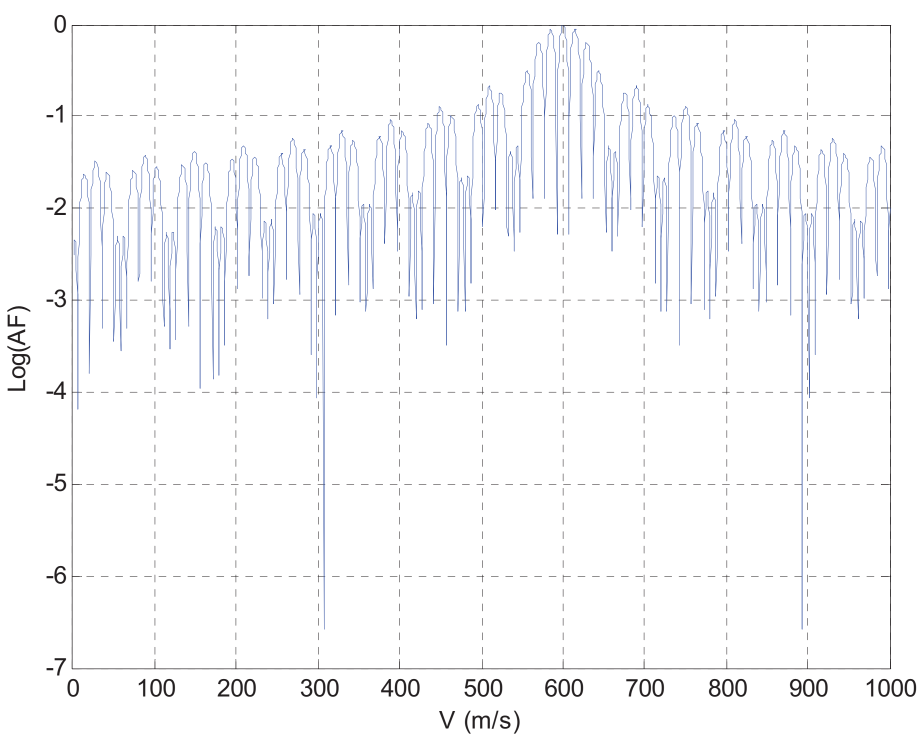

Fig. 9 – Log of the bistatic AF, BT=2500, T_R=1ms, T=250µs, N=2, $\theta_R \approx -\pi/2$, V_a=600m/s, R_a=60Km

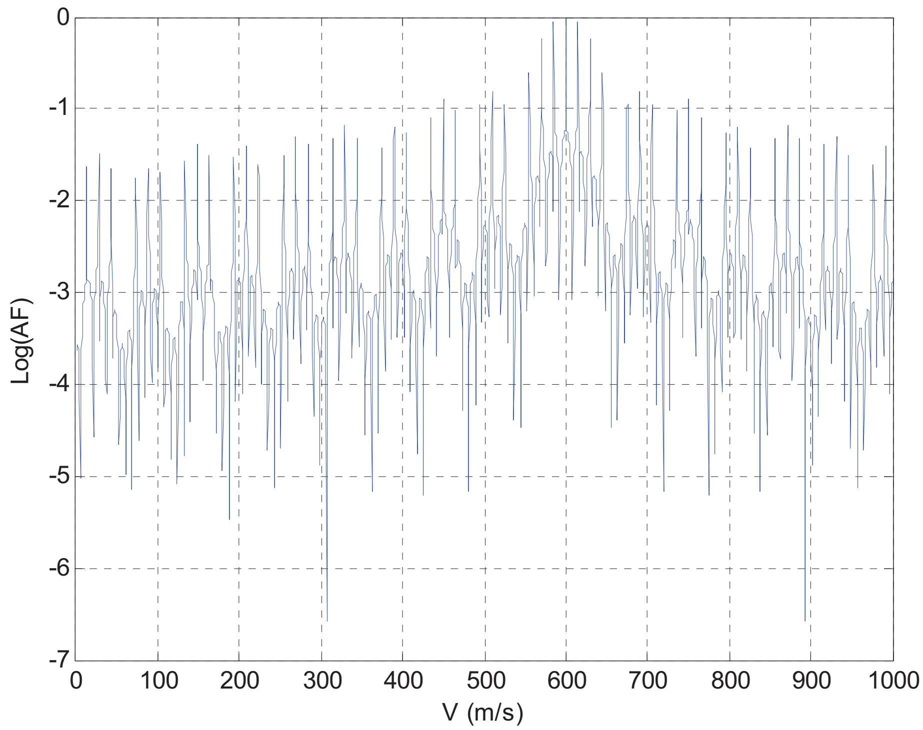

Fig.10 – Log of the bistatic AF, BT=2500, T_R=1ms, T=250μs, N=32, $\theta_R \approx -\pi/2$, V_a=600m/s, R_a=60Km

3 BISTATIC CRAMER-RAO LOWER BOUNDS

Unlike the AF which provides information on the global resolution, the CRLB provides a local measure of estimation accuracy. Both can be used to asses the error properties of the estimates of the signal parameters. In [Van71] the author derived a relationship between CRLB and AF, which has been successfully used in the analysis of passive and active arrays [Dog01]. In the monostatic configuration, [Van71] claims that for the Fisher Information Matrix (FIM) the following relationship holds:

$$\mathbf{J}_M\left(\tau_a,\nu_a\right)=-2SNR\left[\begin{array}{cc}\dfrac{\partial^2\left|X\left(\tau,\nu\right)\right|}{\partial\tau^2} & \dfrac{\partial^2\left|X\left(\tau,\nu\right)\right|}{\partial\tau\partial\nu}\\ \dfrac{\partial^2\left|X\left(\tau,\nu\right)\right|}{\partial\nu\partial\tau} & \dfrac{\partial^2\left|X\left(\tau,\nu\right)\right|}{\partial\nu^2}\end{array}\right]\Bigg|_{\tau=0,\nu=0} \tag{8}$$

where *SNR* is the signal-to-noise power ratio at the receiver. In Appendix A we report the proof of relation (8). From eq. (8) the CRLBs follow: $CRLB(\tau_a)=\left[\mathbf{J}_M(\tau_a,\nu_a)\right]_{1,1}^{-1}$ and $CRLB(\nu_a)=\left[\mathbf{J}_M(\tau_a,\nu_a)\right]_{2,2}^{-1}$.

In the bistatic configuration we should write the AF in terms of the bistatic $\tau(R_R,\theta_R,L)$ and $\nu(R_R,V_B,\theta_R,L)$ and derive it with respect to the useful parameters R_R and V_B. Then

$$\mathbf{J}_B\left(R_R,V_B\right)=-2SNR\left[\begin{array}{cc}\dfrac{\partial^2\left|X\left(R_R,V_B\right)\right|}{\partial {R_R}^2} & \dfrac{\partial^2\left|X\left(R_R,V_B\right)\right|}{\partial R_R\partial V_B}\\ \dfrac{\partial^2\left|X\left(R_R,V_B\right)\right|}{\partial V_B\partial R_R} & \dfrac{\partial^2\left|X\left(R_R,V_B\right)\right|}{\partial {V_B}^2}\end{array}\right]\Bigg|_{R_R=R_a,V_B=V_a} \tag{9}$$

After some algebra, it is possible to verify that, in the monostatic configuration we have:

$$\mathbf{J}_M\left(\tau_a,\nu_a\right)=-2SNR\left[\begin{array}{cc}-\dfrac{\pi^2T^2}{3}+\dfrac{\pi^2T_R^2(1-N^2)}{3} & \dfrac{k\pi^2T^2}{3}\\ \dfrac{k\pi^2T^2}{3} & -\dfrac{k^2\pi^2T^2}{3}\end{array}\right]^{-1} \tag{10}$$

then

$$CRLB(\tau_a) = \frac{3}{2\pi^2 T^2 k^2 SNR}\left[1+\left(\frac{T}{T_R}\right)^2 \frac{1}{N^2-1}\right] \tag{11}$$

and

$$CRLB(\nu_a) = \frac{3}{2\pi^2 T_R^2 SNR\left(N^2-1\right)} \tag{12}$$

These results are in agreement with those obtained in [Dog07].

For the calculation of the CRLBs in the bistatic domain we can partially use the results for the monostatic domain. Following the "chain rule" of the derivative (see Appendix B for details) we can prove that

$$\begin{aligned}\frac{\partial^2\left|X\left(R_R,V_B\right)\right|}{\partial R_R{}^2} &= \left[\mathbf{J}_M\right]_{2,2}\left(\frac{\partial\tau}{\partial R_R}\right)^2 + 2\left[\mathbf{J}_M\right]_{1,2}\frac{\partial\tau}{\partial R_R}\frac{\partial\nu}{\partial R_R} + \left[\mathbf{J}_M\right]_{1,1}\left(\frac{\partial\nu}{\partial R_R}\right)^2 \\ &\quad + \frac{\partial\left|X\left(\tau,\nu\right)\right|}{\partial\tau}\frac{\partial^2\tau}{\partial R_R{}^2} + \frac{\partial\left|X\left(\tau,\nu\right)\right|}{\partial\nu}\frac{\partial^2\nu}{\partial R_R{}^2}\end{aligned} \tag{13}$$

$$\begin{aligned}\frac{\partial^2\left|X\left(R_R,V_B\right)\right|}{\partial V_B{}^2} &= \left[\mathbf{J}_M\right]_{2,2}\left(\frac{\partial\tau}{\partial V_B}\right)^2 + 2\left[\mathbf{J}_M\right]_{1,2}\frac{\partial\tau}{\partial V_B}\frac{\partial\nu}{\partial V_B} + \left[\mathbf{J}_M\right]_{1,1}\left(\frac{\partial\nu}{\partial V_B}\right)^2 \\ &\quad + \frac{\partial\left|X\left(\tau,\nu\right)\right|}{\partial\tau}\frac{\partial^2\tau}{\partial V_B{}^2} + \frac{\partial\left|X\left(\tau,\nu\right)\right|}{\partial\nu}\frac{\partial^2\nu}{\partial V_B{}^2}\end{aligned} \tag{14}$$

$$\begin{aligned}\frac{\partial^2\left|X\left(R_R,V_B\right)\right|}{\partial V_B\partial R_R} &= \frac{\partial^2\left|X\left(R_R,V_B\right)\right|}{\partial R_R\partial V_B} \\ &= \left[\mathbf{J}_M\right]_{2,2}\frac{\partial\tau}{\partial V_B}\frac{\partial\tau}{\partial R_R} + \left[\mathbf{J}_M\right]_{1,2}\frac{\partial\tau}{\partial R_R}\frac{\partial\nu}{\partial V_B} + \frac{\partial\left|X\left(\tau,\nu\right)\right|}{\partial\tau}\frac{\partial^2\tau}{\partial R_R\partial V_B} \\ &\quad + \left[\mathbf{J}_M\right]_{1,2}\frac{\partial\tau}{\partial V_B}\frac{\partial\nu}{\partial R_R} + \left[\mathbf{J}_M\right]_{1,1}\frac{\partial\nu}{\partial R_R}\frac{\partial\nu}{\partial V_B} + \frac{\partial\left|X\left(\tau,\nu\right)\right|}{\partial\nu}\frac{\partial^2\nu}{\partial V_B\partial R_R}\end{aligned} \tag{15}$$

From eq. (6)-(7) we get:

$$\frac{\partial \nu}{\partial R_R} = \frac{f_c}{2c} V_B \frac{L^2 \cos^2 \theta_R}{\left(R_R^2 + L^2 + 2R_R L \sin\theta_R\right)^{3/2} \sqrt{\frac{1}{2} + \frac{R_R + L\sin\theta_R}{2\sqrt{R_R^2 + L^2 + 2R_R L \sin\theta_R}}}} \tag{16}$$

$$\frac{\partial \nu}{\partial V_B} = \frac{2f_c}{c} \sqrt{\frac{1}{2} + \frac{R_R + L\sin\theta_R}{2\sqrt{R_R^2 + L^2 + 2R_R L \sin\theta_R}}} \tag{17}$$

$$\frac{\partial \tau}{\partial R_R} = \frac{1}{c}\left(1 + \frac{R_R + L\sin\theta_R}{\sqrt{R_R^2 + L^2 + 2R_R L \sin\theta_R}}\right) \tag{18}$$

$$\frac{\partial^2 \nu}{\partial R_R \partial V_B} = \frac{1}{V_B}\frac{\partial \nu}{\partial R_R} \tag{19}$$

$$\frac{\partial^2 \tau}{\partial {R_R}^2} = \frac{L^2 \cos^2 \theta_R}{c\left(R_R^2 + L^2 + 2R_R L \sin\theta_R\right)^{3/2}} \tag{20}$$

$$\frac{\partial^2 \nu}{\partial {R_R}^2} = \frac{-\left[6\left(R_R^2 + L^2 + 2R_R L\sin\theta_R\right)^{1/2}\left(R_R + L\sin\theta_R\right) + \left(R_R^2 + L^2 + 2R_R L\sin\theta_R\right) + 5\left(R_R + L\sin\theta_R\right)^2\right]}{4c\left(\sqrt{2} f_c V_B L^2 \cos^2\theta_R\right)^{-1}\left(R_R^2 + L^2 + 2R_R L\sin\theta_R\right)^{9/4}\left[\left(R_R^2 + L^2 + 2R_R L\sin\theta_R\right)^{1/2} + \left(R_R + L\sin\theta_R\right)\right]^{3/2}} \tag{21}$$

$$\frac{\partial \tau}{\partial V_B} = \frac{\partial^2 \tau}{\partial R_R \partial V_B} = \frac{\partial^2 \tau}{\partial {V_B}^2} = \frac{\partial^2 \nu}{\partial {V_B}^2} = 0 \tag{22}$$

For L=0, bistatic CRLBs coincide with monostatic CRLBs.

4 NUMERICAL ANALYSIS

The CRLBs are plotted in Figs. 11-14 as a function of the baseline length *L*, the target angle θ_R, and the number of subpulses *N* in each transmitted burst. It is evident that, for all the parameter values we tested, the bistatic CRLBs ($CRLB_B$) are higher than the monostatic CRLBs ($CRLB_M$). The bistatic CRLBs get even worse for target angles θ_R close to $-\pi/2$, where they tend to infinity. This behavior is in agreement with the shape of the bistatic AF plotted in Fig.5c, where the AF exhibit and almost step-wise shape.

To highlight the differences between monostatic and bistatic domain we plot in Figs. 15-22 the log of the ratio between $CRLB_B$ and $CRLB_M$ as a function of the baseline length *L* and the true position of the target R_a. For high values of *BT* we observe that generally the $CRLB_B$ are higher than the $CRLB_M$, particularly for the range and when the distance between the receiver and the target is orthogonal to the baseline. When *BT* is low, the $CRLB_B$ show some gain with respect to the monostatic scenario, even for $\theta_R \cong -\pi/2$ as shown in Figs. 19 and 21.

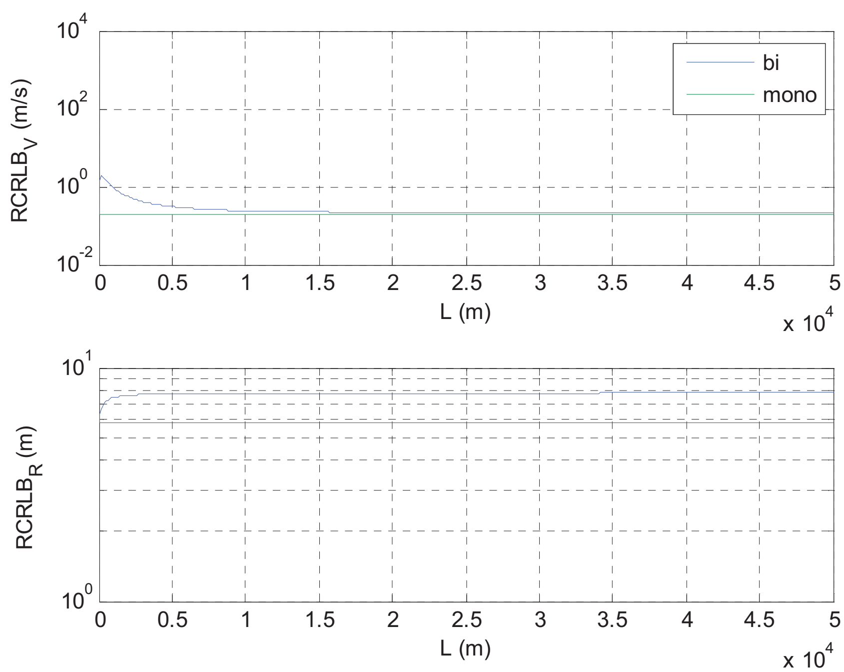

Fig. 11 – RCRLB as a function of bistatic baseline length *L*, *BT*=2500, T_R=1ms, *T*=250µs, *N*=32, $\theta_R = \pi/2$, V_a=600 m/s, R_a=60Km, *SNR*=0dB

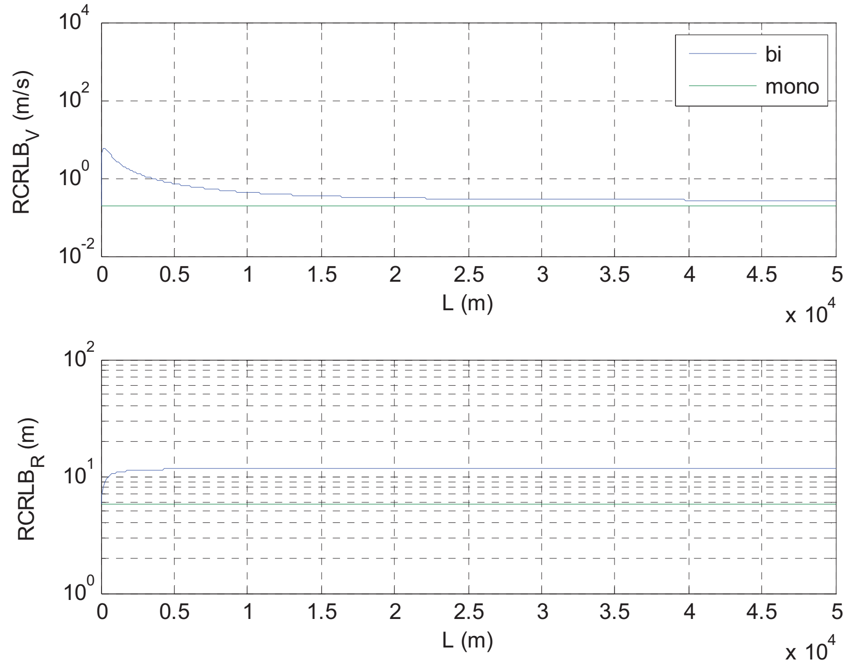

Fig. 12 – RCRLB as a function of bistatic baseline length L, BT=2500, T_R=1ms, T=250μs, N=32, $\theta_R = \pi$, V_a=600 m/s, R_a=60Km, SNR=0dB.

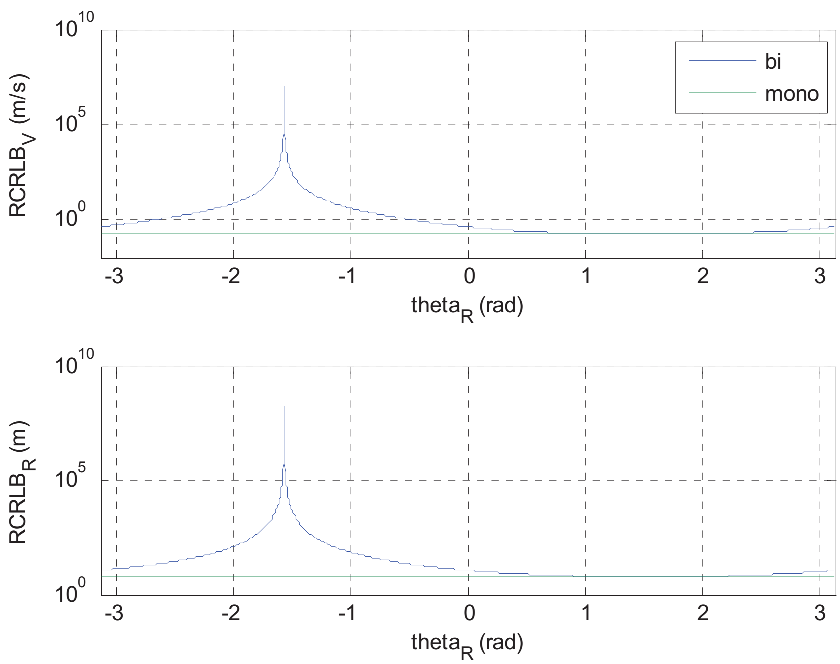

Fig. 13 – RCRLB as a function of target angle θ_R, L=10Km, BT=2500, T_R=1ms, T=250μs,

N=32, V_a=600 m/s, R_a=60Km, SNR=0dB

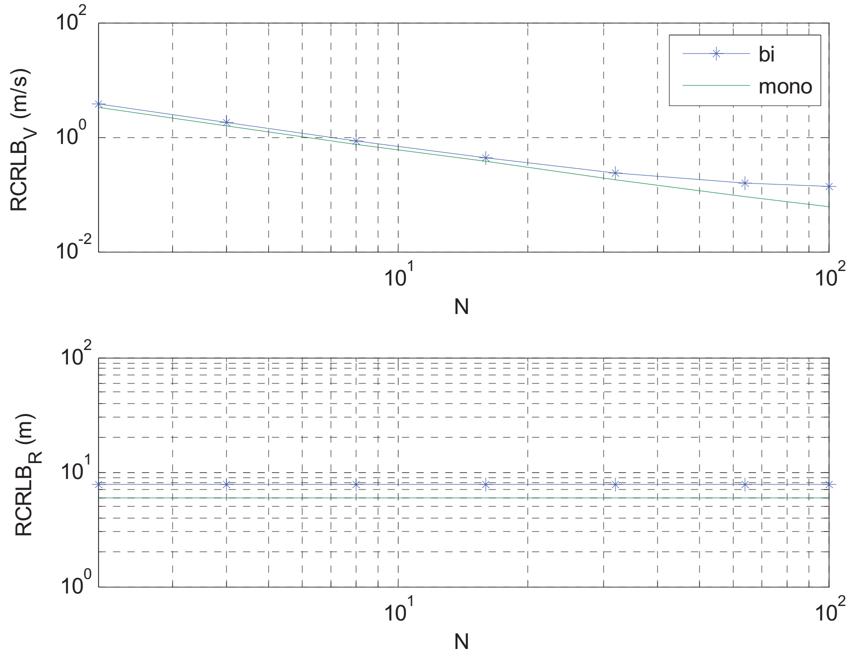

Fig. 14 – RCRLB as a function of the number of pulses N, L=10Km, BT=2500, T_R=1ms, T=250μs, V_a=600 m/s, R_a=60Km, $\theta_R = \pi/6$, SNR=0dB.

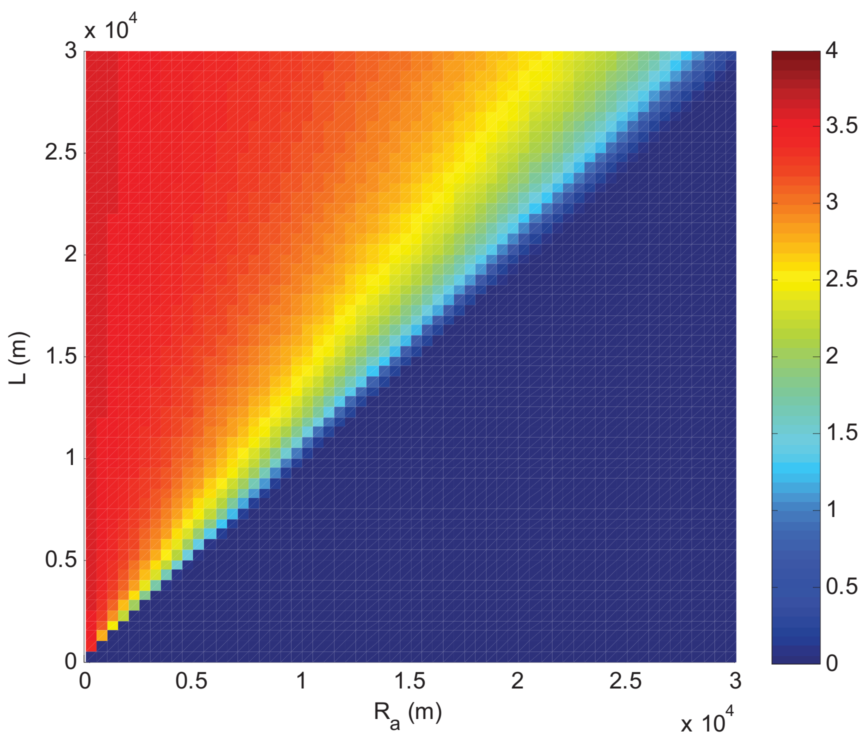

Fig. 15 - Log-ratio between CRLB$_B$ and CRLB$_M$ for the range, BT=2500, T_R =1ms, T=250μs, N=32, $\theta_R \cong -\pi/2$, V_a =600m/s.

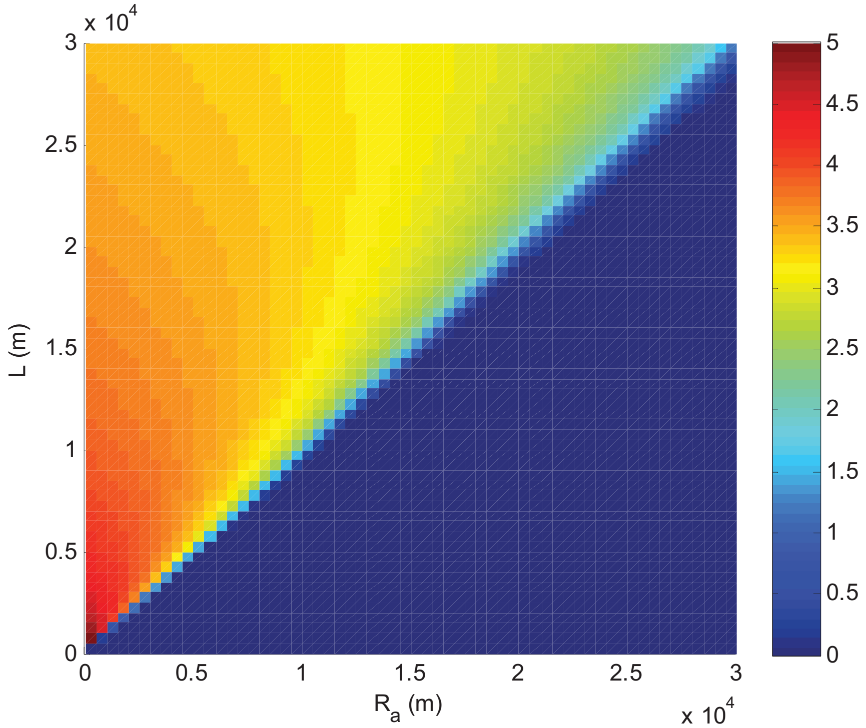

Fig. 16 - Log-ratio between $CRLB_B$ and $CRLB_M$ for the velocity, BT=2500, T_R =1ms, T=250μs, N=32, $\theta_R \cong -\pi/2$, V_a =600m/s.

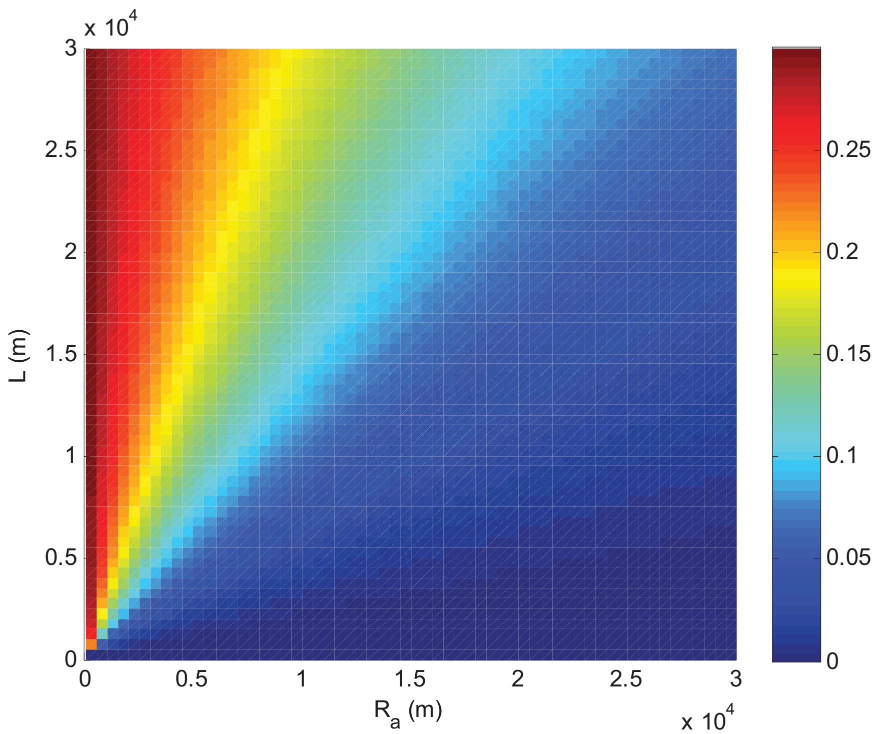

Fig. 17 - Log-ratio between $CRLB_B$ and $CRLB_M$ for the range, BT=2500, T_R =1ms, T=250μs, N=32, $\theta_R = \pi$, V_a =600m/s.

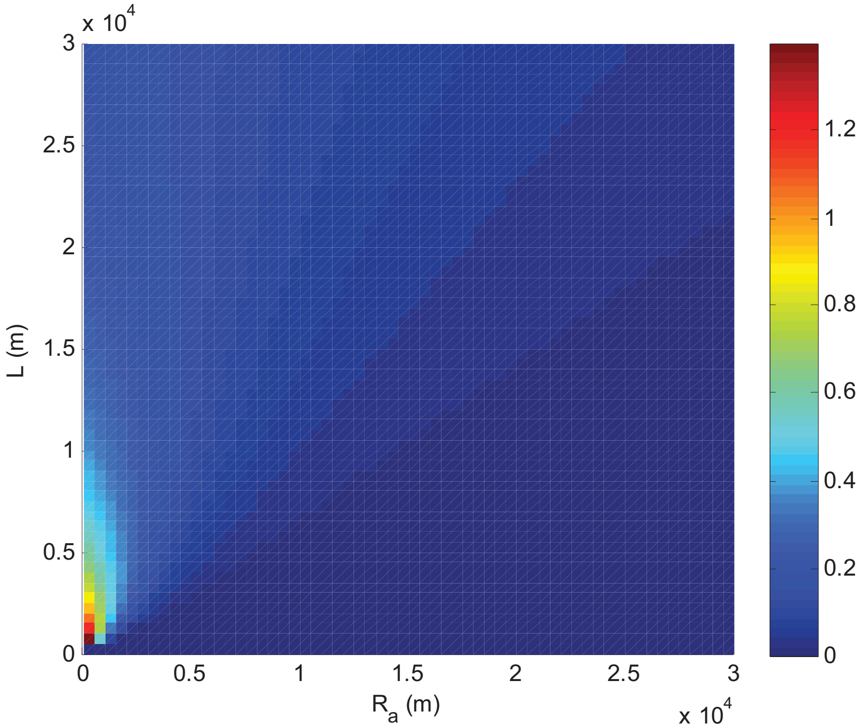

Fig. 18 - Log-ratio between $CRLB_B$ and $CRLB_M$ for the velocity, BT=2500, T_R =1ms, T=250μs, N=32, $\theta_R = \pi$, V_a =600m/s

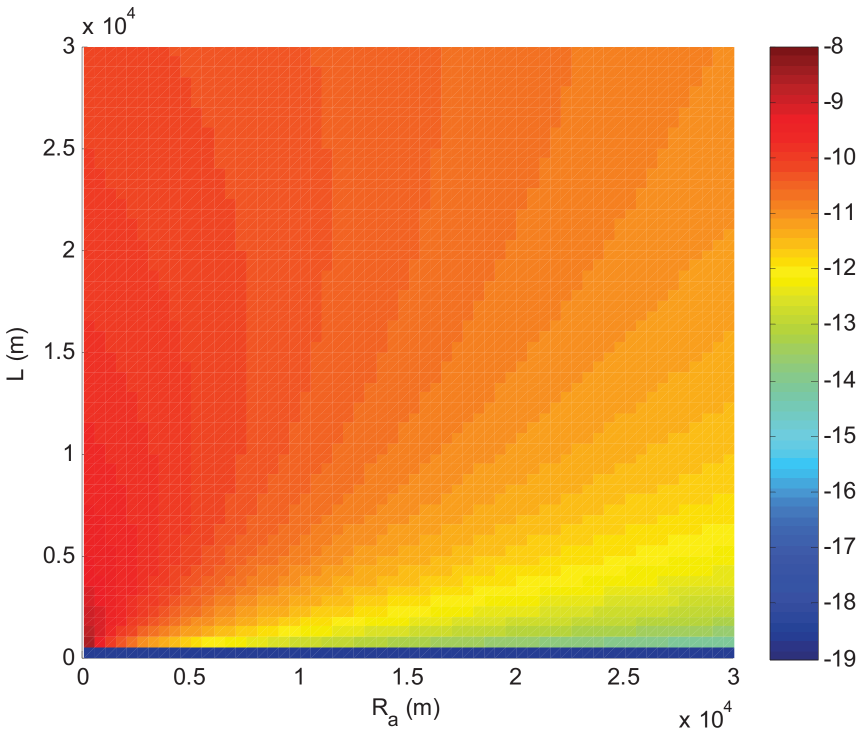

Fig. 19 - Log-ratio between $CRLB_B$ and $CRLB_M$ for the range, BT=40, T_R =1s, T=0.1s, N=8, $\theta_R = \pi$, V_a =600m/s

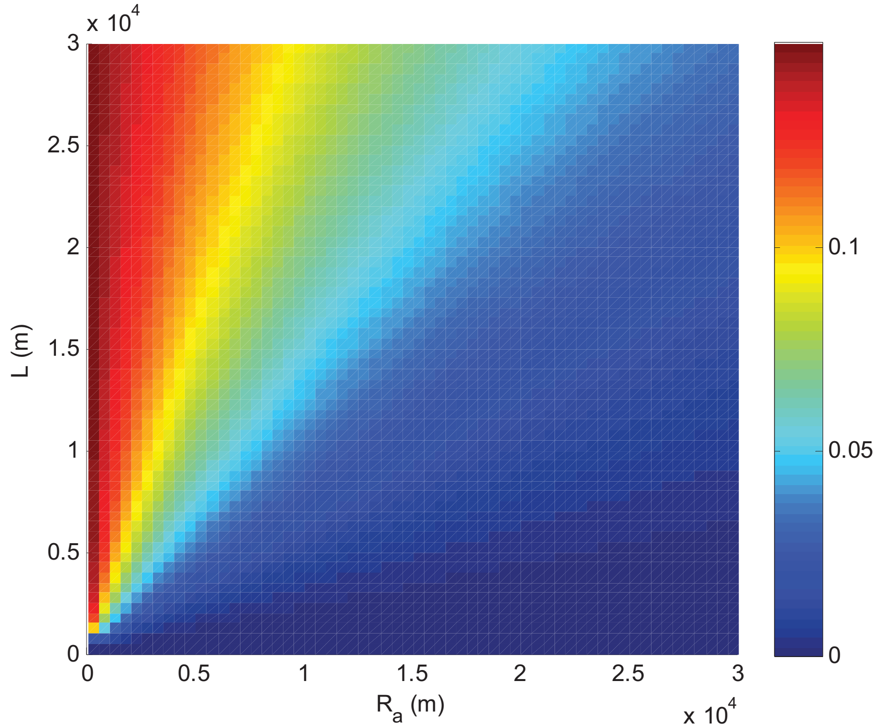

Fig. 20 - Log-ratio between $CRLB_B$ and $CRLB_M$ for the velocity, BT=40, T_R =1s, T=0.1s, N=8, $\theta_R = \pi$, V_a =600m/s

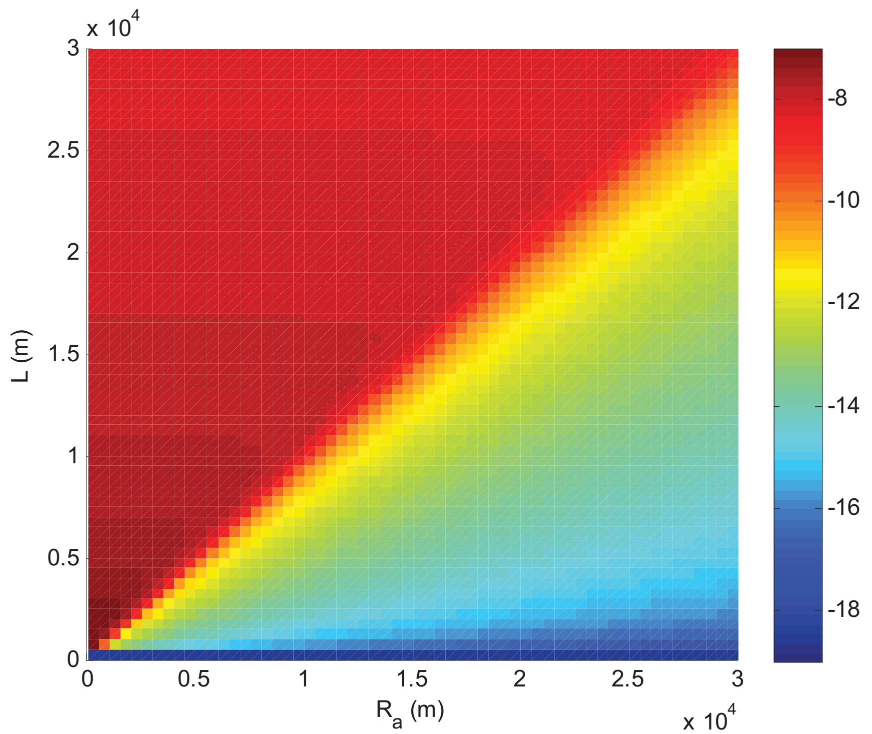

Fig. 21 - Log-ratio between $CRLB_B$ and $CRLB_M$ for the range, BT=40, T_R =1s, T=0.1s, N=8, $\theta_R \cong -\pi/2$, V_a =600m/s

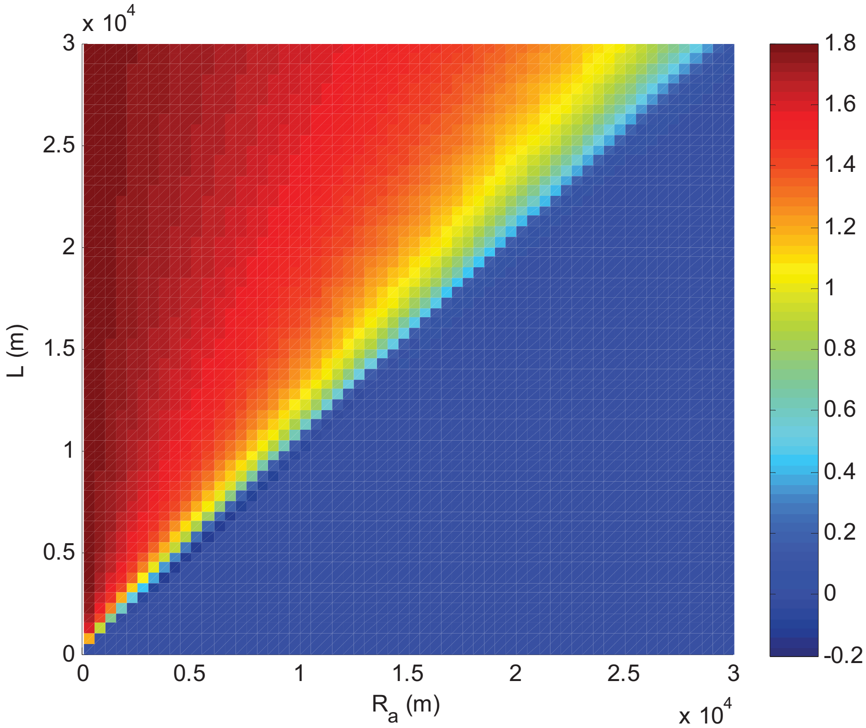

Fig. 22 - Log-ratio between $CRLB_B$ and $CRLB_M$ for the velocity, BT=40, T_R =1s, T=0.1s, N=8, $\theta_R \cong -\pi/2$, V_a =600m/s.

5 OPTIMAL SELECTION OF THE TX-RX PAIR IN A MULTISTATIC RADAR NETWORK

The CRLB study carried out on the bistatic geometry can be applied for the selection of the TX-RX pair in a multistatic radar network. Multistatic radar utilises multiple transmitters and receivers to provide several different monostatic and bistatic channels of observation, leading to an increase in the information on a particular area of surveillance. The information gain obtained through this spatial diversity can give rise to a number of advantages over both the individual monostatic and bistatic cases in typical radar functions, such as detection, parameter estimation, tracking and identification.

We verified in previous sessions that the performance of each bistatic channel heavily depends upon the geometry of the scenario and the position of the target with respect to each receiver and transmitter. In this paragraph we approach the problem of optimally selecting the transmitter-receiver (TX-RX) pair, based on the information provided by the CRLB for the bistatic geometry of each TX-RX pair. The best pair is defined as that exhibiting the lowest bistatic CRLB for the target velocity or range. These results can be used for the dynamical selection of the TX-RX signals for the tracking of a radar target moving along a trajectory in a multistatic scenario.

In our scenario we considered a map of dimension $L_x = 20km$ and $L_y = 20km$ and we placed five transmitters and four receiver in this area. In particular, we placed the transmitters at coordinates:

$$
\begin{aligned}
T^{(1)} &= \left(x_T^{(1)}, y_T^{(1)}\right) = \left(5km, 15km\right) \\
T^{(2)} &= \left(x_T^{(2)}, y_T^{(2)}\right) = \left(15km, 15km\right) \\
T^{(3)} &= \left(x_T^{(3)}, y_T^{(3)}\right) = \left(10km, 10km\right) \\
T^{(4)} &= \left(x_T^{(4)}, y_T^{(4)}\right) = \left(5km, 5km\right) \\
T^{(5)} &= \left(x_T^{(5)}, y_T^{(5)}\right) = \left(15km, 5km\right)
\end{aligned}
\tag{23}
$$

and the receivers at coordinates:

$$
\begin{aligned}
R^{(1)} &= \left(x_R^{(1)}, y_R^{(1)}\right) = \left(5km, 10km\right) \\
R^{(2)} &= \left(x_R^{(2)}, y_R^{(2)}\right) = \left(10km, 15km\right) \\
R^{(3)} &= \left(x_R^{(3)}, y_R^{(3)}\right) = \left(10km, 5km\right) \\
R^{(4)} &= \left(x_R^{(4)}, y_R^{(4)}\right) = \left(15km, 10km\right)
\end{aligned}
\tag{24}
$$

Therefore, there are $N_T \times N_R = 5 \times 4 = 20$ pairs of transmitter–receiver that we considered as independent bistatic systems. The 20 resulting pairs of Tx-Rx are listed in Table 1.

We assume that each transmitter sends a burst of $N = 8$ chirp pulses with a compression ratio $BT = 2500$ and a pulse repetition interval $PRI = 10^{-3}\sec$. The carrier frequency of the system is $f_C = 3 \cdot 10^8 / 2\pi \ Hz$.

For each point of the analyzed area and for each of the 20 bistatic systems we calculated the root Cramér-Rao lower bound (RCRLB) of the target range and of the target velocity. In particular, we assumed that, in each point of the analyzed area, the target has a velocity vector aligned to the *x* axis and with intensity of 500 *m*/sec.

As verified**,** the RCRLB of the target range and of the target velocity are a function of the range from receiver to target R_R, the baseline *L*, the look angle of the receiver θ_R, the radial velocity V_a and the signal-to-noise power-ratio (*SNR*). All these parameters depend on the configuration of the bistatic triangle, that is, on the coordinates of the target, the transmitter and the receiver. Bistatic geometry also affects the received echo power, because the path loss factor in this case is $\left(R_T R_R\right)^2$ [Sko01]. In particular the *SNR* can be written as:

$$SNR = \frac{SNR_C \cdot \left(L_x^2 + L_y^2\right)^2}{\left(R_T R_R\right)^2} = \frac{SNR_C \cdot L^2}{\left(R_T R_R\right)^2} \tag{35}$$

where SNR_C is a constant parameter. We assumed that $SNR_C = 10dB$, that is, we assumed that if both the transmitter and the receiver are located in $(0,0)$ and the target is located in $\left(L_x, L_y\right)$ [1], then $SNR = 10dB$.

Figures 23-42 are colour coded maps representing the RCRLB_B of the target range and of the target velocity in each point of the analyzed area. In particular, Figure *i*-(a) represents the RCRLB_B of the target range, measured in $dB(m)$, for the *i*th bistatic system; while Figure *i*-(b) represents the RCRLB_B of the target velocity, in $dB(m/\sec)$, for the *i*th bistatic system.

As apparent from the results, the RCRLB of each bistatic system is strongly related to the bistatic geometry. It is clear that the effects of geometry factors are more prominent as the target approaches the baseline, that is, when $R_R \le L$ and the receiver look angle θ_R

approaches $-\pi/2$. Moreover, when the target is on the baseline, the resulting delay is *L*/*c* and the radial velocity is zero, and therefore resolution is totally lost. However, it is evident that the effects of the bistatic geometry are less noticeable when the distance to the target increases; in this case the bistatic system behaves more and more as a monostatic system Therefore, the performances of each bistatic system are strongly related to the configuration of the bistatic triangle, that is, to the positions of the transmitter, the receiver and the target.

It is clear that using different transmitting and receiving systems, the target can be seen by different bistatic configuration; therefore, knowing the coordinates of each transmitter and each receiver of the whole system, it is possible to calculate, for each point of the analyzed area, which is the transmitter-receiver pair having the best performances, that is the minimum $CRLB_B$.

Figures 43-(b) and 44-(b) show, in a colour coded map, the transmitter-receiver pair which has the minimum $RCRLB_B$ for each point of the analyzed area. The colormap of these figures in divided into 20 colours, each of which is associated with one of the 20 bistatic systems listed in Table 1.

Figures 43-(a) and 44-(a) show the minimum $RCRLB_B$ of the target range and the target velocity, respectively, that is the value of the RCRLB which is provided by the transmitter-receiver pair which has the minimum RCRLB.

Figures 45-66 show same results as in Fig. 23-42 but obtained by choosing different transmitter-receiver configurations. In particular, the positions of the 5 transmitters and the 4 receivers have been randomly chosen inside the analyzed area.

[1] *Lx* and *Ly* are the projections of the baseline *L* on the *x* and *y* axis respectively

Pair 1	$T^{(1)}$-$R^{(1)}$
Pair 2	$T^{(1)}$-$R^{(2)}$
Pair 3	$T^{(1)}$-$R^{(3)}$
Pair 4	$T^{(1)}$-$R^{(4)}$
Pair 5	$T^{(2)}$-$R^{(1)}$
Pair 6	$T^{(2)}$-$R^{(2)}$
Pair 7	$T^{(2)}$-$R^{(3)}$
Pair 8	$T^{(2)}$-$R^{(4)}$
Pair 9	$T^{(3)}$-$R^{(1)}$
Pair 10	$T^{(3)}$-$R^{(2)}$
Pair 11	$T^{(3)}$-$R^{(3)}$
Pair 12	$T^{(3)}$-$R^{(4)}$
Pair 13	$T^{(4)}$-$R^{(1)}$
Pair 14	$T^{(4)}$-$R^{(2)}$
Pair 15	$T^{(4)}$-$R^{(3)}$
Pair 16	$T^{(4)}$-$R^{(4)}$
Pair 17	$T^{(5)}$-$R^{(1)}$
Pair 18	$T^{(5)}$-$R^{(2)}$
Pair 19	$T^{(5)}$-$R^{(3)}$
Pair 20	$T^{(5)}$-$R^{(4)}$

Table 1: Analyzed bistatic systems.

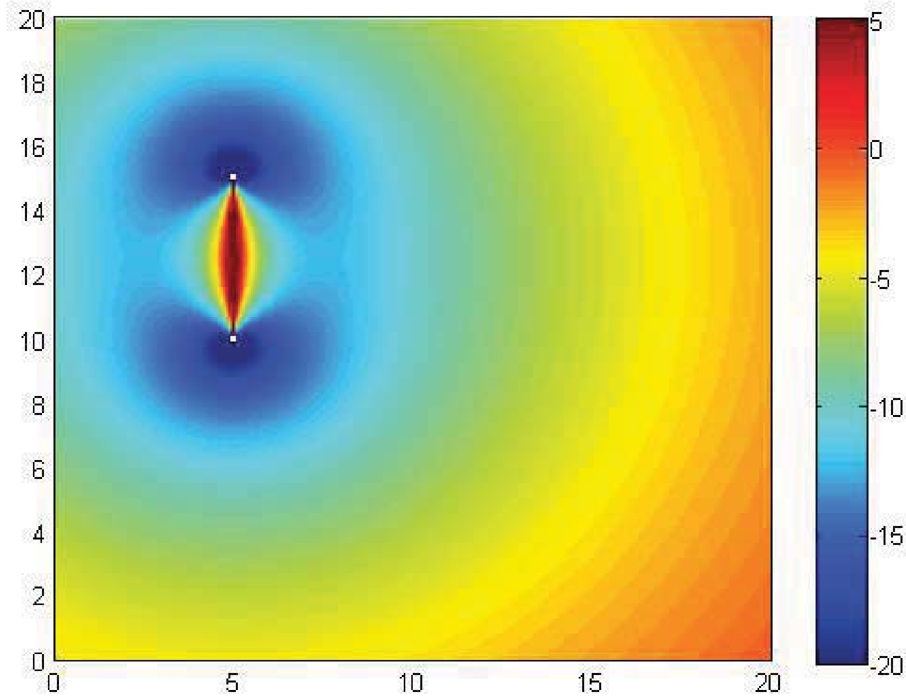

Figure 23-(a) - Bistatic RCRLB of the target range [dB(m)]. *Pair 1.*

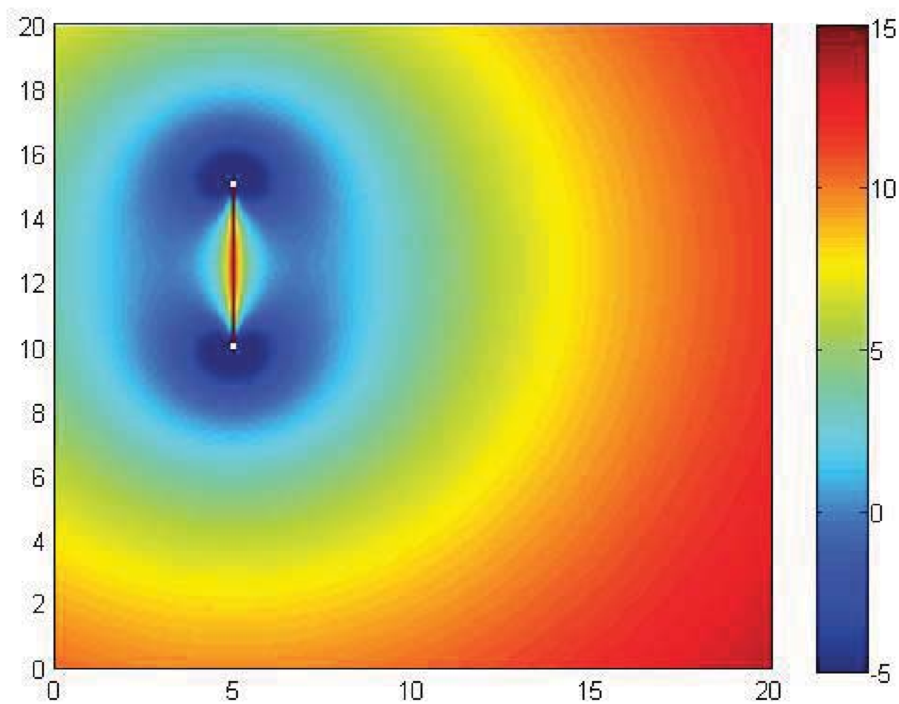

Figure 23-(b): Bistatic RCRLB of the target velocity [dB(m/sec)]. *Pair 1.*

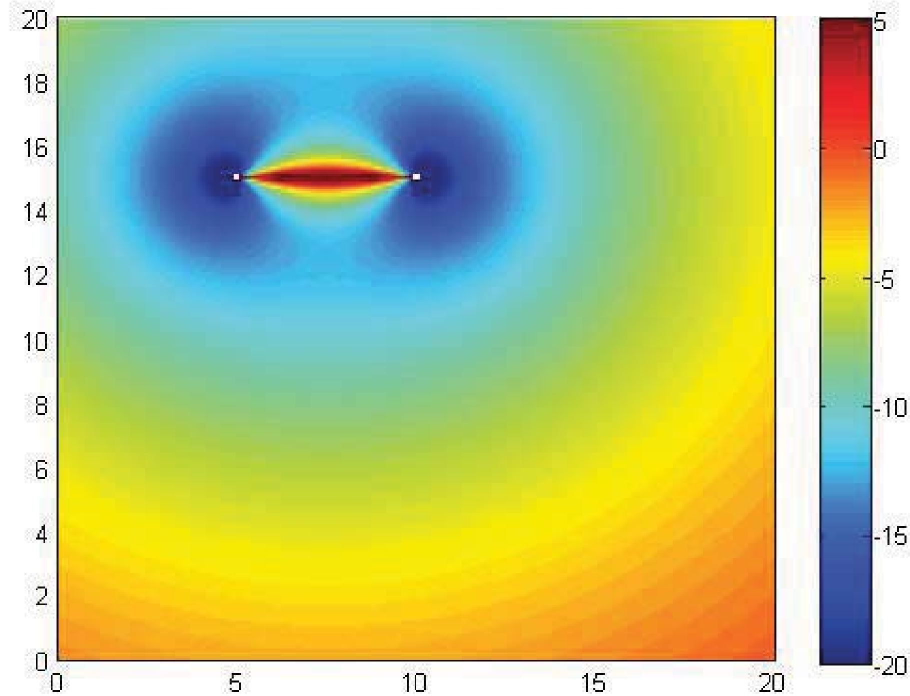

Figure 24-(a): Bistatic RCRLB of the target range [dB(m)]. *Pair 2*.

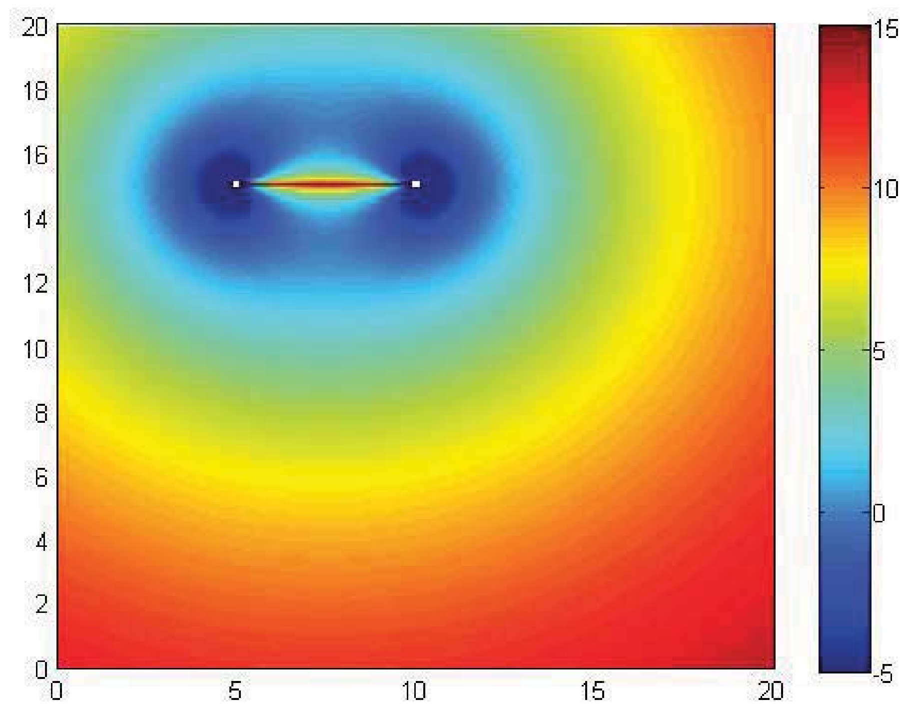

Figure 24-(b): Bistatic RCRLB of the target velocity [dB(m/sec)]. *Pair 2.*

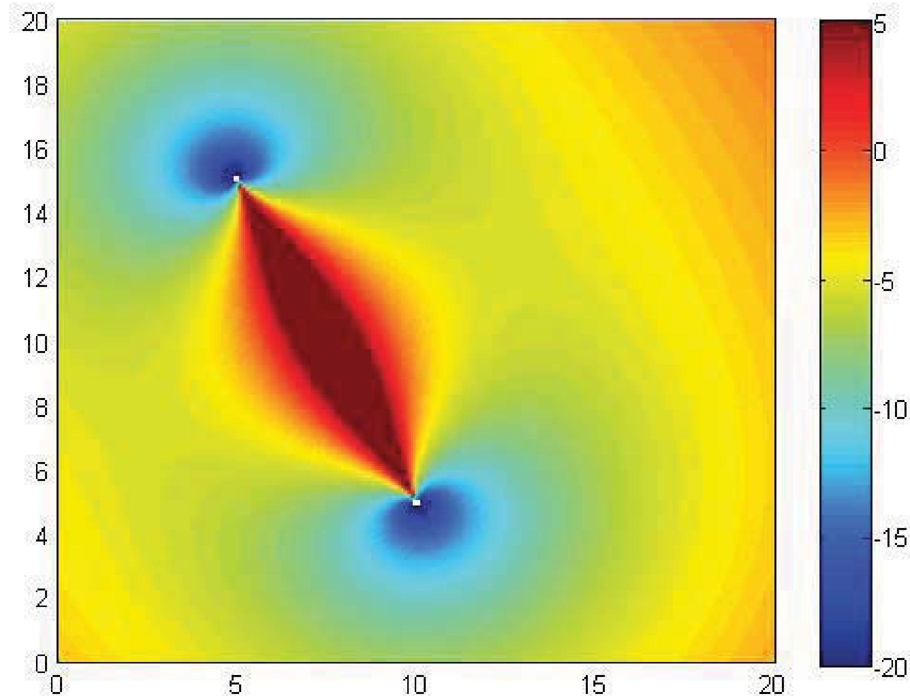

Figure 25-(a): Bistatic RCRLB of the target range [dB(m)]. *Pair 3*.

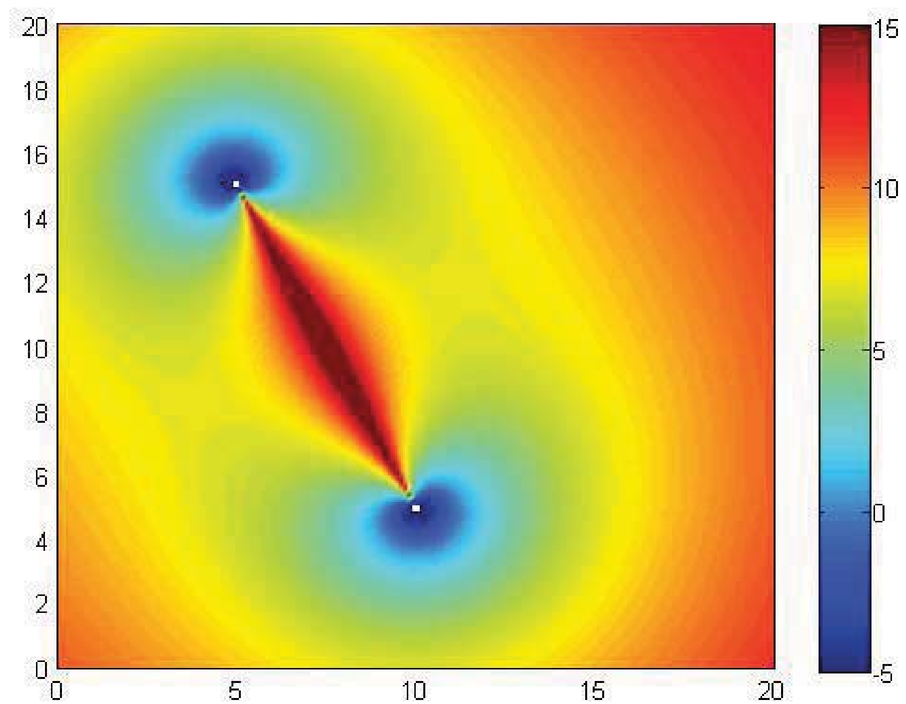

Figure 25-(b): Bistatic RCRLB of the target velocity [dBm/sec]. *Pair 3.*

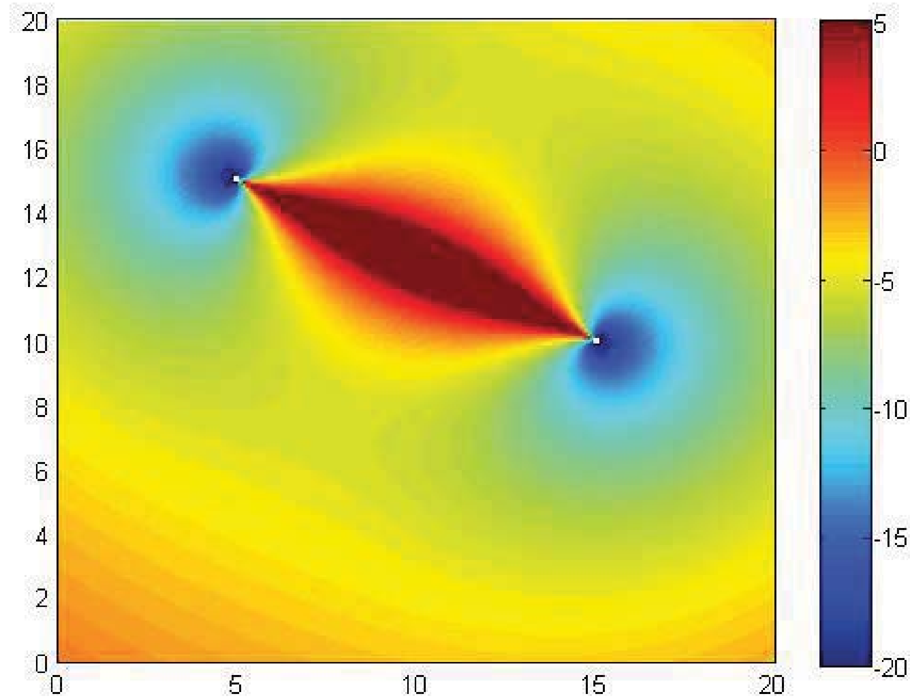

Figure 26-(a): Bistatic RCRLB of the target Range [dBm]. *Pair 4*.

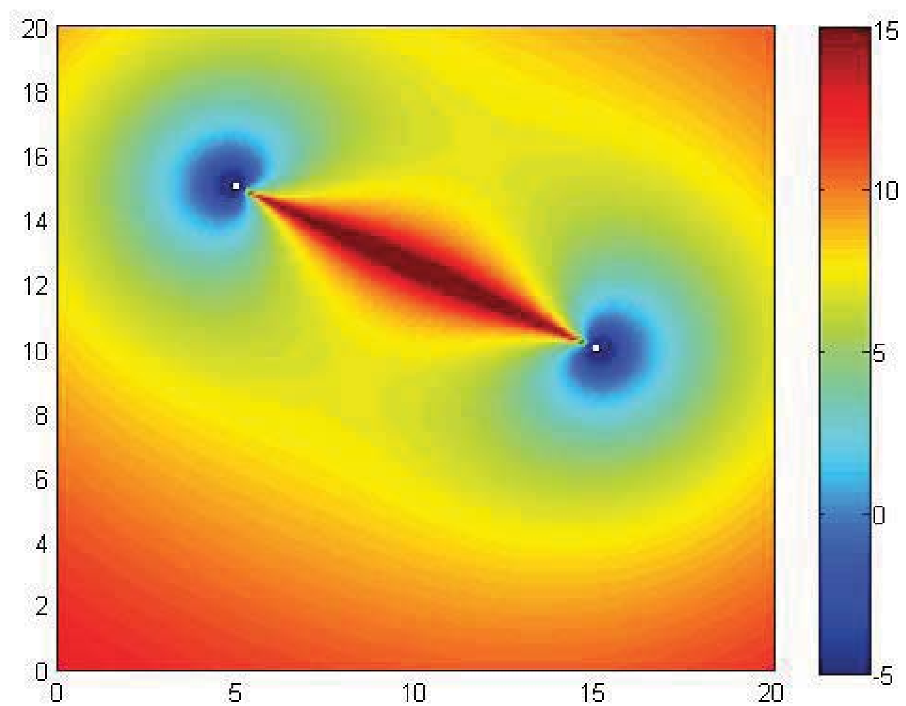

Figure 26-(b): Bistatic RCRLB of the target velocity [dBm/sec]. *Pair 4.*

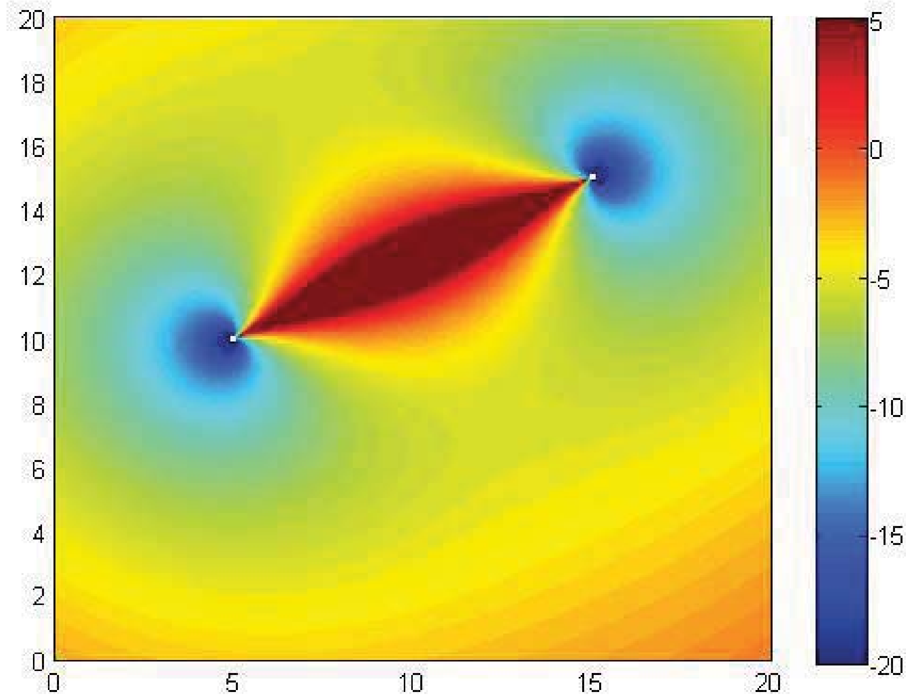

Figure 27-(a): Bistatic RCRLB of the target Range [dBm]. *Pair 5*.

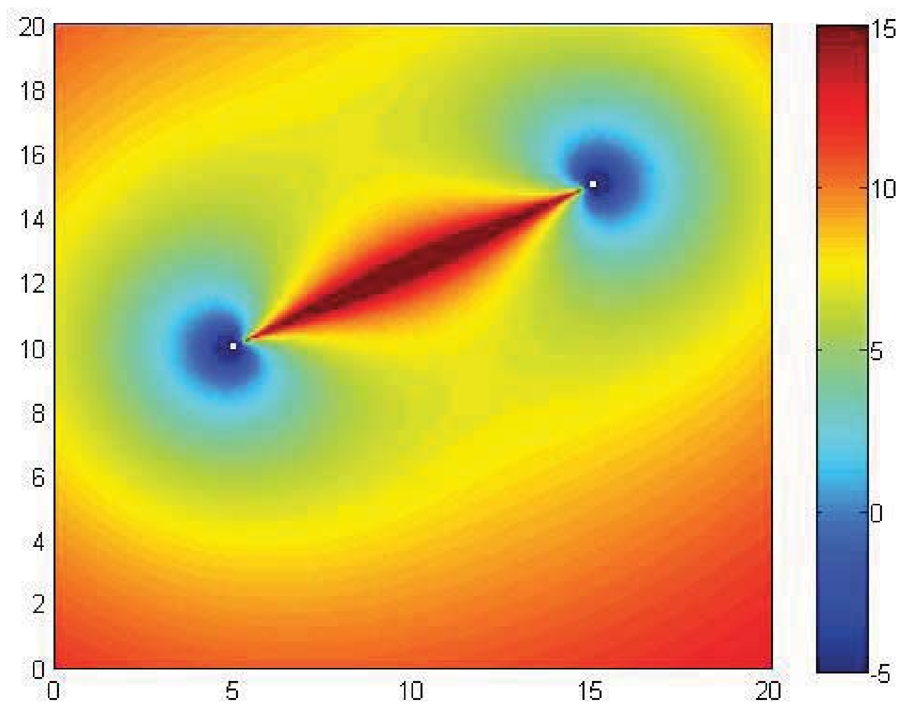

Figure 27-(b): Bistatic RCRLB of the target velocity [dBm/sec]. *Pair 5.*

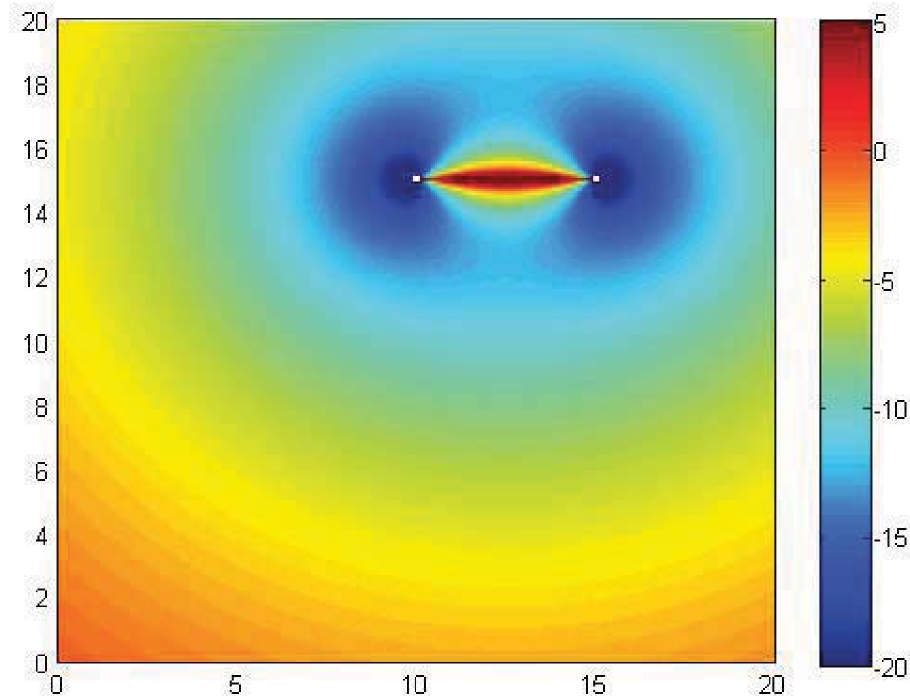

Figure 28-(a): Bistatic RCRLB of the target Range [dBm]. *Pair 6*.

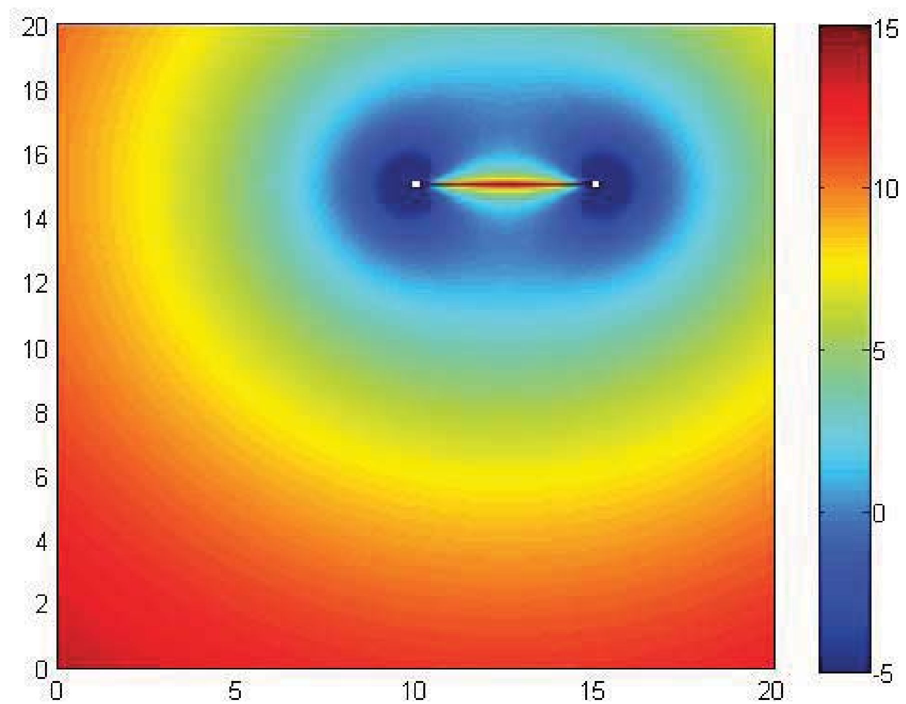

Figure 28-(b): Bistatic RCRLB of the target velocity [dBm/sec]. *Pair 6.*

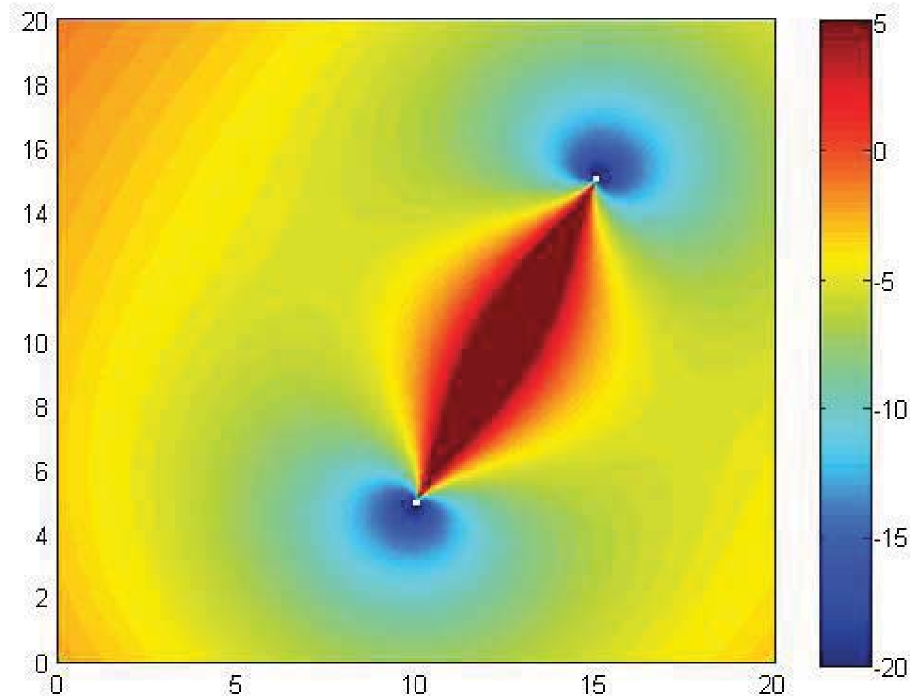

Figure 29-(a): Bistatic RCRLB of the target Range [dBm]. *Pair 7*.

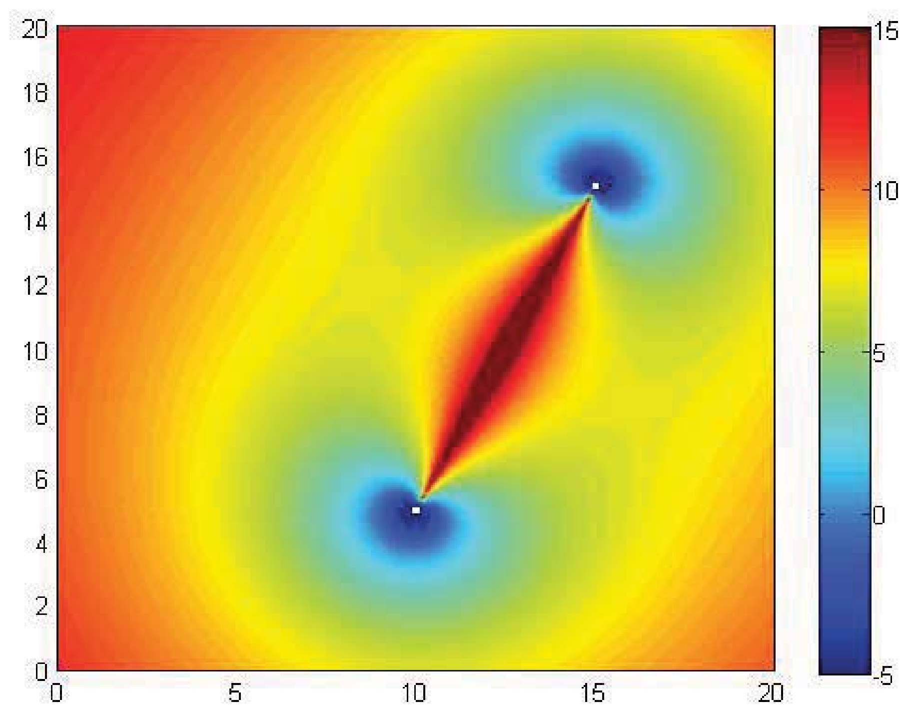

Figure 29-(b): Bistatic RCRLB of the target velocity [dBm/sec]. *Pair 7.*

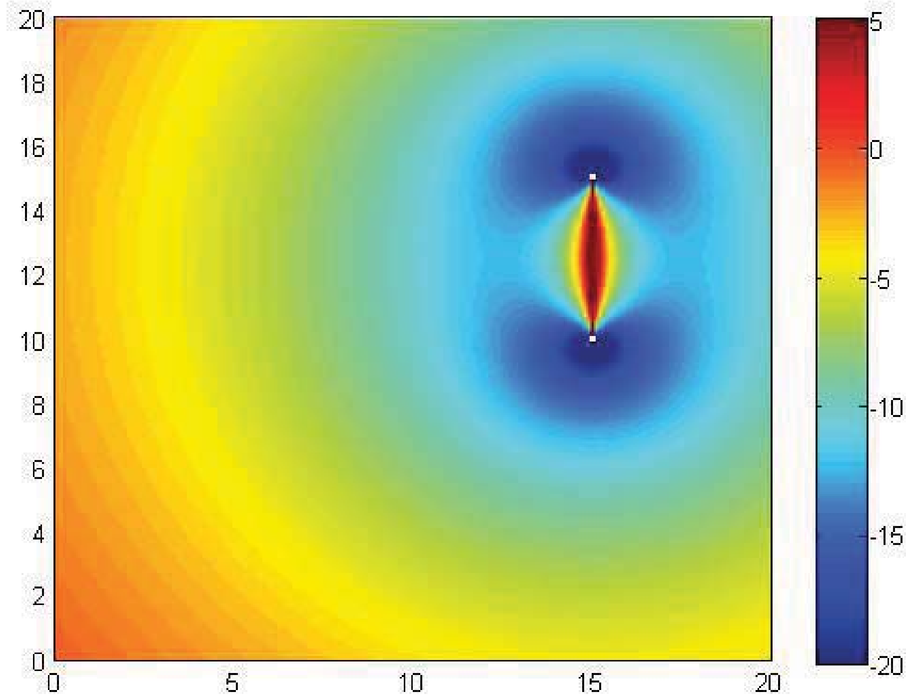

Figure 30-(a): Bistatic RCRLB of the target Range [dBm]. *Pair 8*.

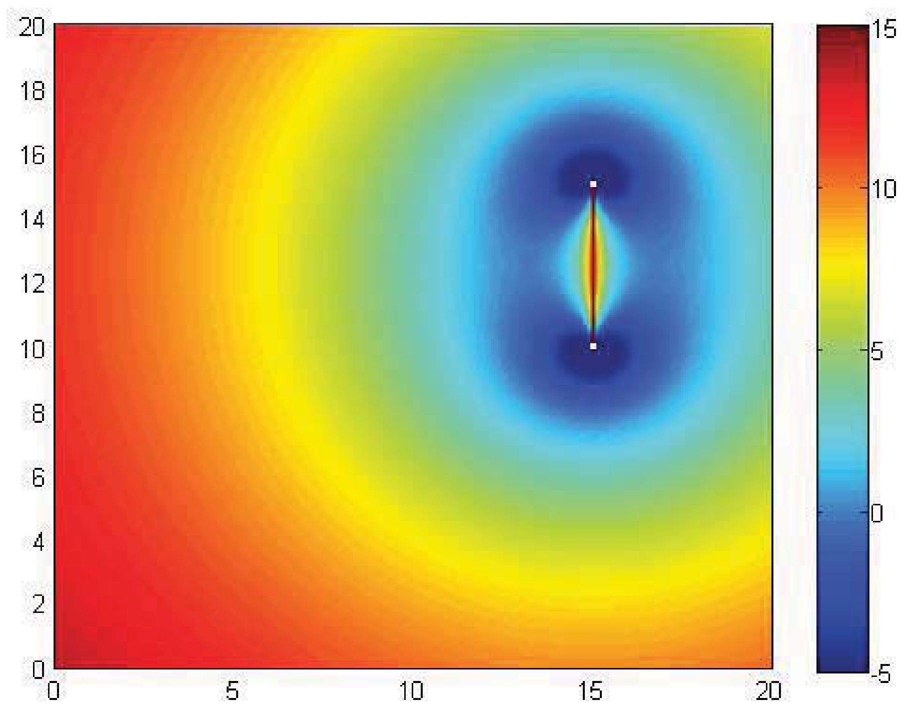

Figure 30-(b): Bistatic RCRLB of the target velocity [dBm/sec]. *Pair 8.*

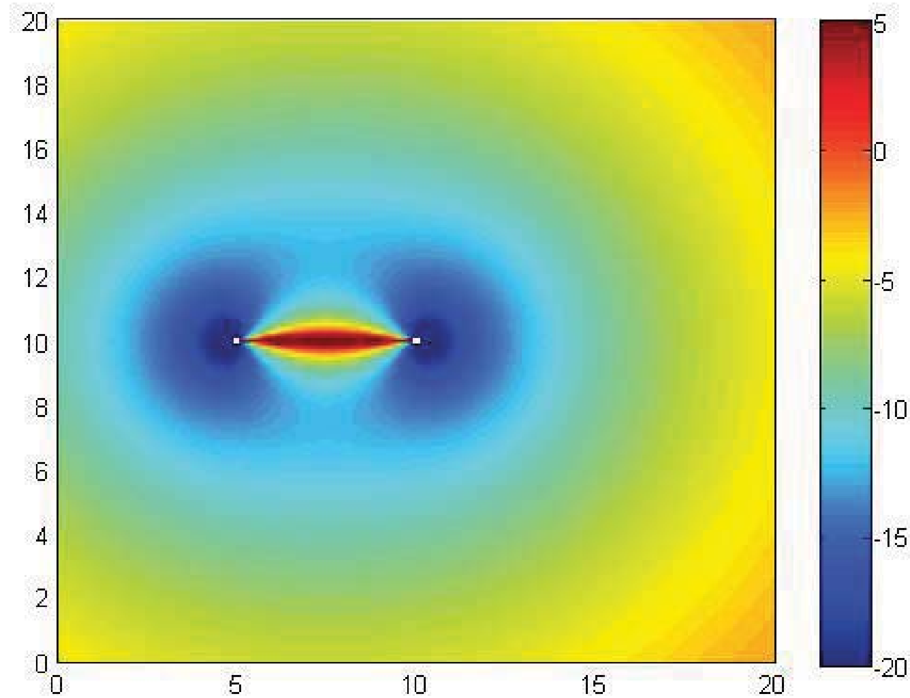

Figure 31-(a): Bistatic RCRLB of the target Range [dBm]. *Pair 9*.

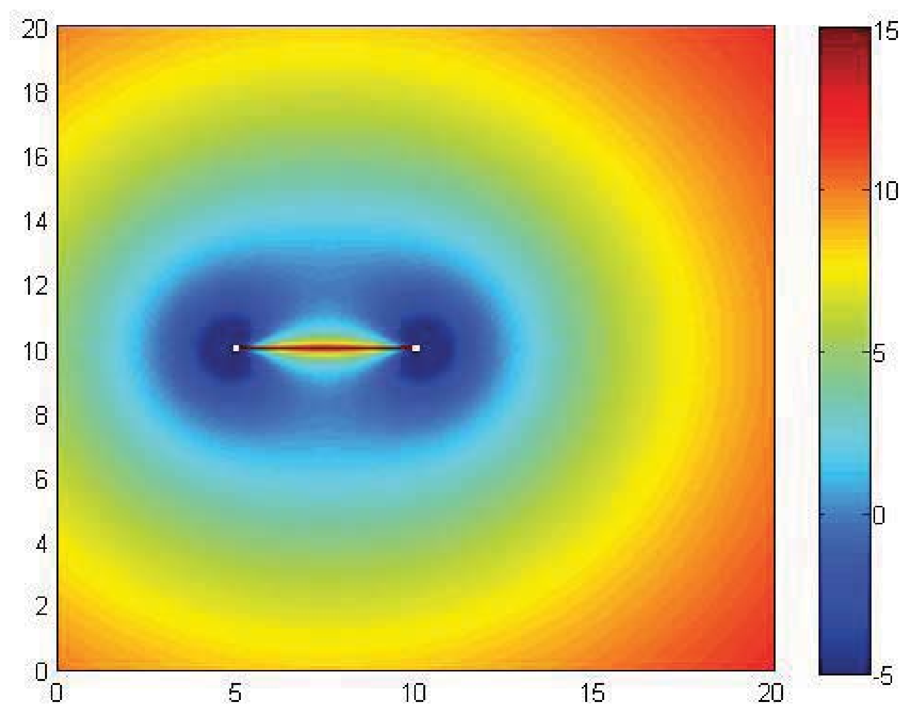

Figure 31-(b): Bistatic RCRLB of the target velocity [dBm/sec]. *Pair 9.*

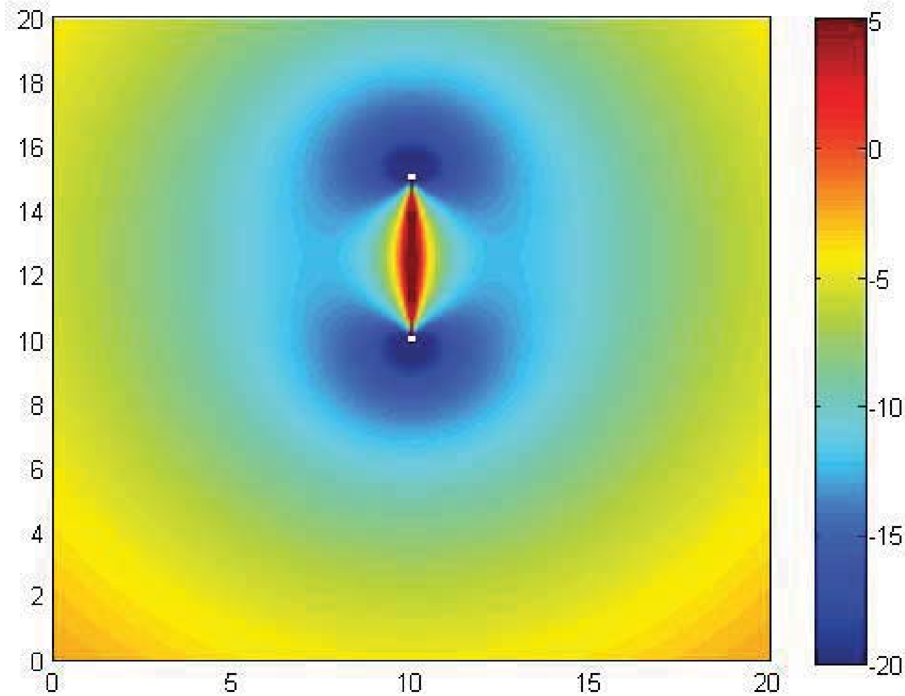

Figure 32-(a): Bistatic RCRLB of the target Range [dBm]. *Pair 10*.

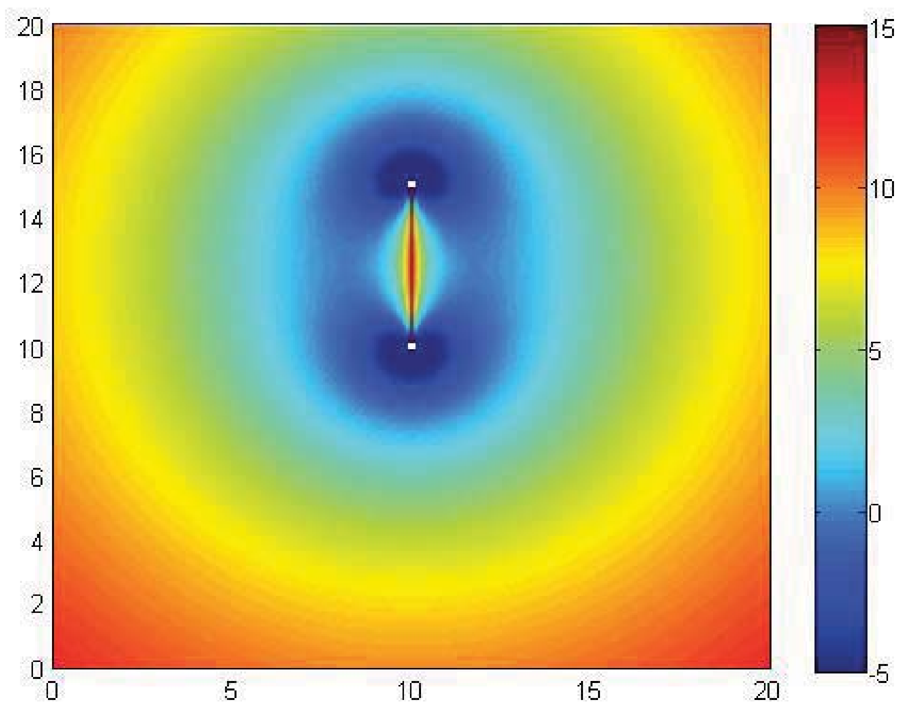

Figure 32-(b): Bistatic RCRLB of the target velocity [dBm/sec]. *Pair 10.*

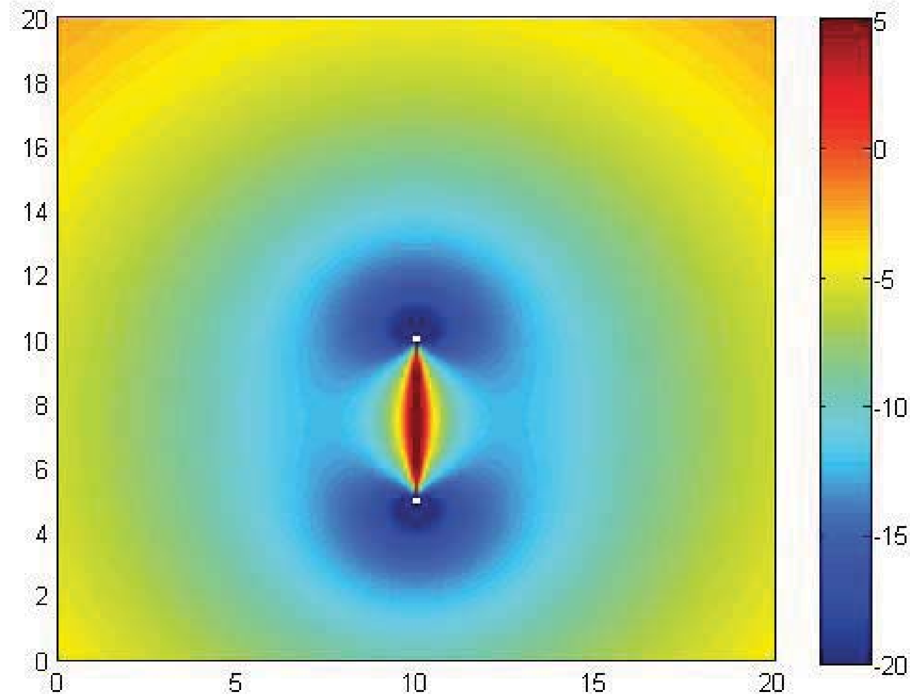

Figure 33-(a): Bistatic RCRLB of the target Range [dBm]. *Pair 11*.

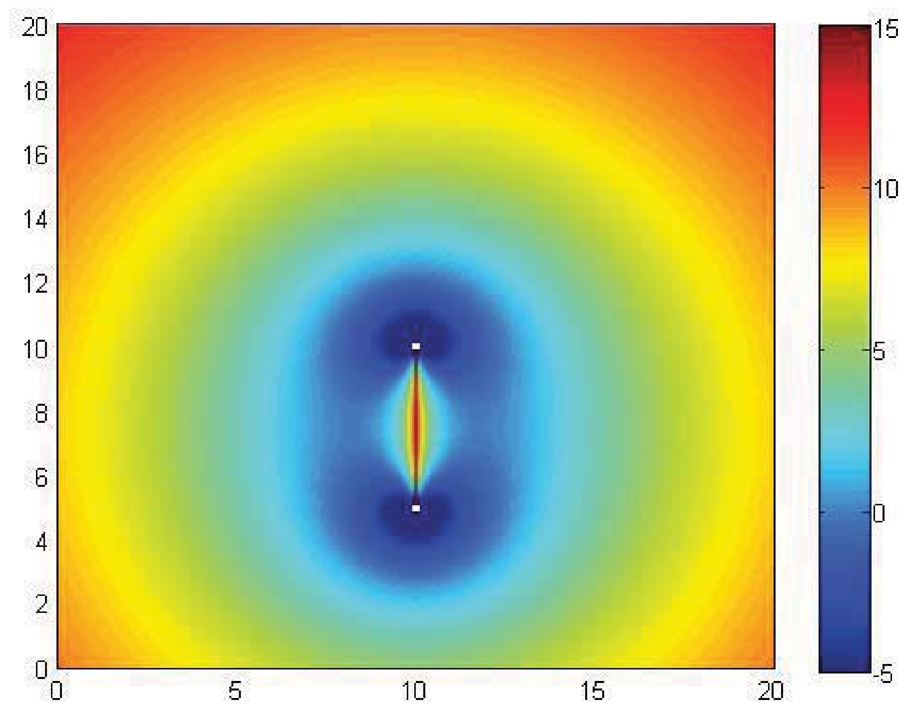

Figure 33-(b): Bistatic RCRLB of the target velocity [dBm/sec]. *Pair 11*.

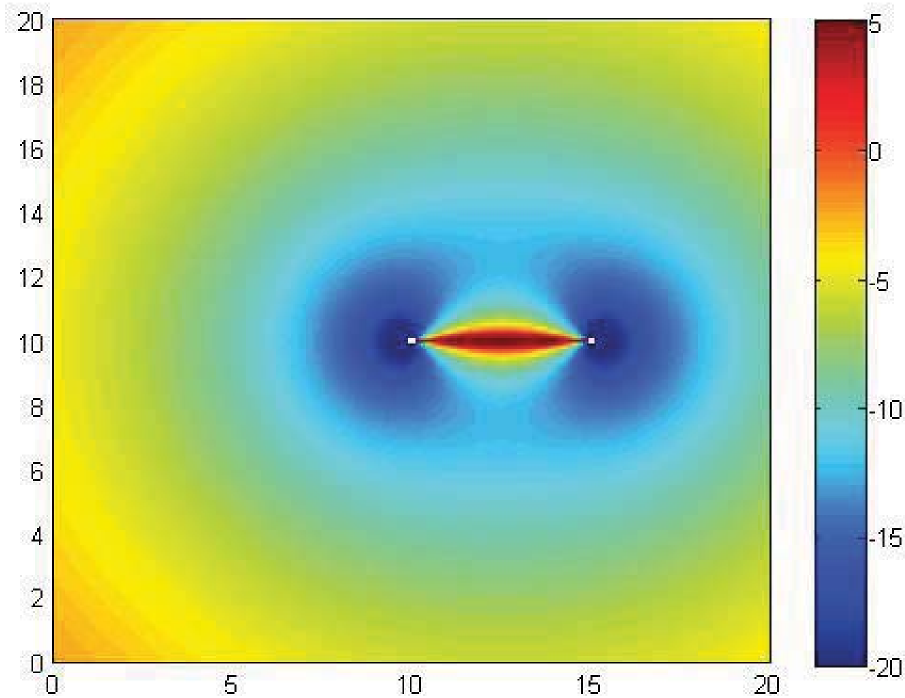

Figure 34-(a): Bistatic RCRLB of the target Range [dBm]. *Pair 12*.

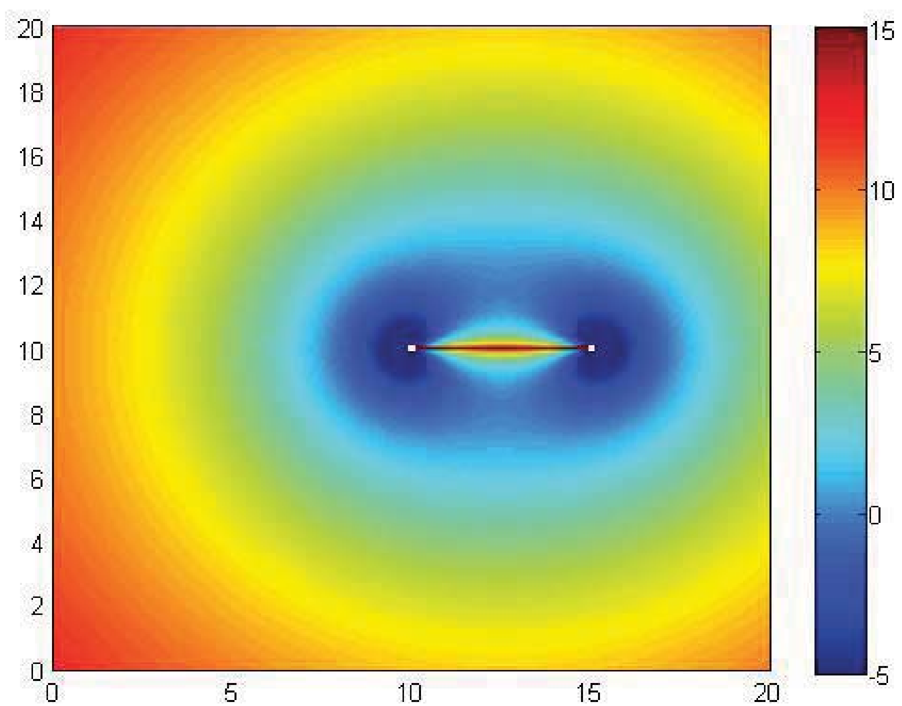

Figure 34-(b): Bistatic RCRLB of the target velocity [dBm/sec]. *Pair 12*.

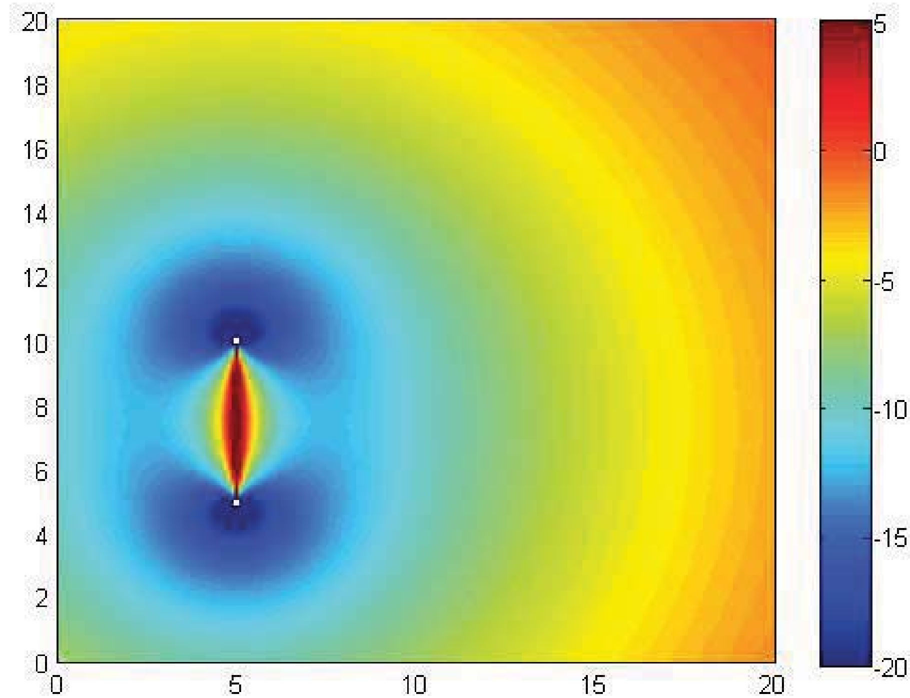

Figure 35-(a): Bistatic RCRLB of the target Range [dBm]. *Pair 13*.

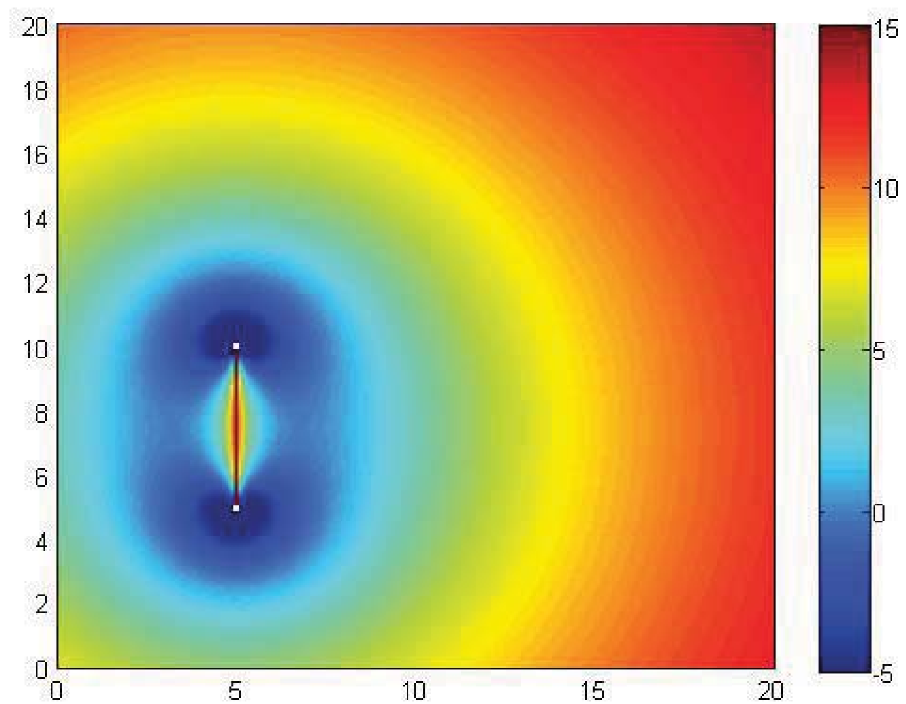

Figure 35-(b): Bistatic RCRLB of the target velocity [dBm/sec]. *Pair 13*.

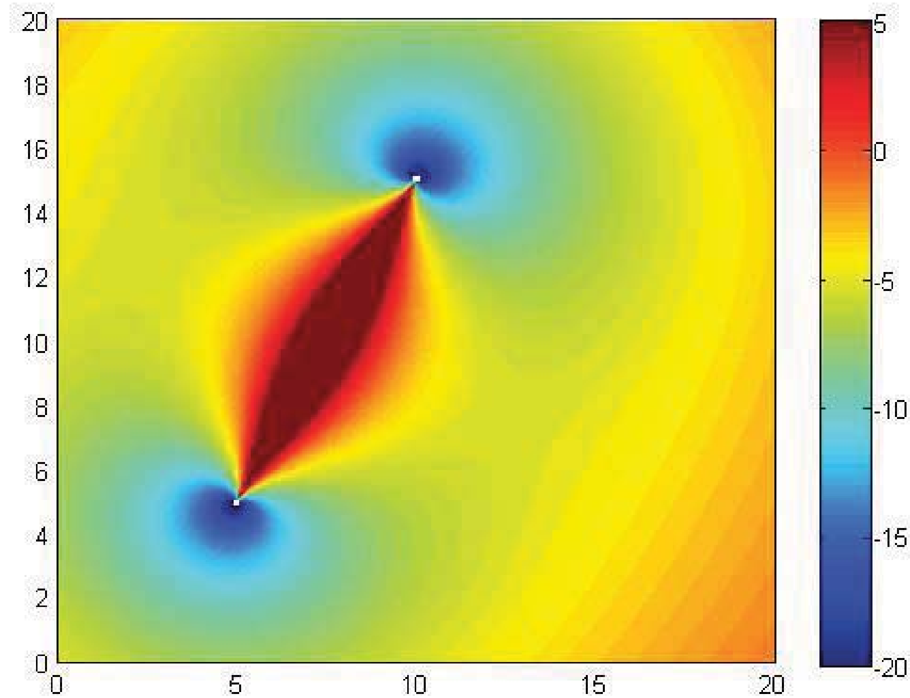

Figure 36-(a): Bistatic RCRLB of the target Range [dBm]. *Pair 14*.

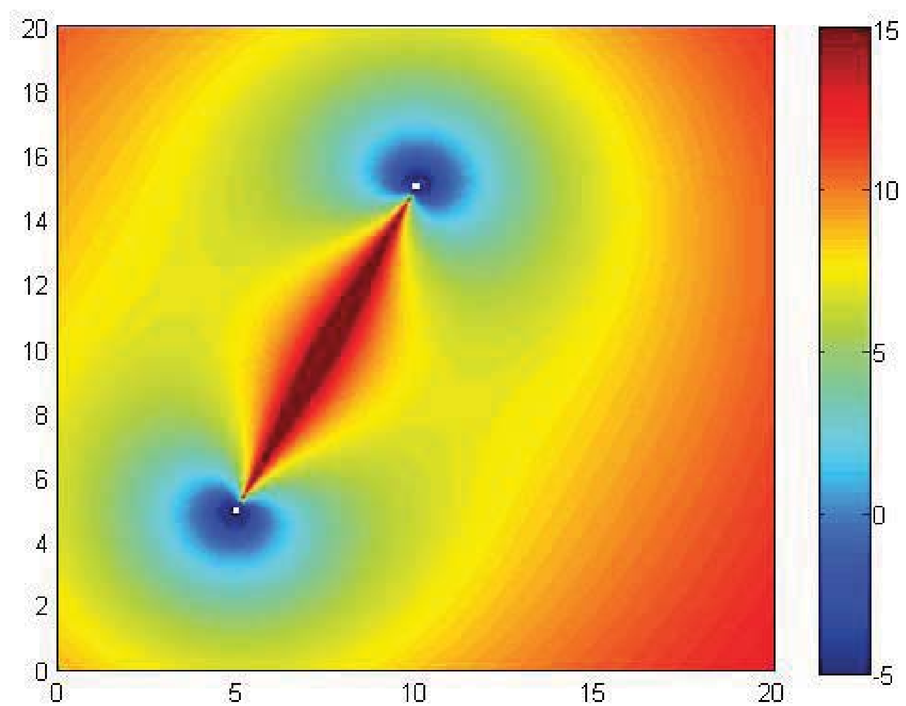

Figure 36-(b): Bistatic RCRLB of the target velocity [dBm/sec]. *Pair 14.*

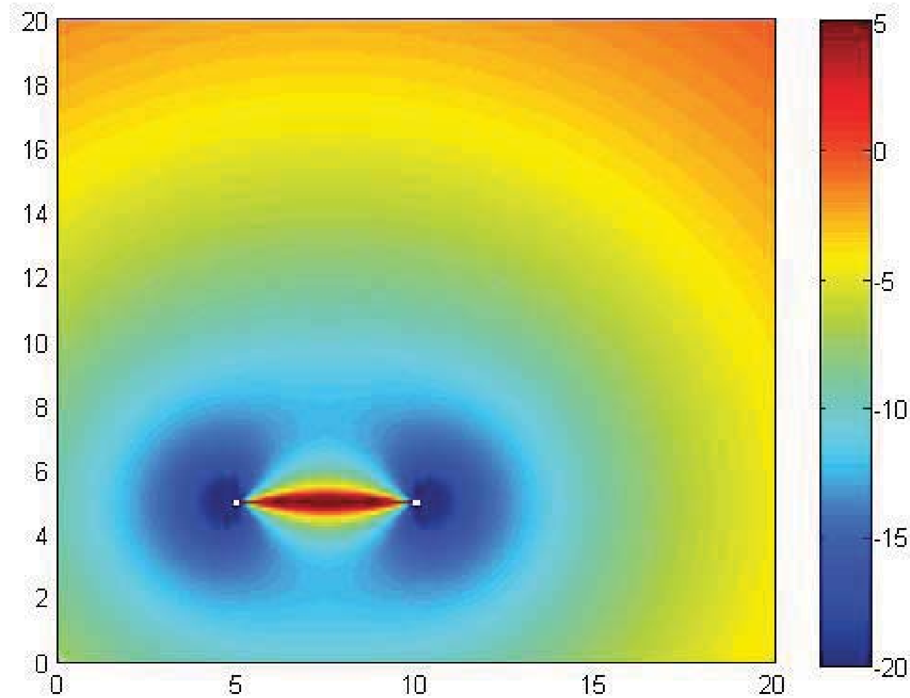

Figure 37-(a): Bistatic RCRLB of the target Range [dBm]. *Pair 15*.

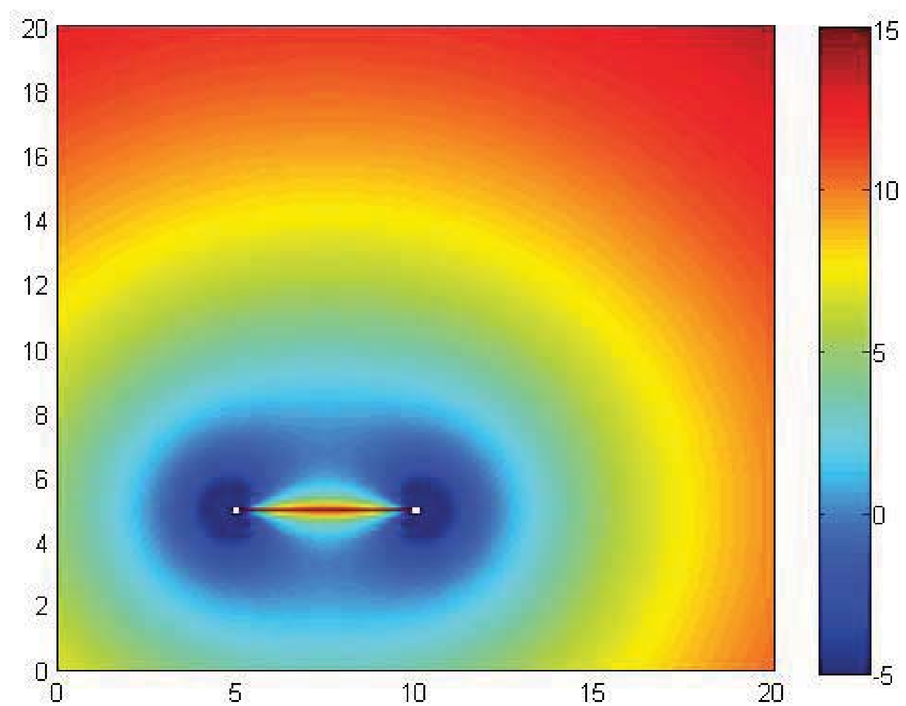

Figure 37-(b): Bistatic RCRLB of the target velocity [dBm/sec]. *Pair 15*.

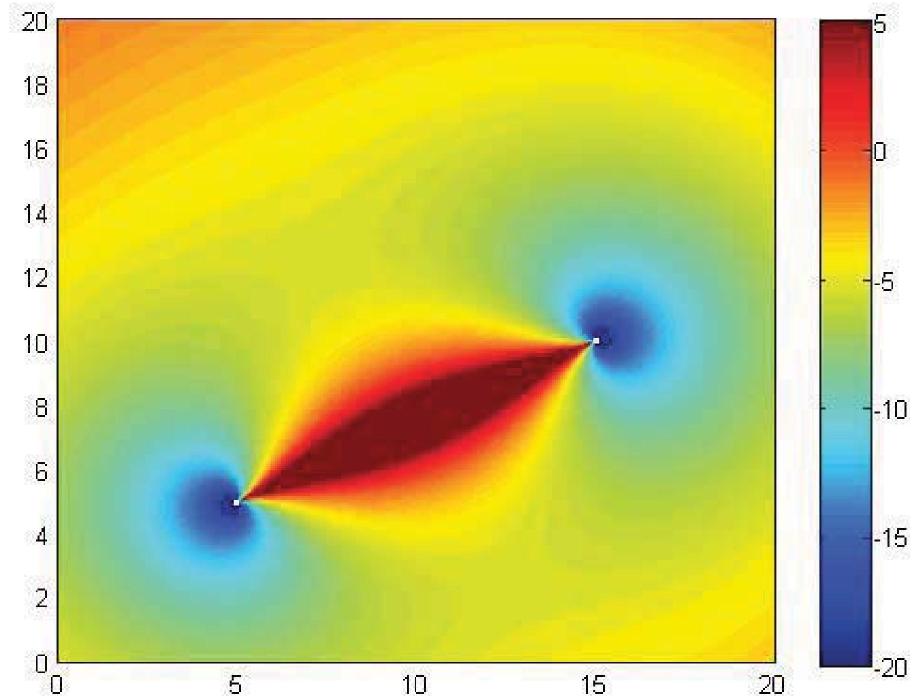

Figure 38-(a): Bistatic RCRLB of the target Range [dBm]. *Pair 16*.

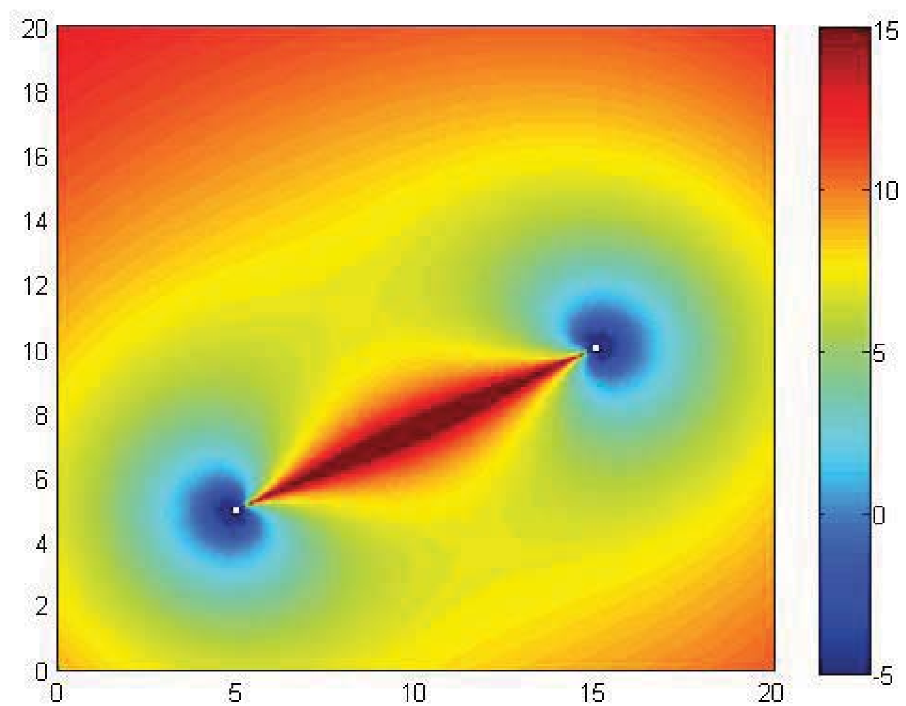

Figure 38-(b): Bistatic RCRLB of the target velocity [dBm/sec]. *Pair 16.*

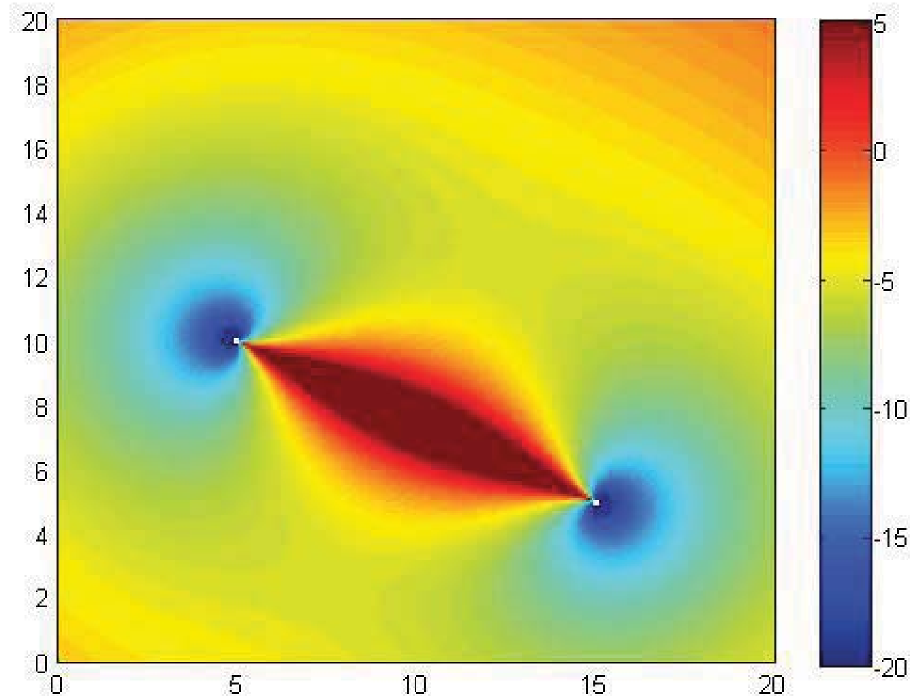

Figure 39-(a): Bistatic RCRLB of the target Range [dBm].   *Pair 17*.

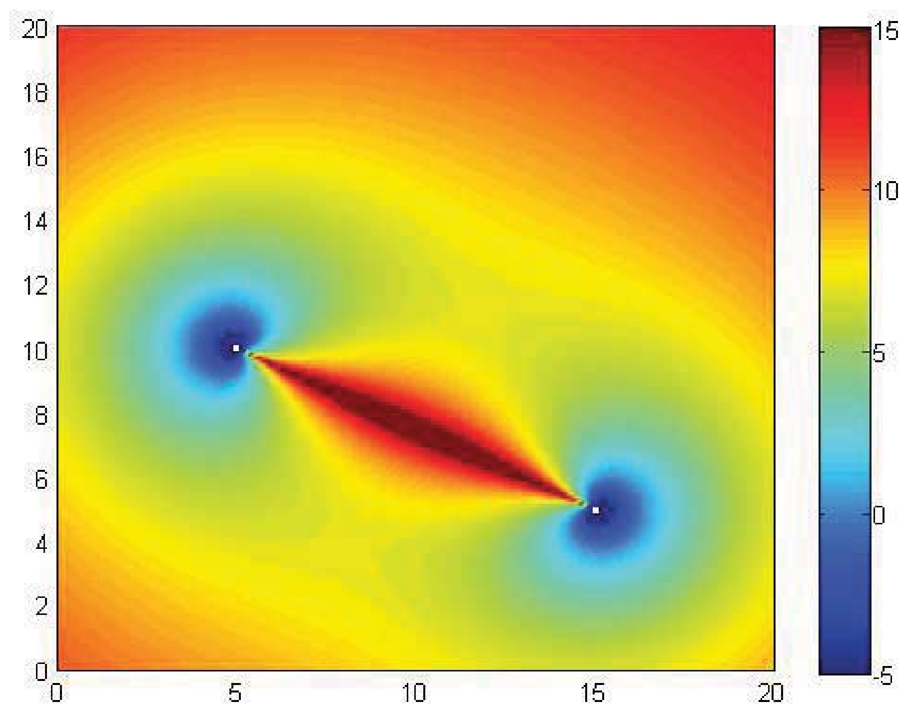

Figure 39-(b): Bistatic RCRLB of the target velocity [dBm/sec].   *Pair 17*.

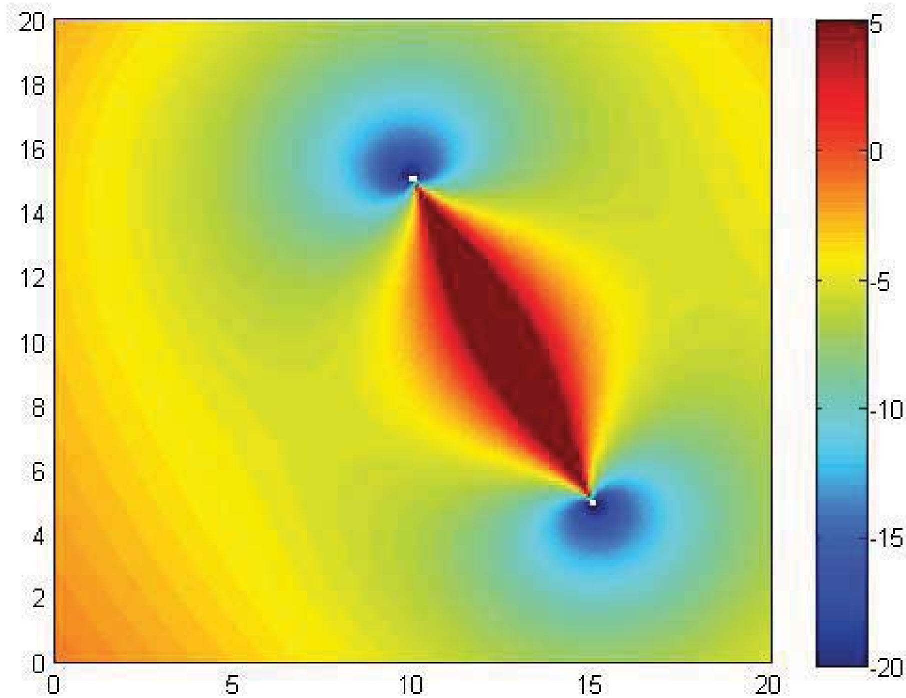

Figure 40-(a): Bistatic RCRLB of the target Range [dBm]. *Pair 18*.

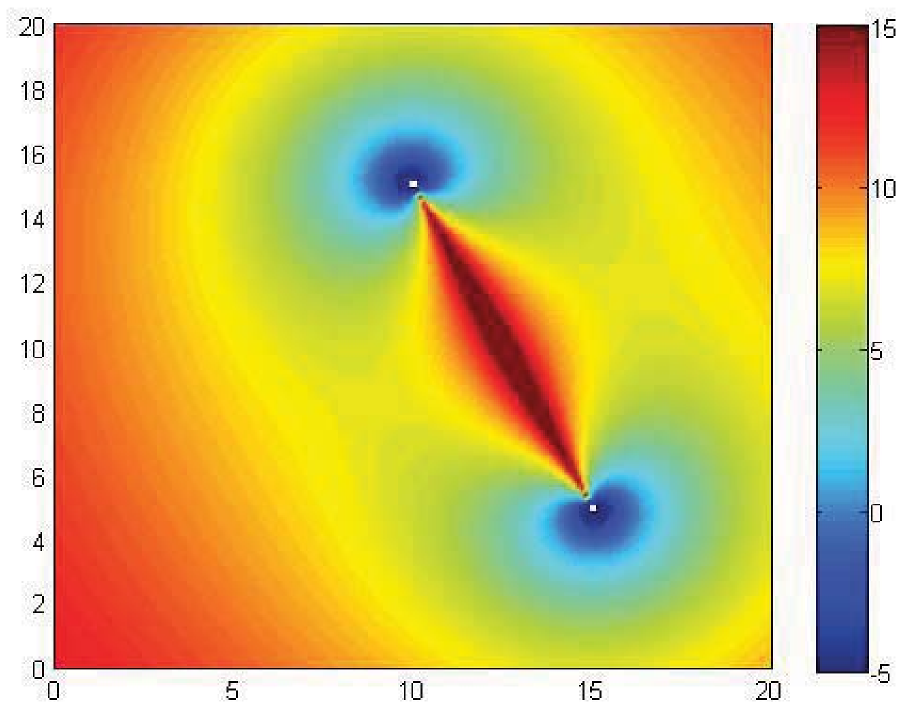

Figure 40-(b): Bistatic RCRLB of the target velocity [dBm/sec]. *Pair 18.*

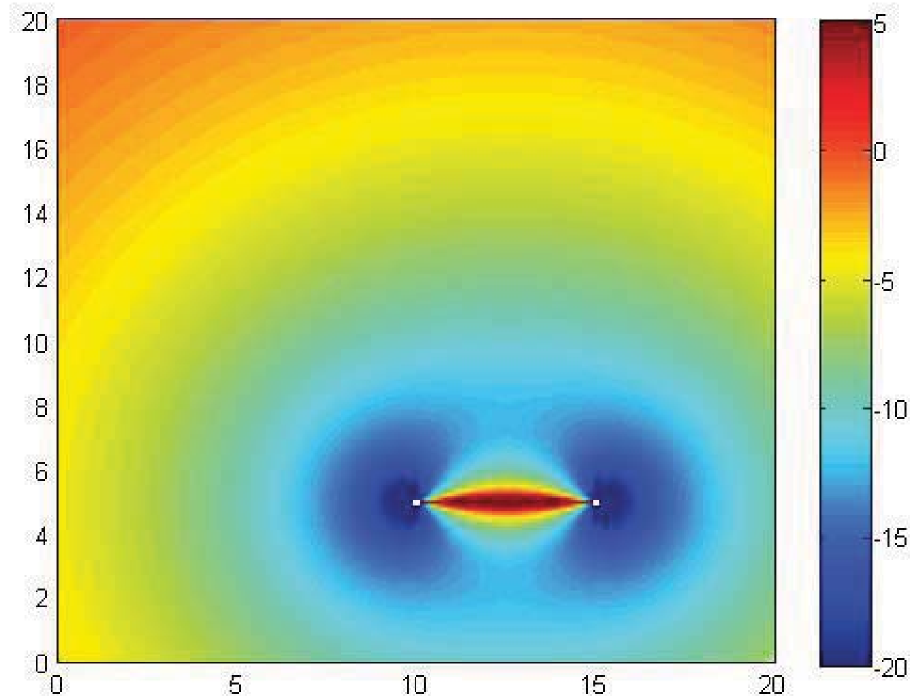

Figure 41-(a): Bistatic RCRLB of the target Range [dBm]. *Pair 19*.

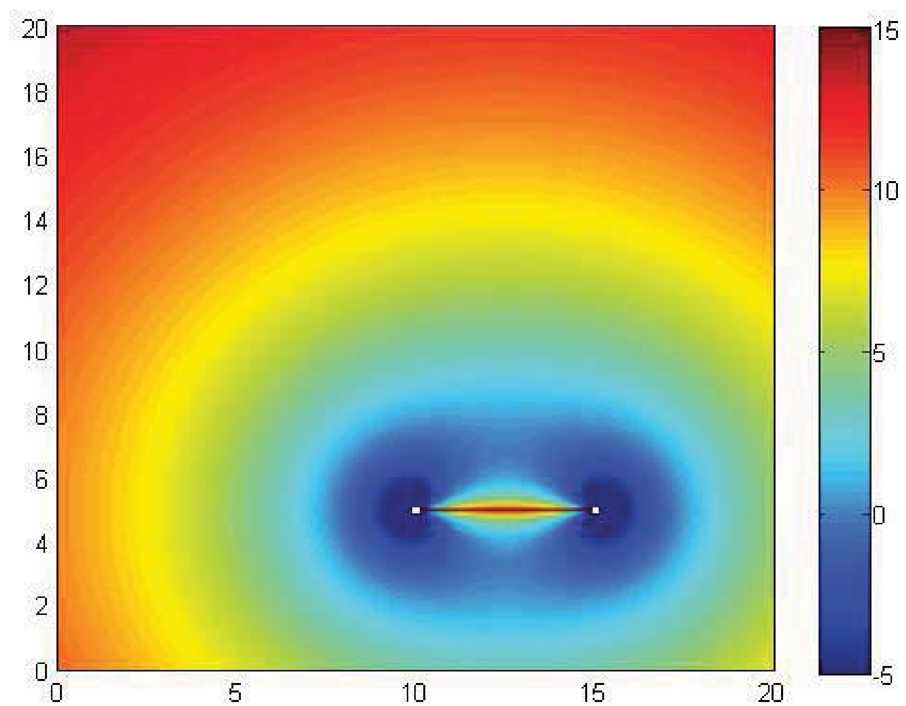

Figure 41-(b): Bistatic RCRLB of the target velocity [dBm/sec]. *Pair 19.*

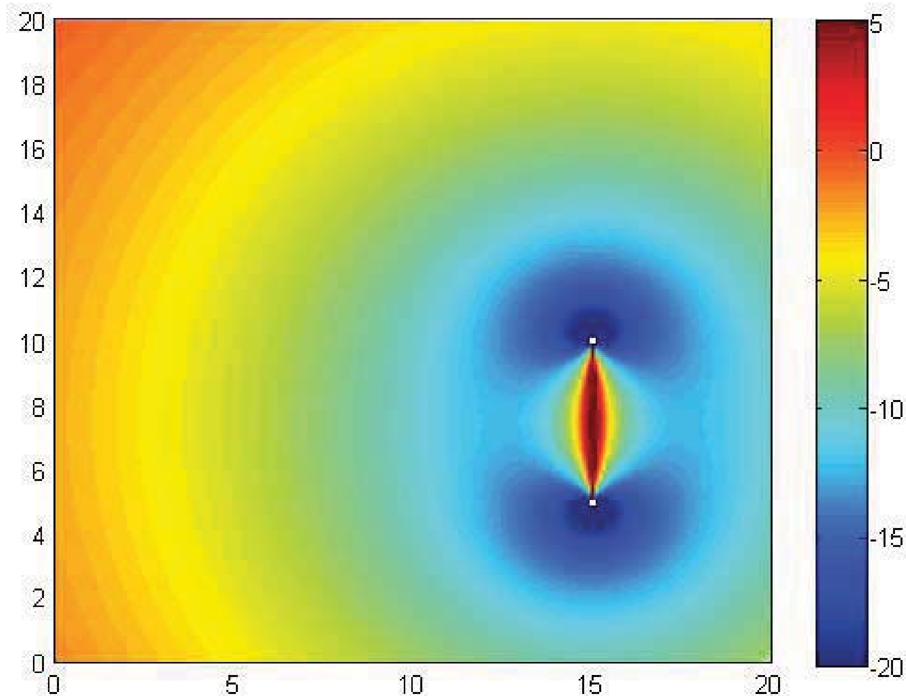

Figure 42-(a): Bistatic RCRLB of the target Range [dBm]. *Pair 20*.

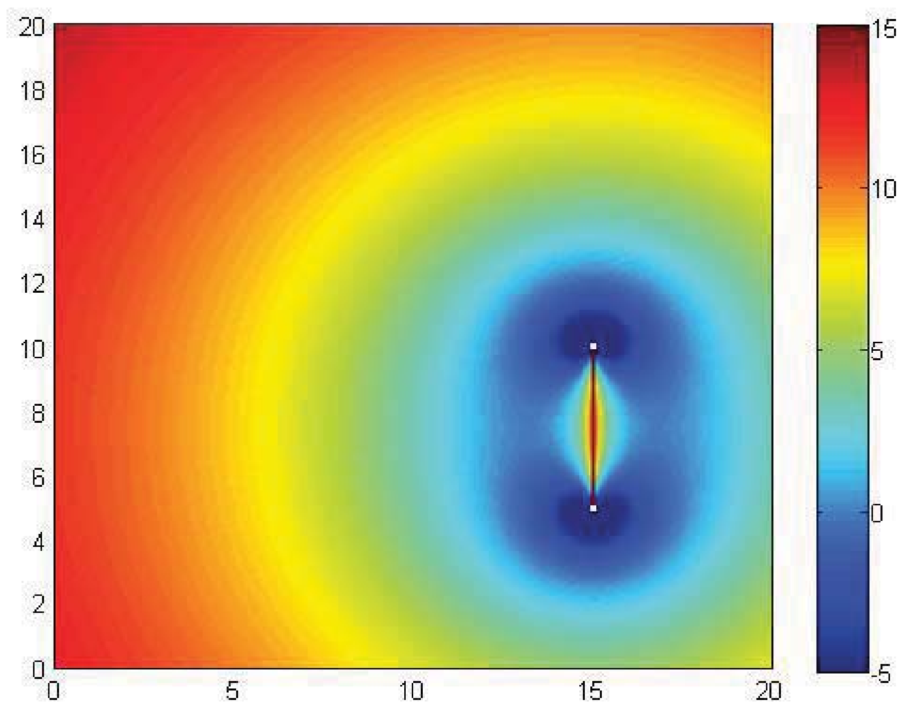

Figure 42-(b): Bistatic RCRLB of the target velocity [dBm/sec]. *Pair 20*.

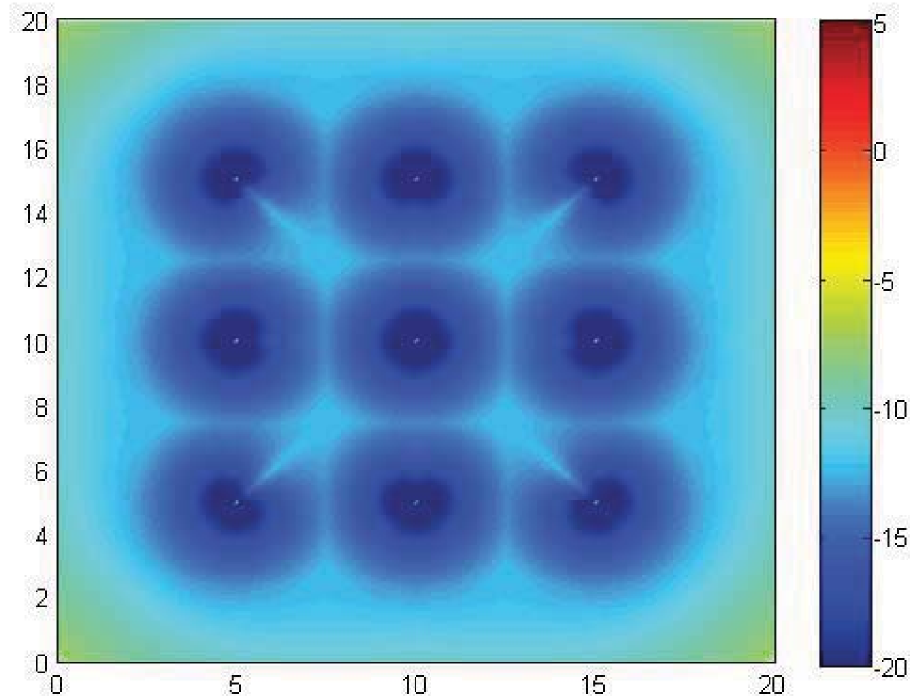

Figure 43-(a): Minimum RCRLB of the target range [dBm].

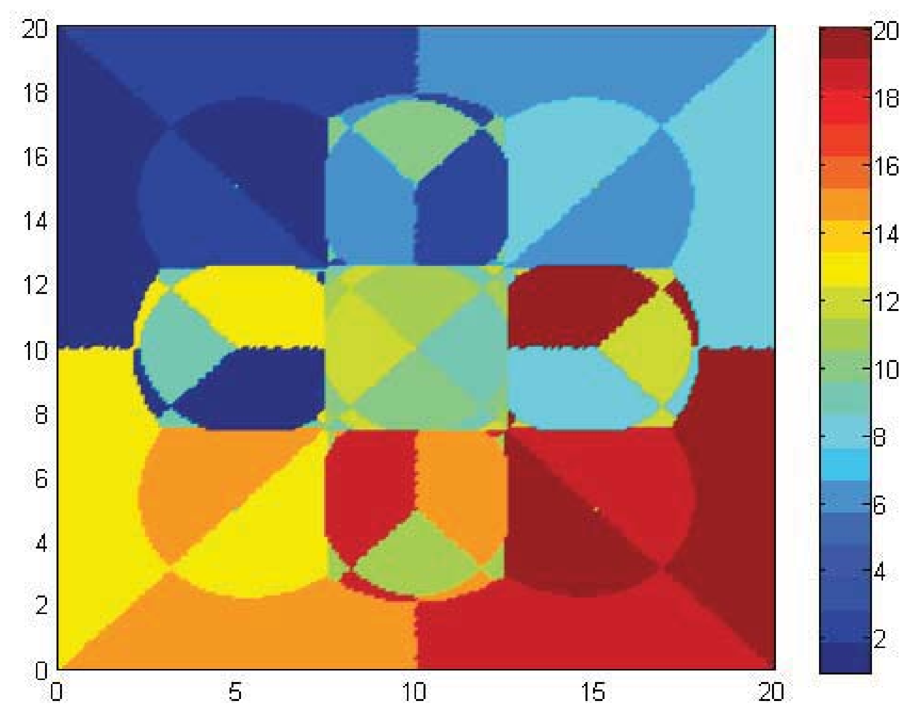

Figure 43-(b): Optimum pair map for target range estimation.

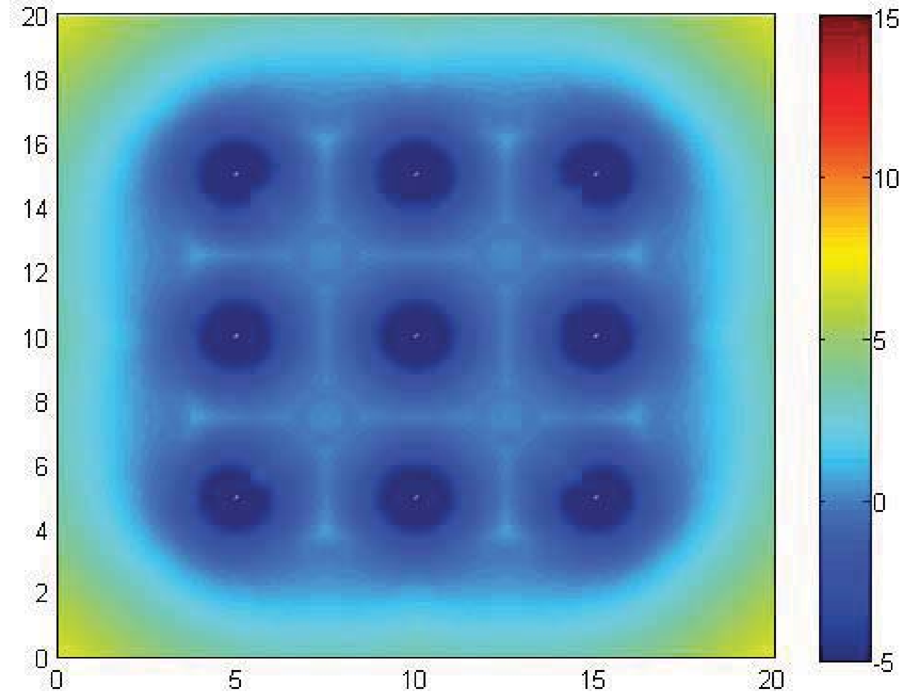

Figure 44-(a): Minimum RCRLB of the target velocity [dBm/sec].

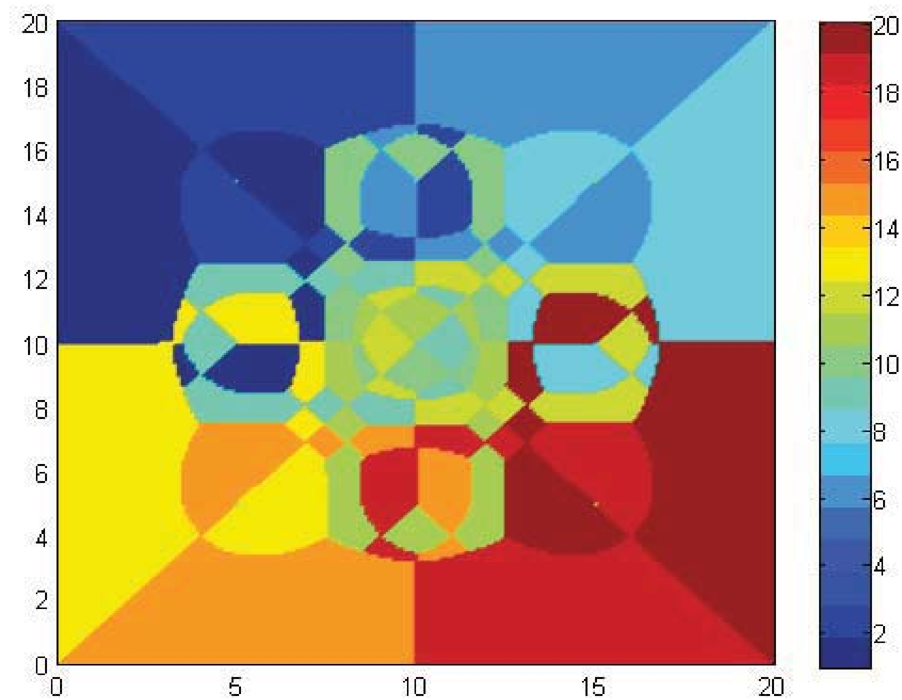

Figure 44-(b): Optimum pair map for target velocity estimation.

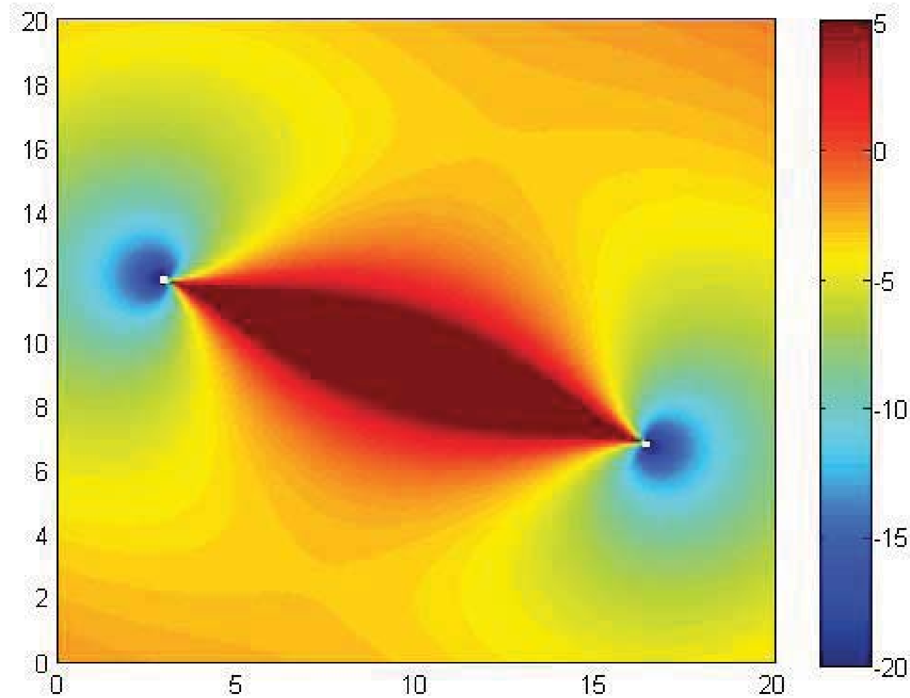

Figure 45-(a): Bistatic RCRLB of the target Range [dBm]. *Pair 1*, 2^{nd} configuration

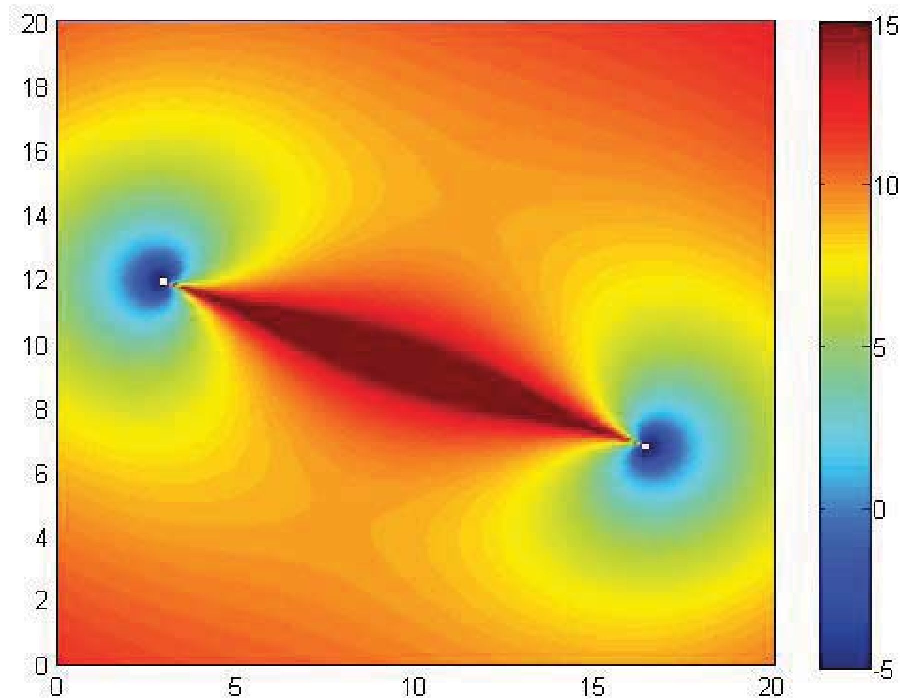

Figure 45-(b): Bistatic RCRLB of the target velocity [dBm/sec]. *Pair 1*, 2^{nd} configuration

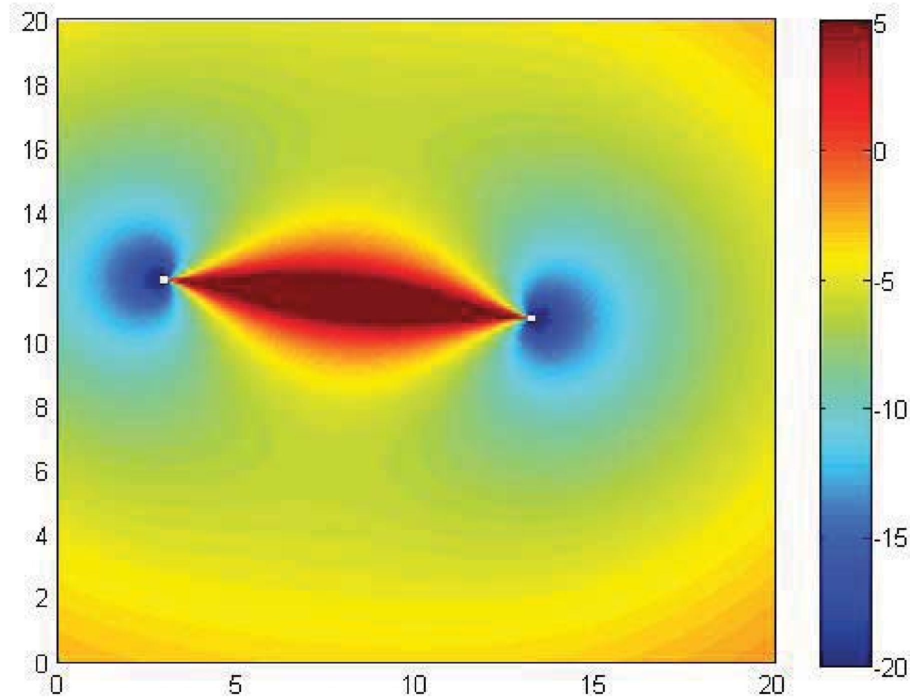

Figure 46-(a): Bistatic RCRLB of the target Range [dBm]. *Pair 2*, 2nd configuration

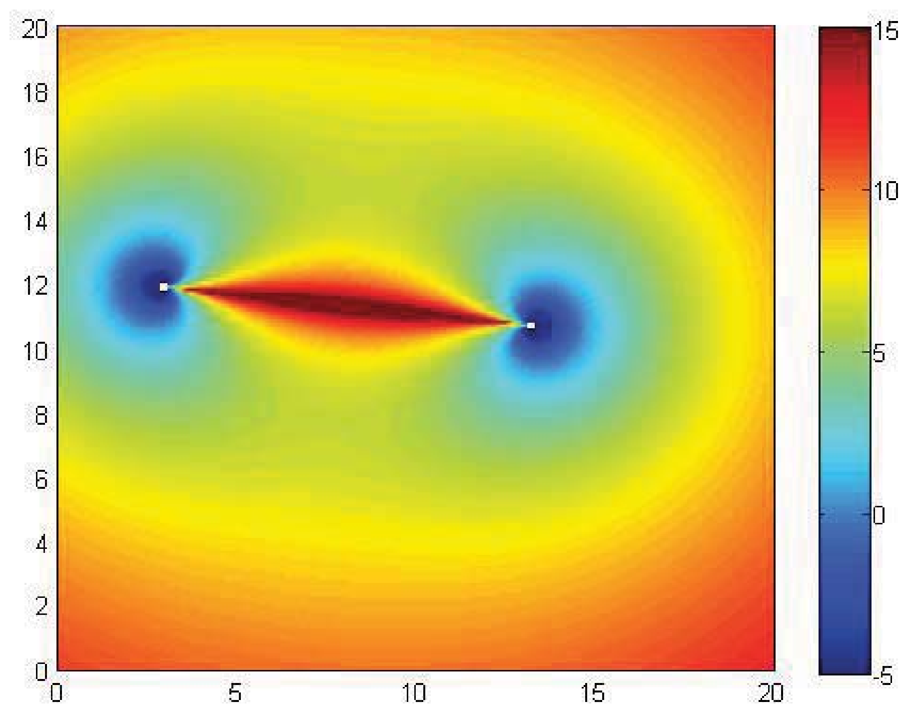

Figure 46-(b): Bistatic RCRLB of the target velocity [dBm/sec]. *Pair 2*, 2nd configuration.

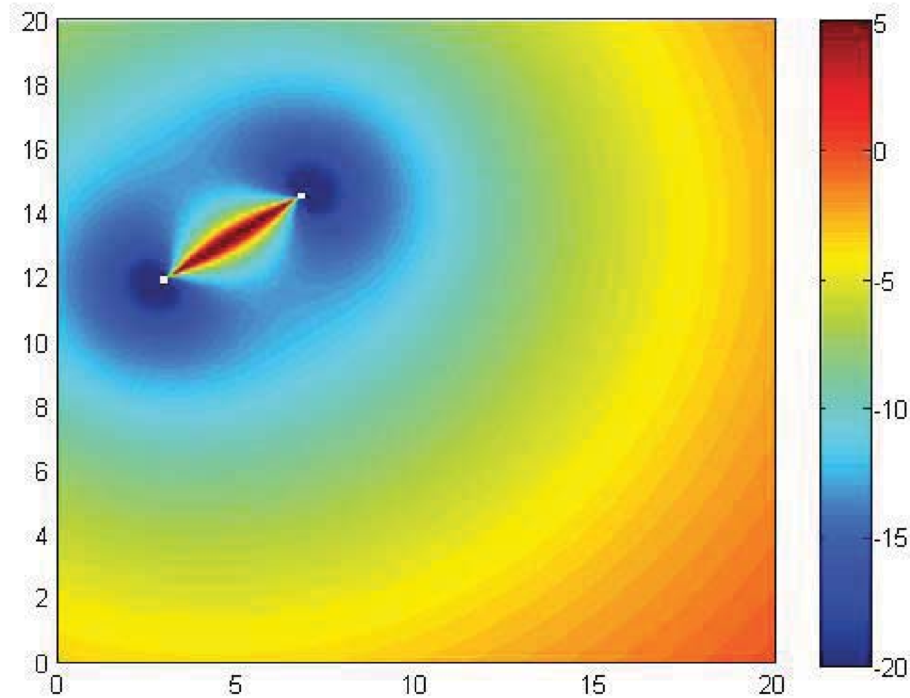

Figure 47-(a): Bistatic RCRLB of the target Range [dBm]. *Pair 3*, 2^{nd} configuration

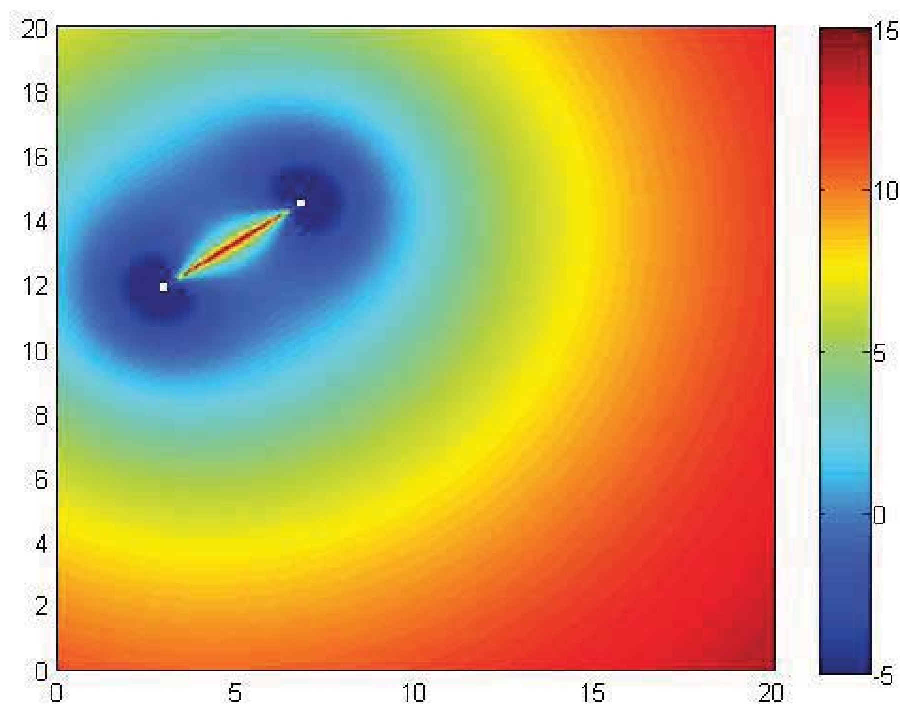

Figure 47-(b): Bistatic RCRLB of the target velocity [dBm/sec]. *Pair 3*, 2^{nd} configuration

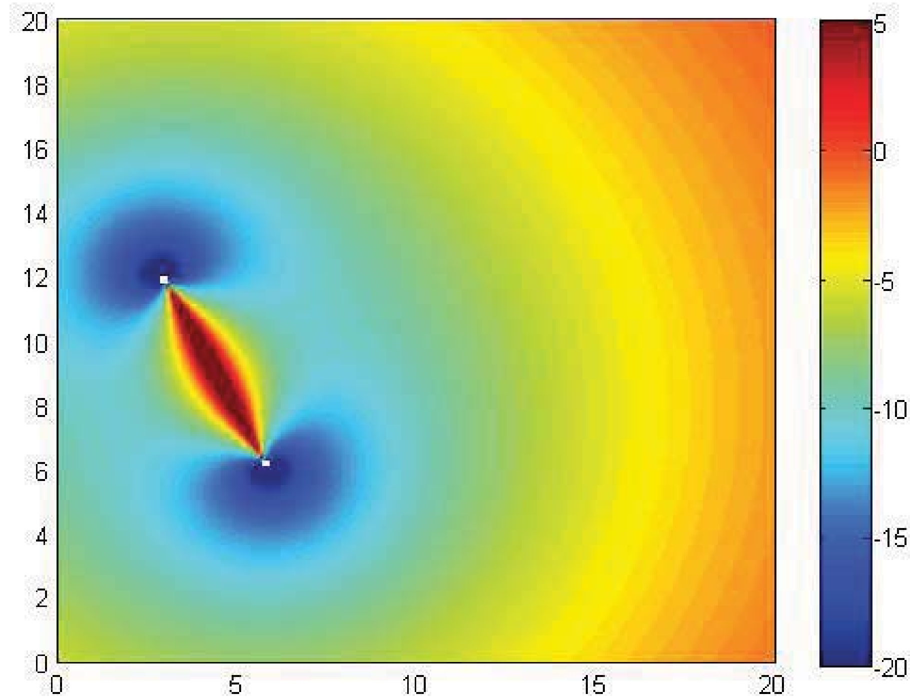

Figure 48-(a): Bistatic RCRLB of the target Range [dBm]. *Pair 4*, 2nd configuration

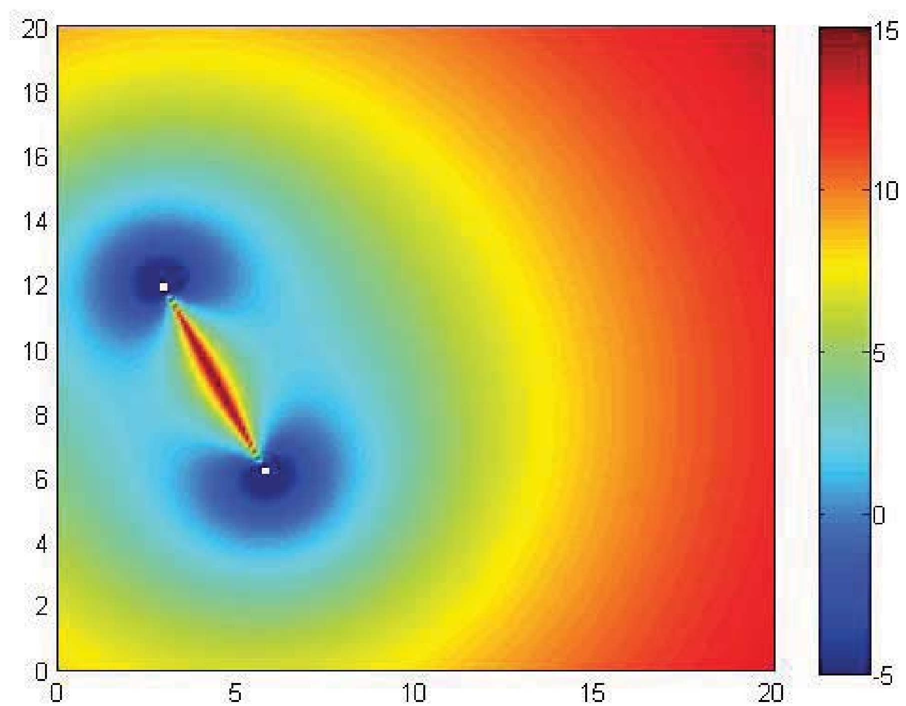

Figure 48-(b): Bistatic RCRLB of the target velocity [dBm/sec]. *Pair ,* 2nd configuration.

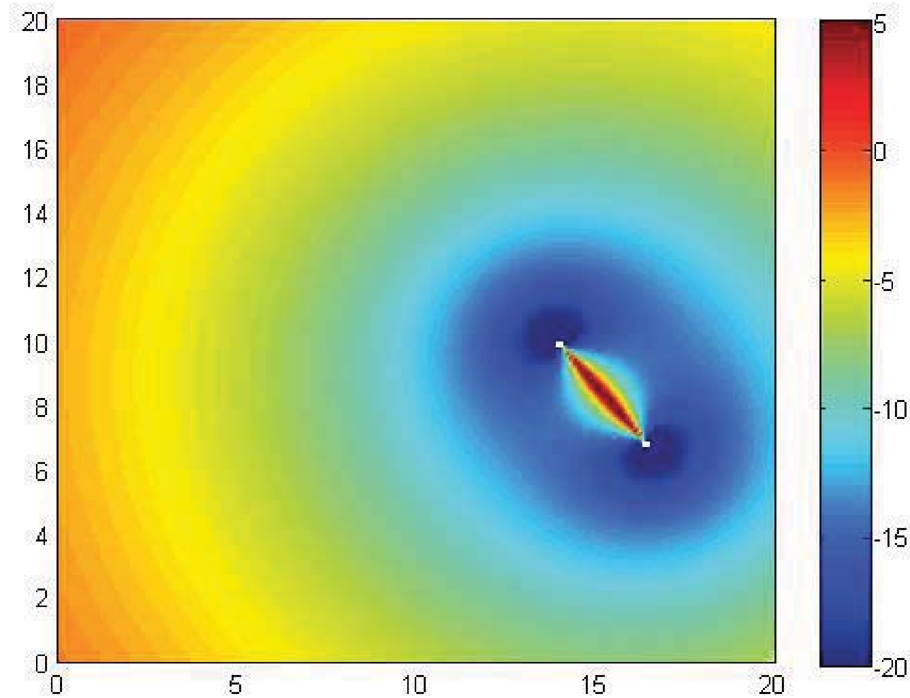

Figure 49-(a): Bistatic RCRLB of the target Range [dBm]. *Pair 5*. 2nd configuration

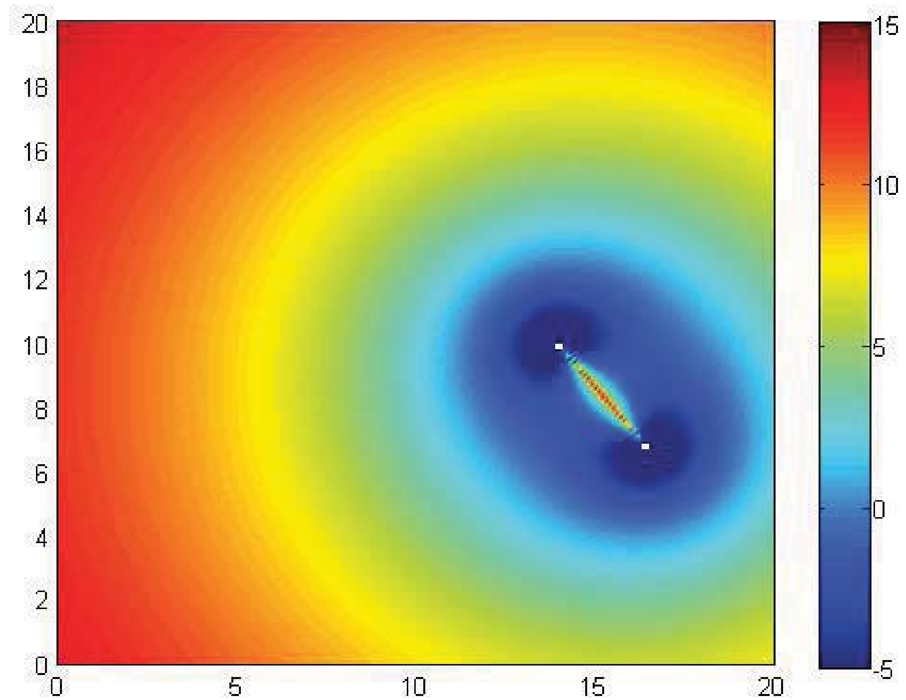

Figure 49-(b): Bistatic RCRLB of the target velocity [dBm/sec]. *Pair 5.* 2nd configuration

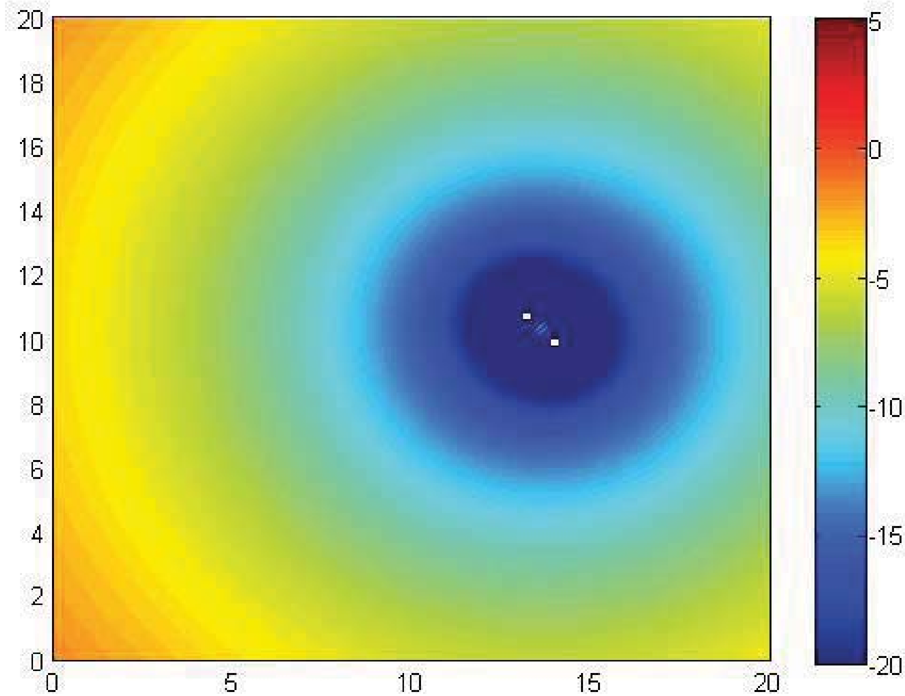

Figure 50-(a): Bistatic RCRLB of the target Range [dBm]. *Pair 6*. 2nd configuration

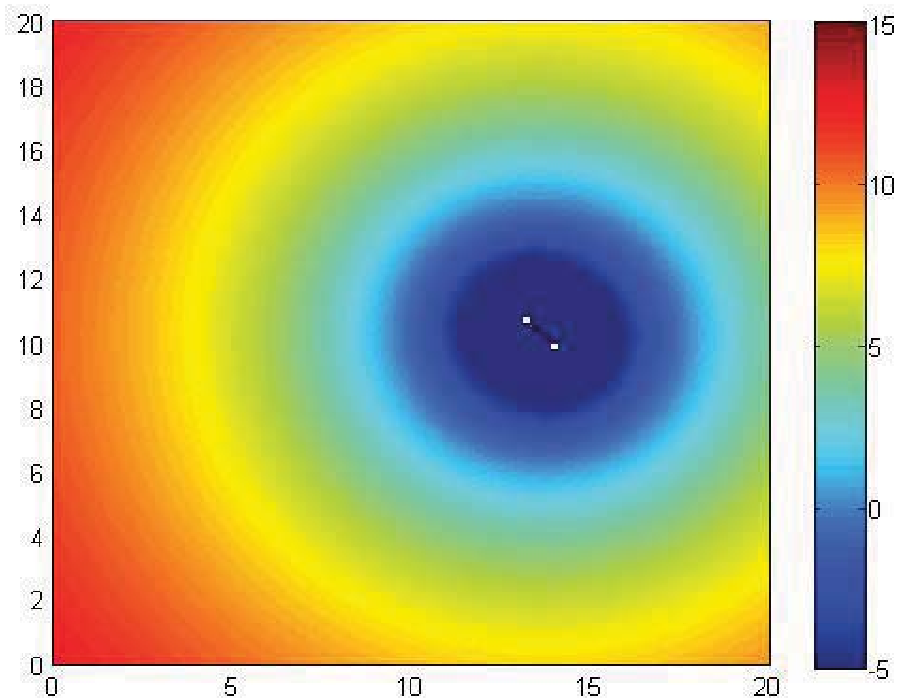

Figure 50-(b): Bistatic RCRLB of the target velocity [dBm/sec]. *Pair 6.* 2nd configuration

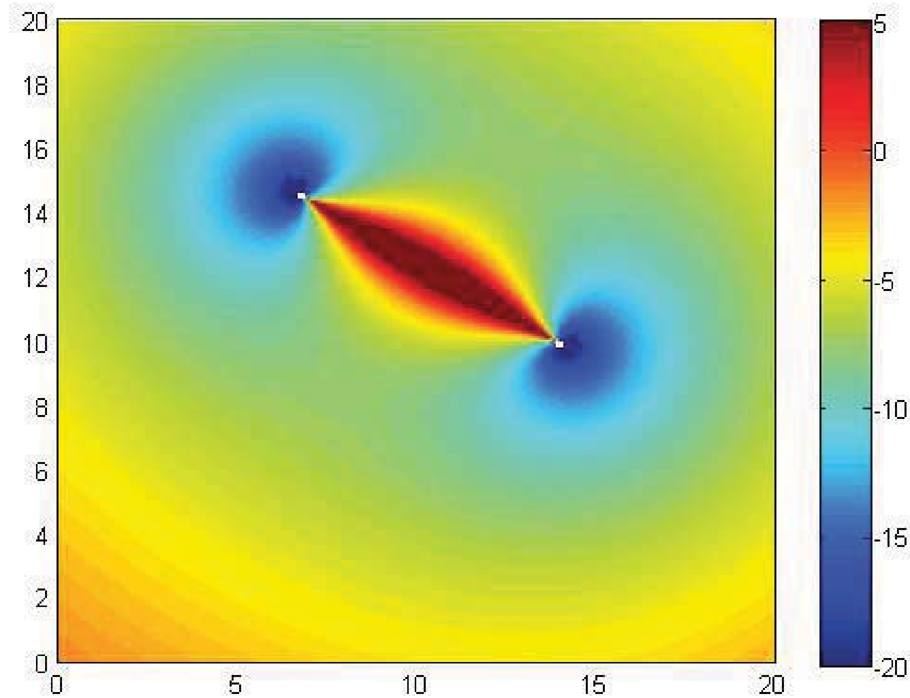

Figure 51-(a): Bistatic RCRLB of the target Range [dBm]. *Pair 7*. 2nd configuration

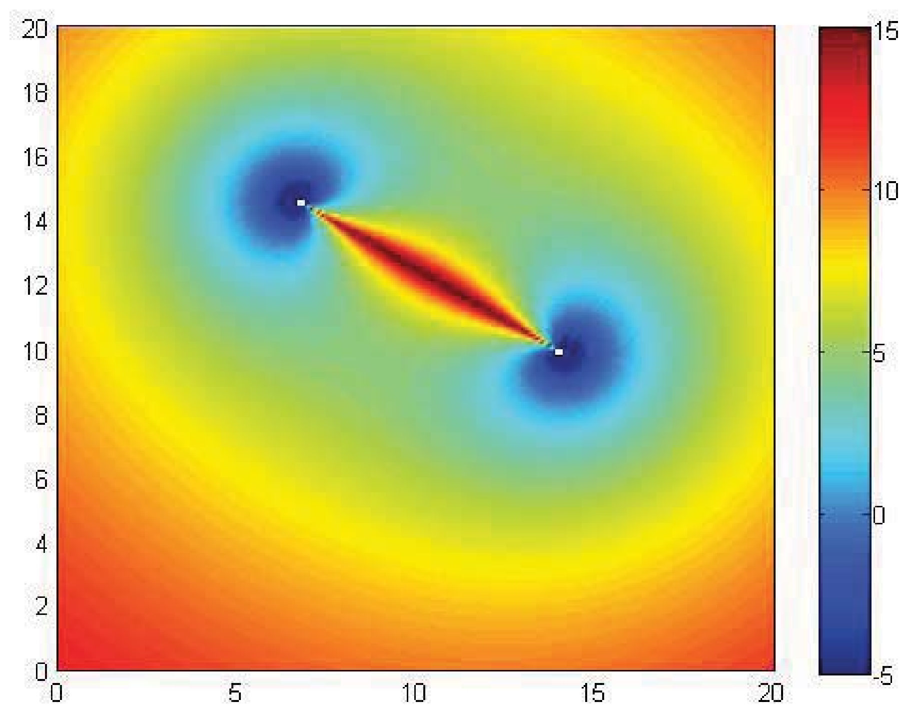

Figure 51-(b): Bistatic RCRLB of the target velocity [dBm/sec]. *Pair 7*2nd configuration.

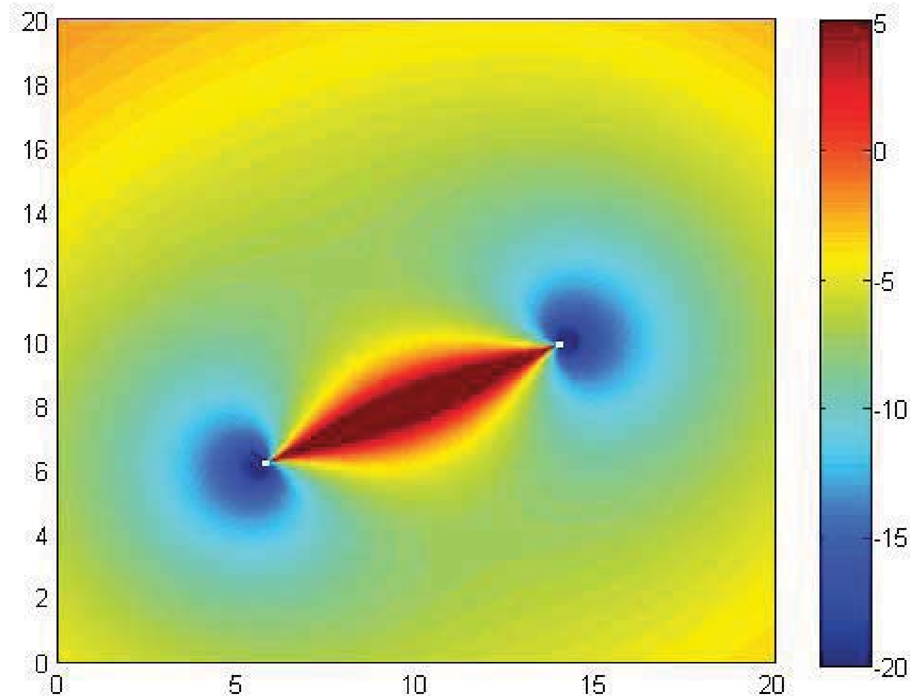

Figure 52-(a): Bistatic RCRLB of the target Range [dBm]. *Pair 8*. 2nd configuration

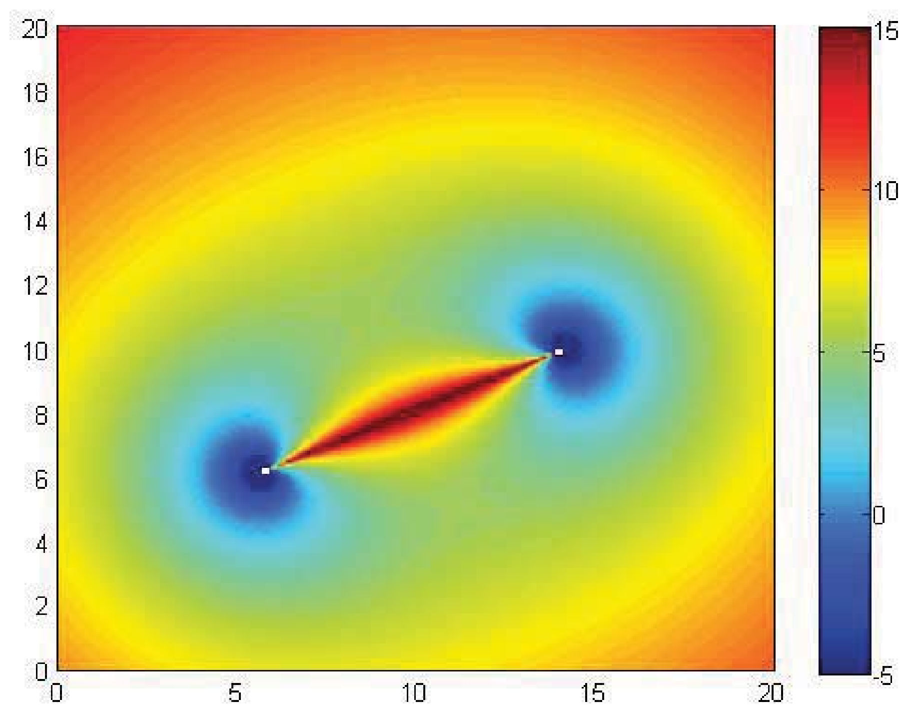

Figure 52-(b): Bistatic RCRLB of the target velocity [dBm/sec]. *Pair 8.* 2nd configuration

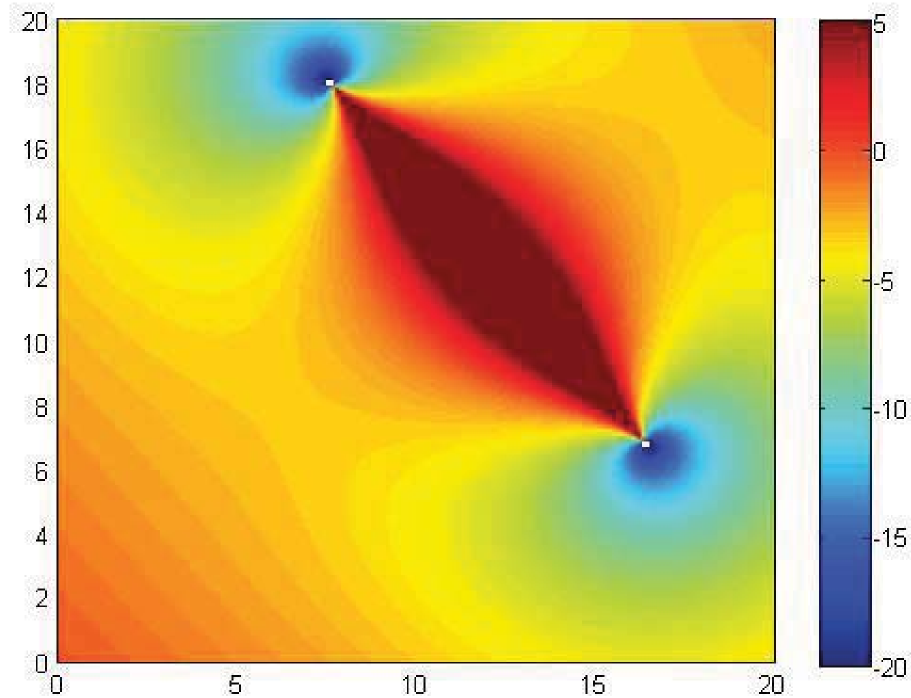

Figure 53-(a): Bistatic RCRLB of the target Range [dBm]. *Pair 9*. 2nd configuration

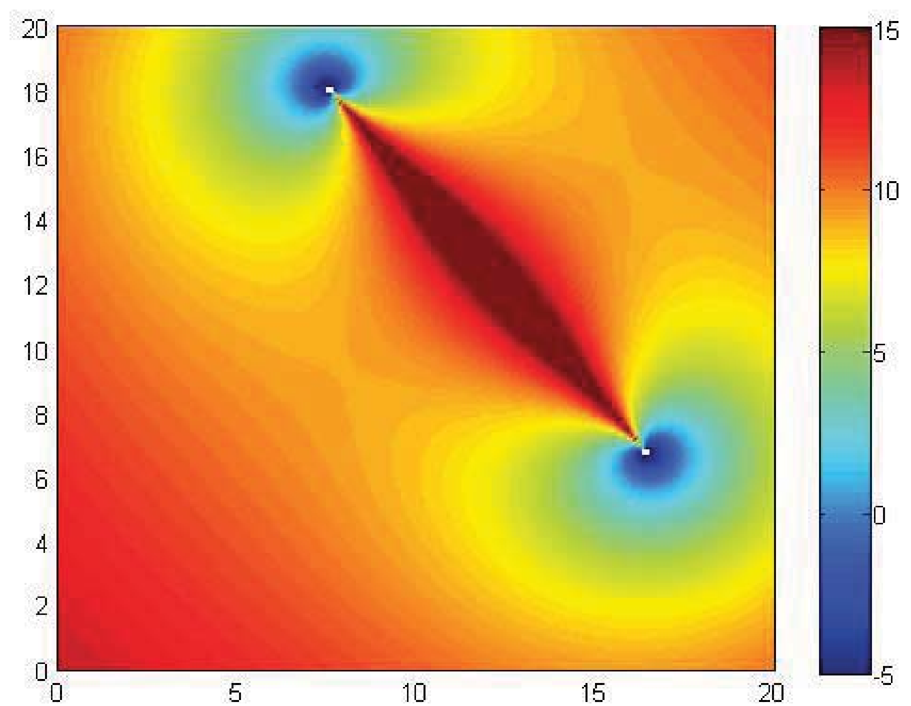

Figure 53-(b): Bistatic RCRLB of the target velocity [dBm/sec]. *Pair 9.* 2nd configuration

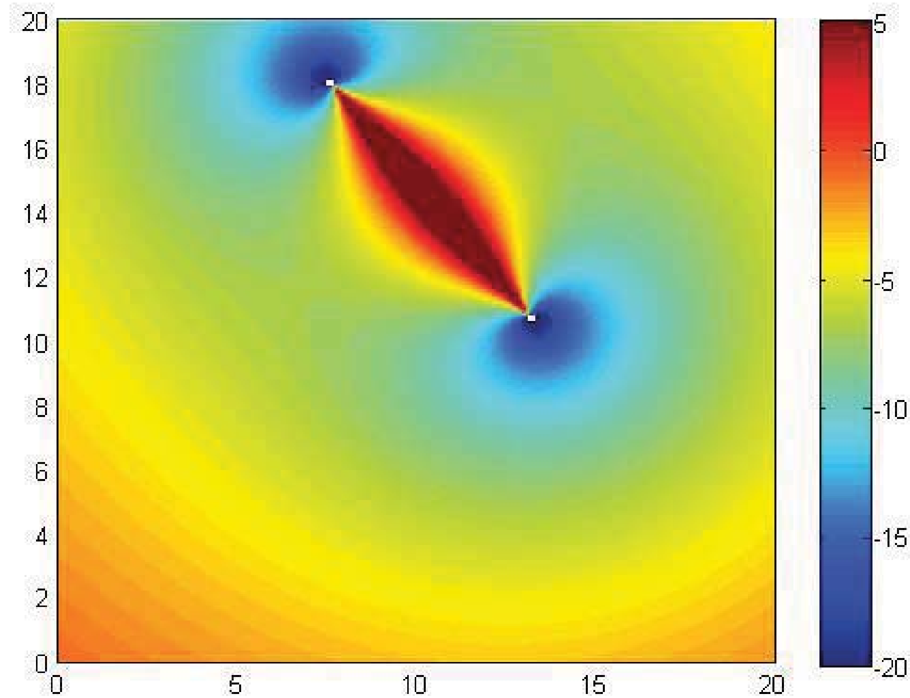

Figure 54-(a): Bistatic RCRLB of the target Range [dBm]. *Pair 10*. 2nd configuration

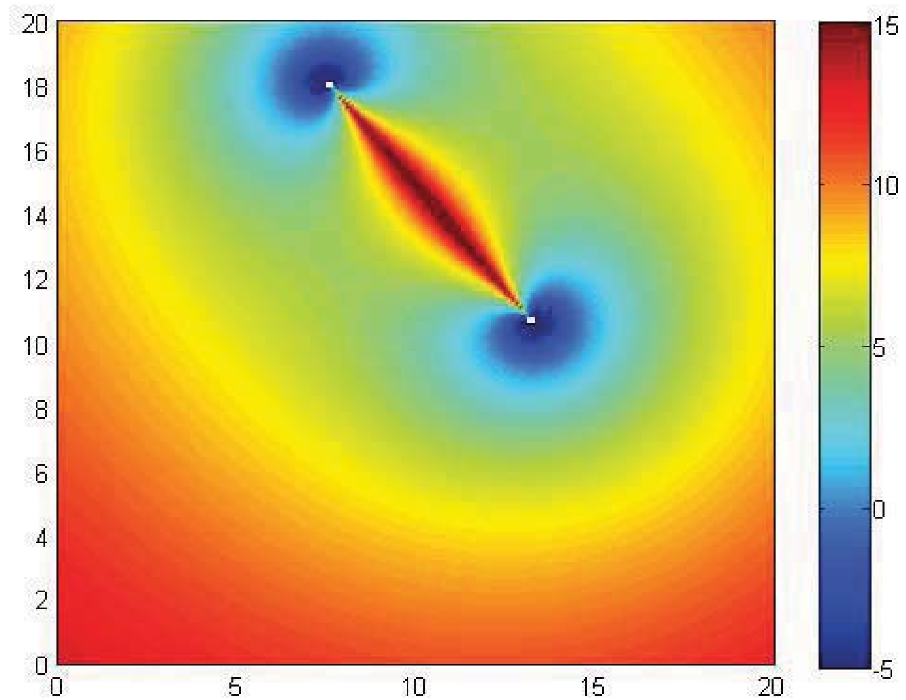

Figure 54-(b): Bistatic RCRLB of the target velocity [dBm/sec]. *Pair 10.* 2nd configuration

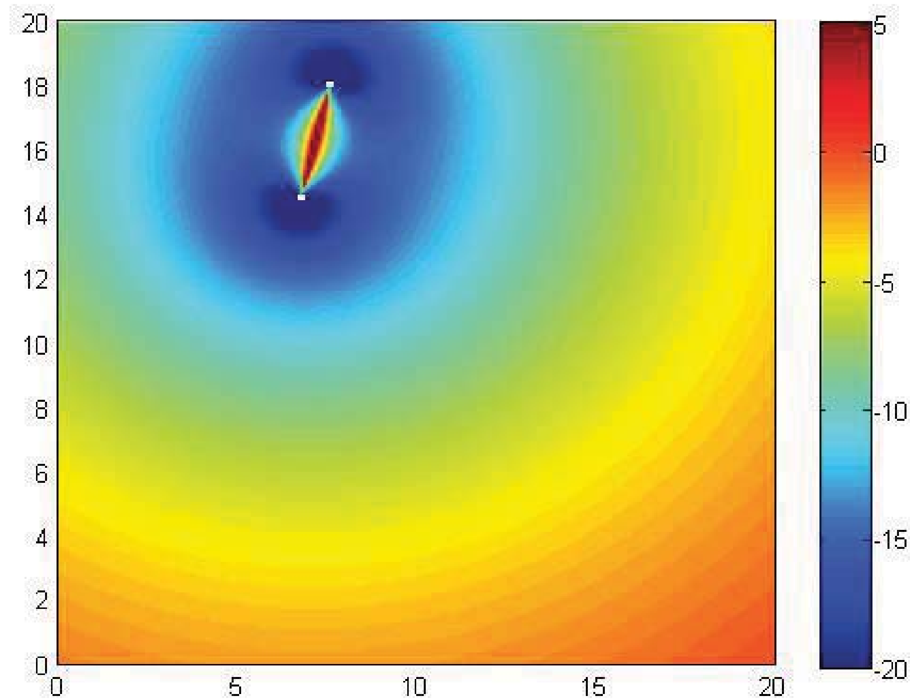

Figure 55-(a): Bistatic RCRLB of the target Range [dBm]. *Pair 11*. 2nd configuration

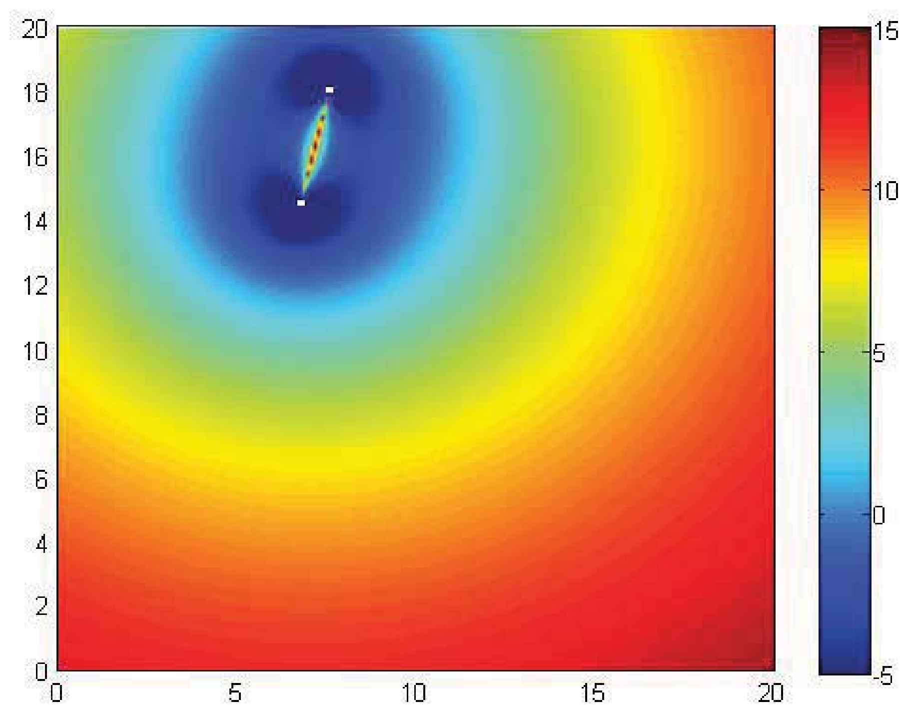

Figure 55-(b): Bistatic RCRLB of the target velocity [dBm/sec]. *Pair 11.* 2nd configuration

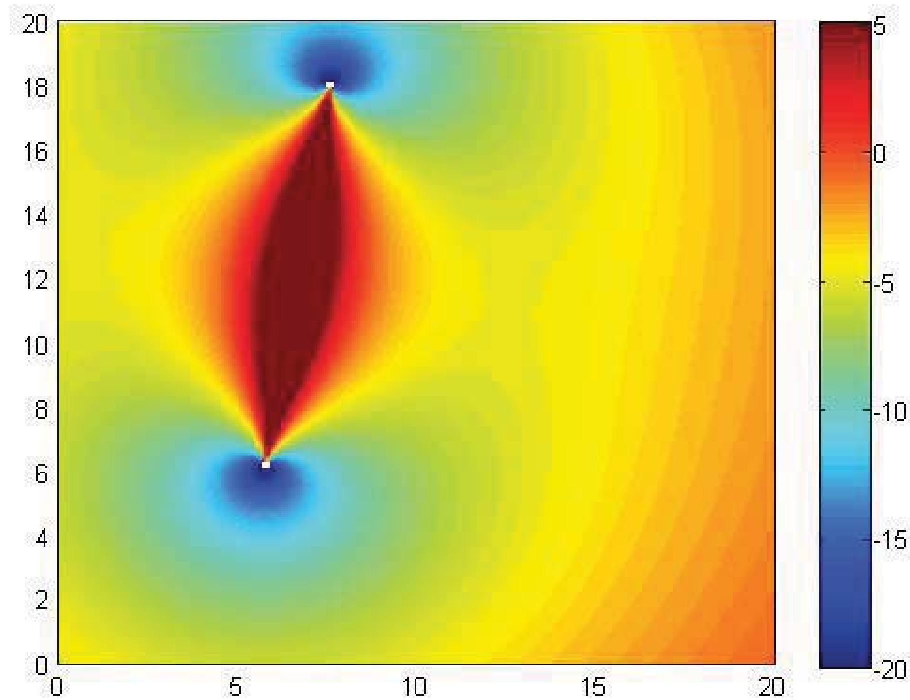

Figure 56-(a): Bistatic RCRLB of the target Range [dBm]. *Pair 12*. 2nd configuration

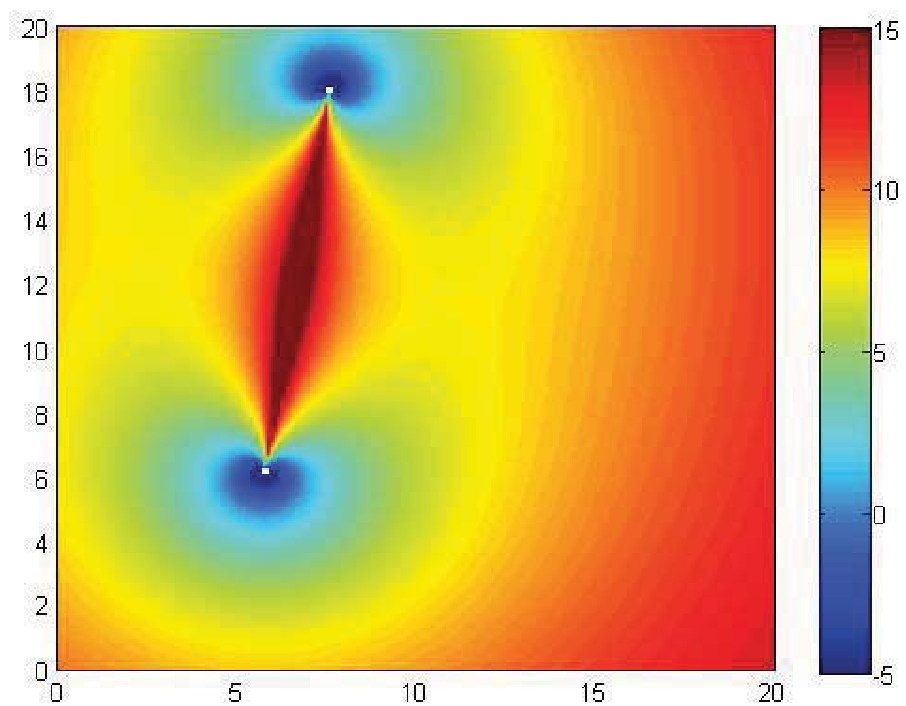

Figure 56-(b): Bistatic RCRLB of the target velocity [dBm/sec]. *Pair 12.* 2nd configuration

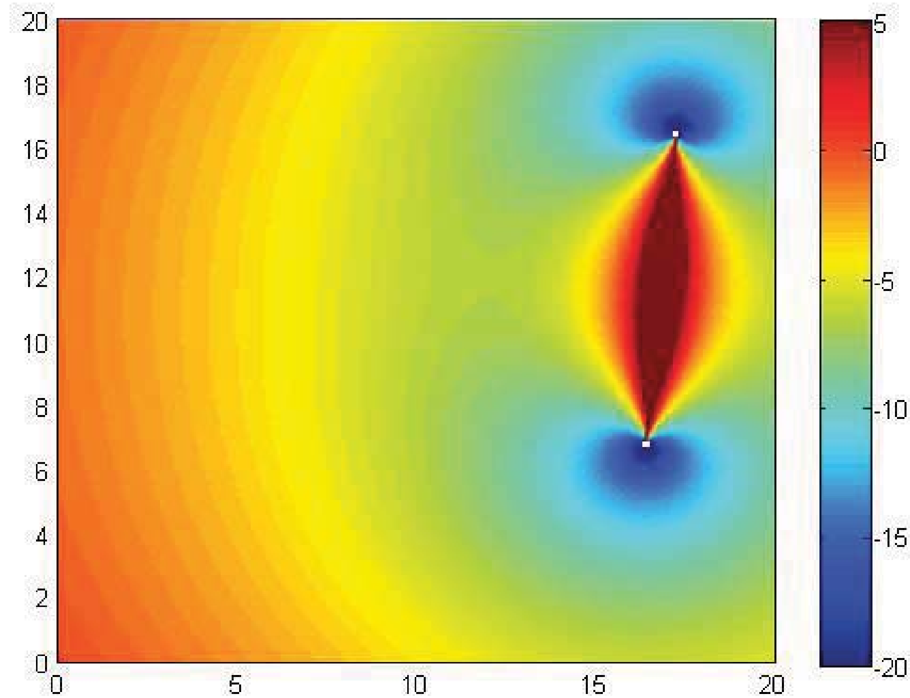

Figure 57-(a): Bistatic RCRLB of the target Range [dBm]. *Pair 13*. 2nd configuration

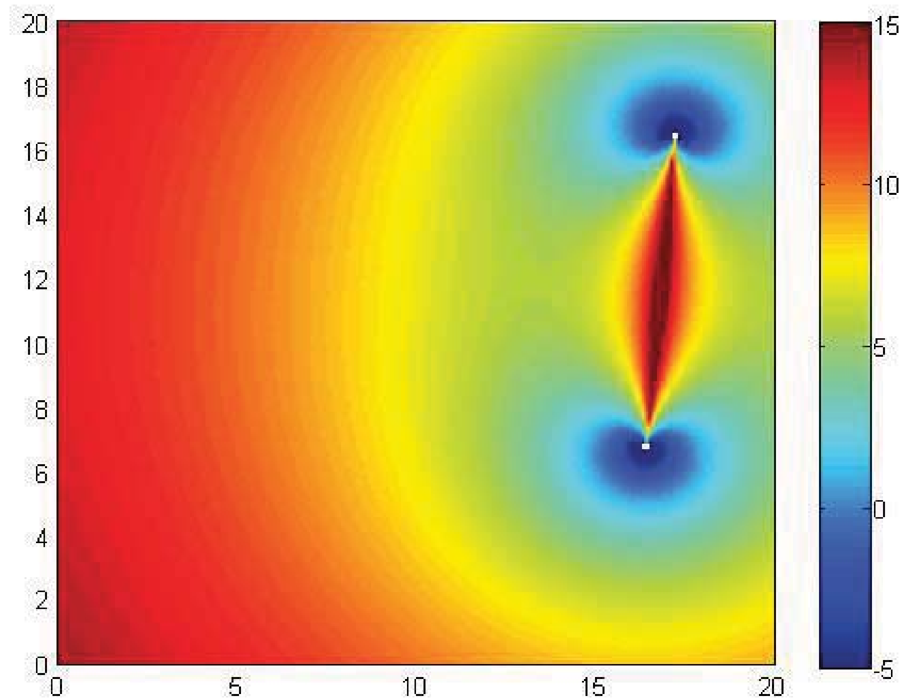

Figure 57-(b): Bistatic RCRLB of the target velocity [dBm/sec]. *Pair 13.* 2nd configuration

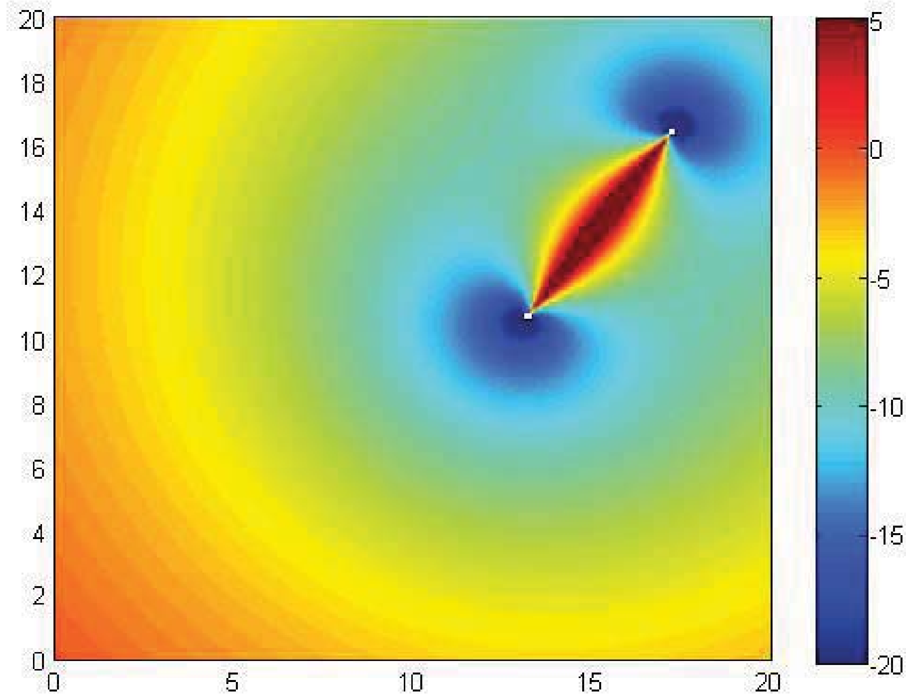

Figure 58-(a): Bistatic RCRLB of the target Range [dBm]. *Pair 14*. 2nd configuration

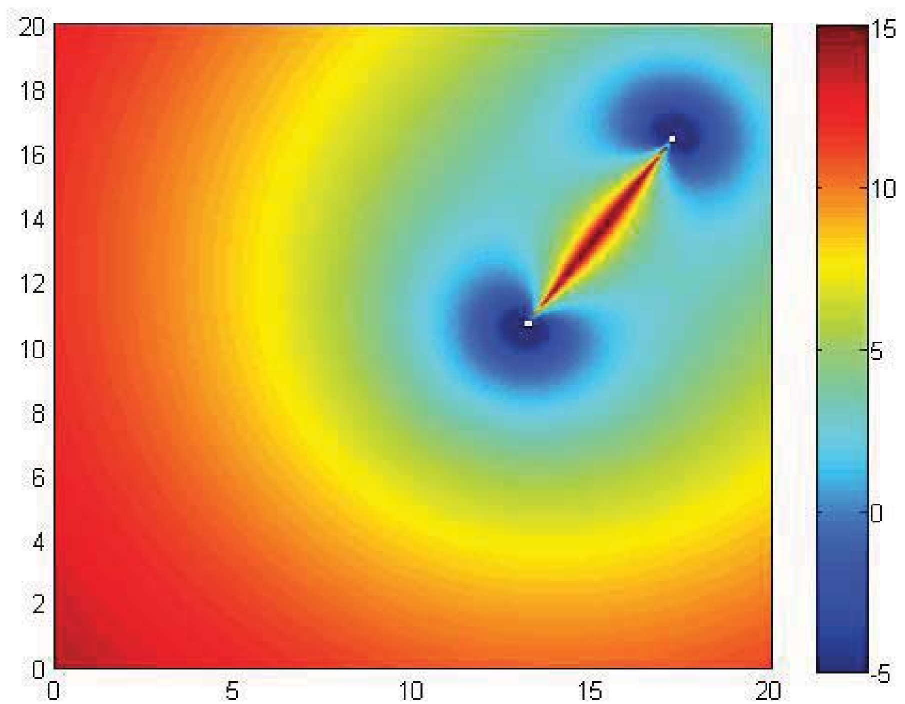

Figure 58-(b): Bistatic RCRLB of the target velocity [dBm/sec]. *Pair 14.* 2nd configuration

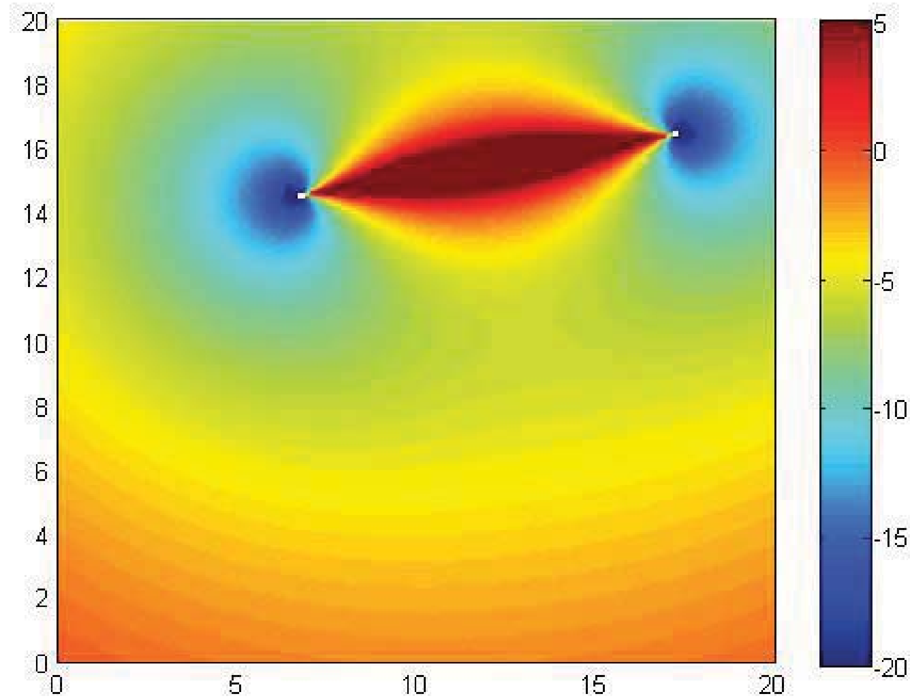

Figure 59-(a): Bistatic RCRLB of the target Range [dBm]. *Pair 15*. 2nd configuration

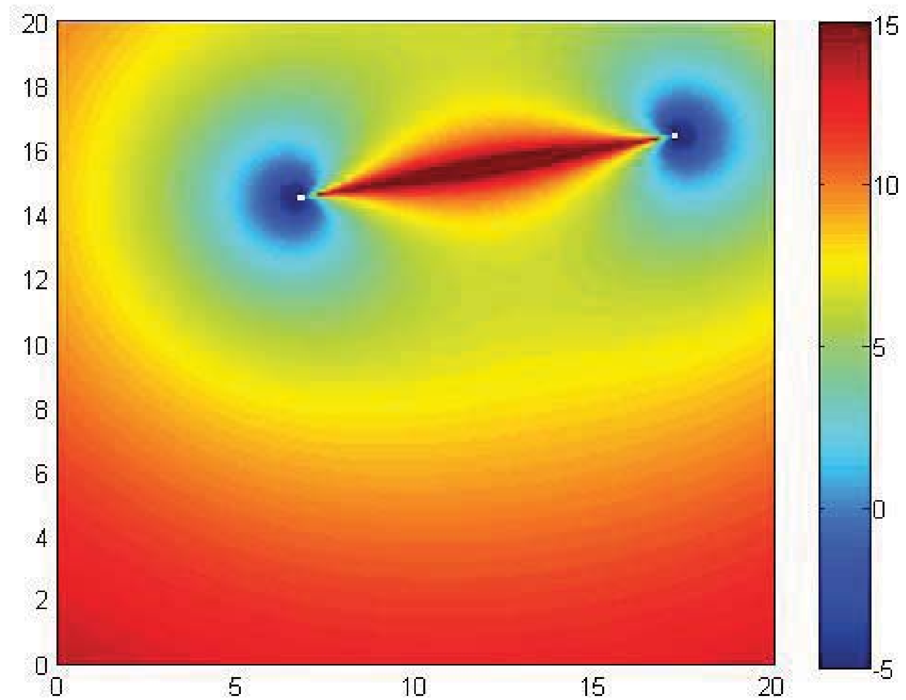

Figure 59-(b): Bistatic RCRLB of the target velocity [dBm/sec]. *Pair 15.* 2nd configuration

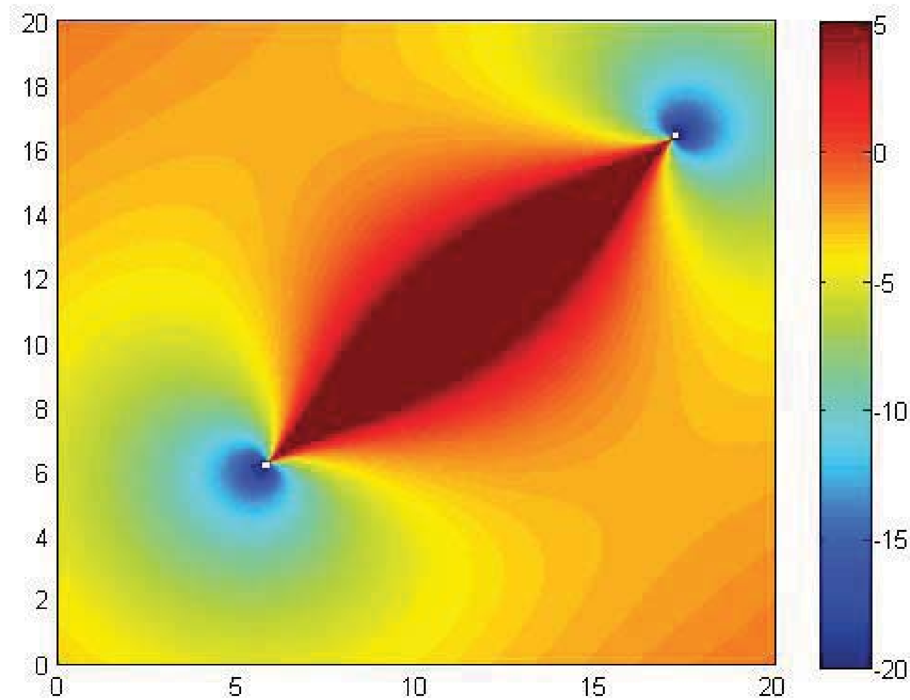

Figure 60-(a): Bistatic RCRLB of the target Range [dBm]. *Pair 16*. 2nd configuration

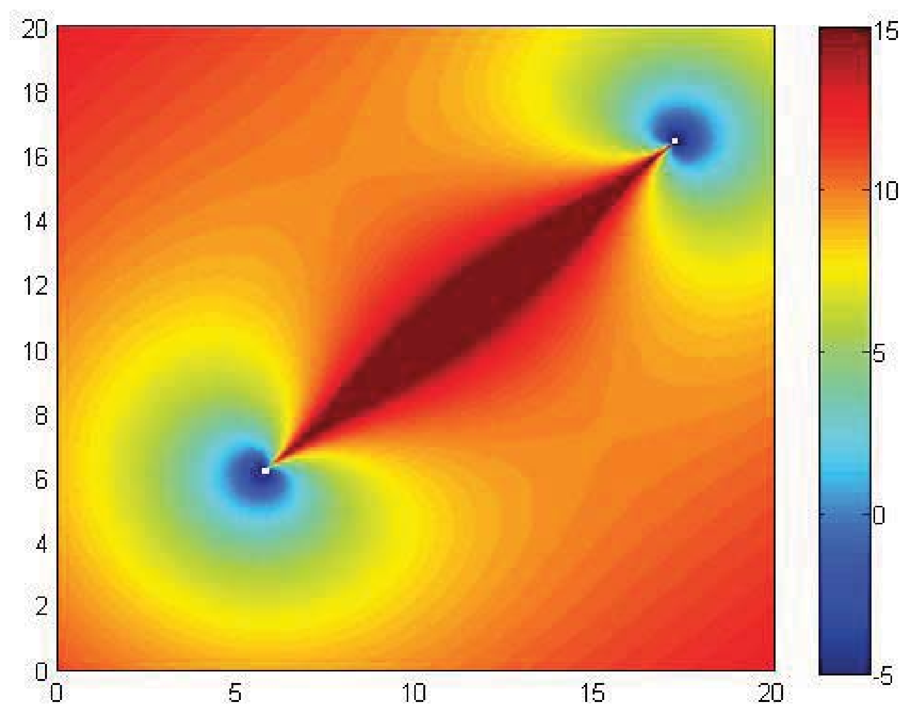

Figure 60-(b): Bistatic RCRLB of the target velocity [dBm/sec]. *Pair 16,* 2nd configuration.

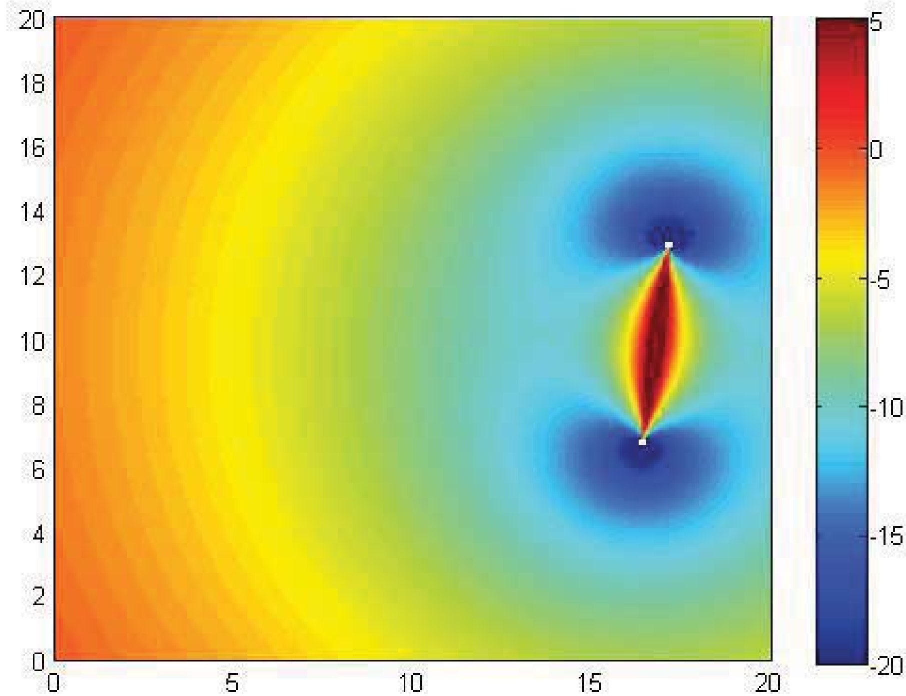

Figure 61-(a): Bistatic RCRLB of the target Range [dBm]. *Pair 17*. 2nd configuration

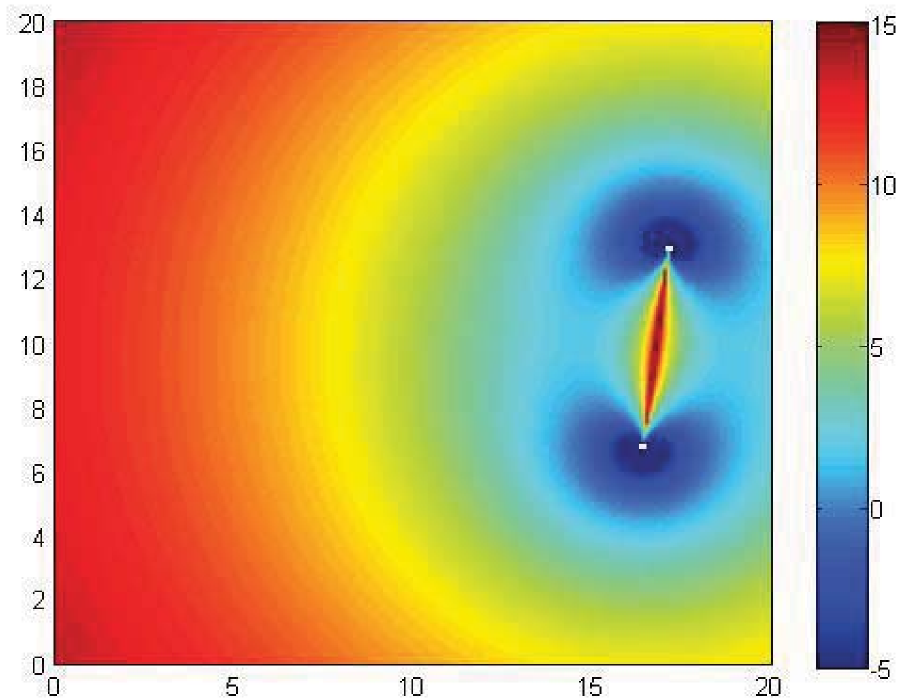

Figure 61-(b): Bistatic RCRLB of the target velocity [dBm/sec]. *Pair 17.* 2nd configuration

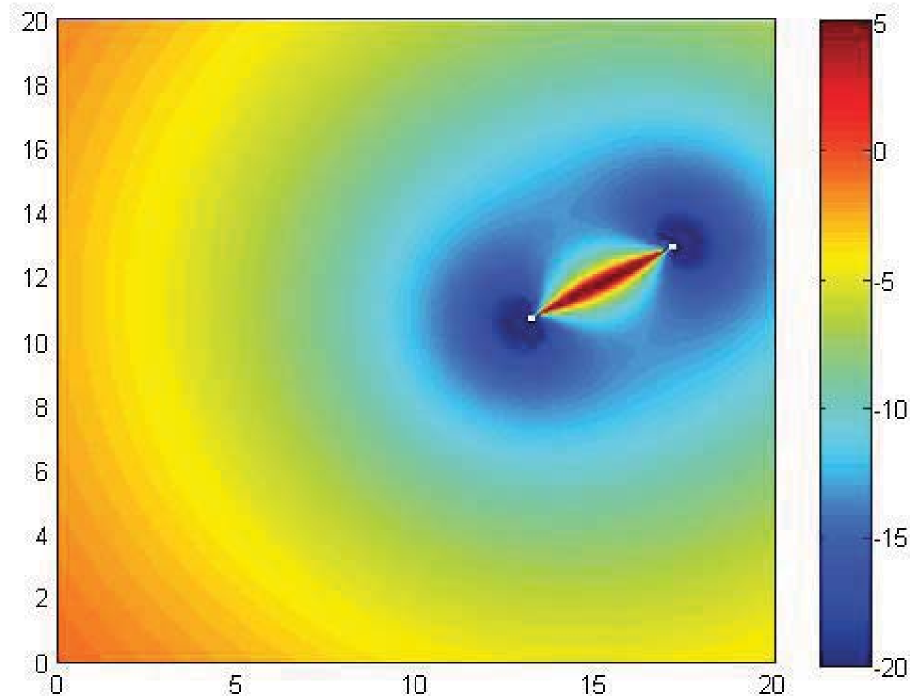

Figure 62-(a): Bistatic RCRLB of the target Range [dBm]. *Pair 18*. 2nd configuration

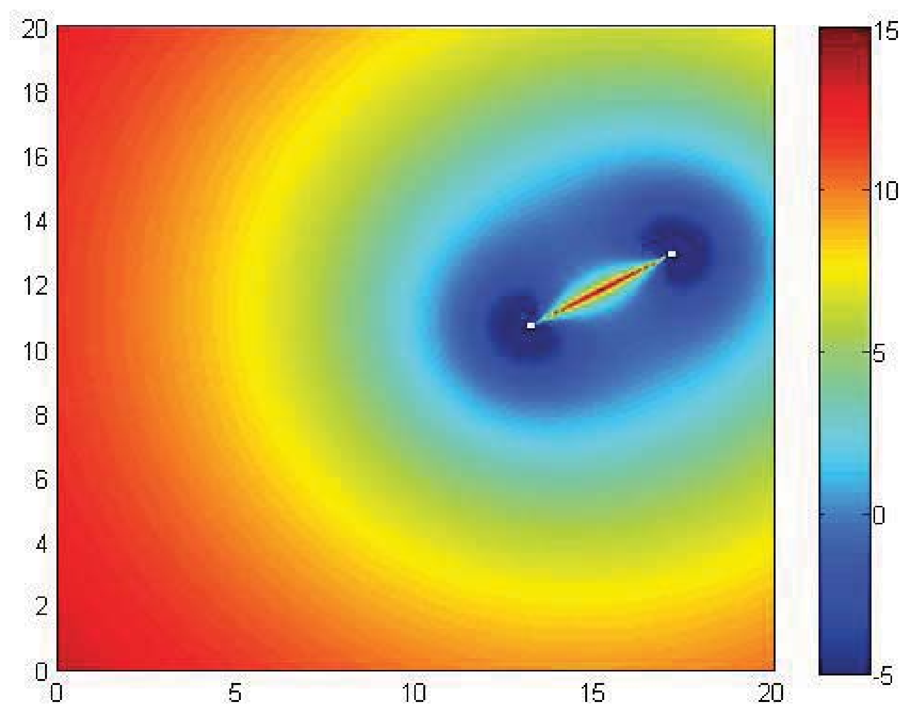

Figure 62-(b): Bistatic RCRLB of the target velocity [dBm/sec]. *Pair 18.* 2nd configuration

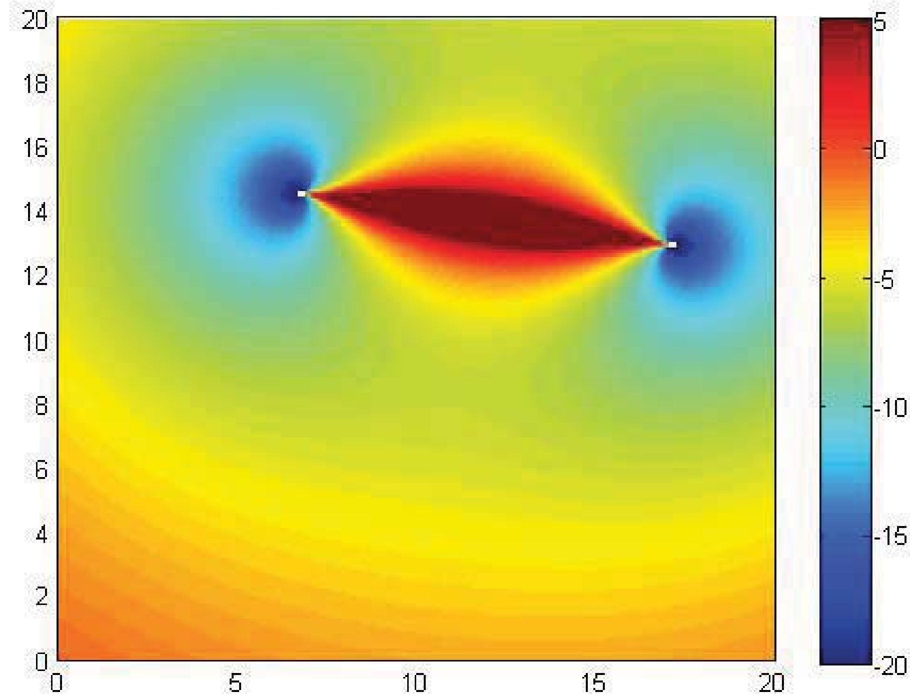

Figure 63-(a): Bistatic RCRLB of the target Range [dBm]. *Pair 19*. 2nd configuration

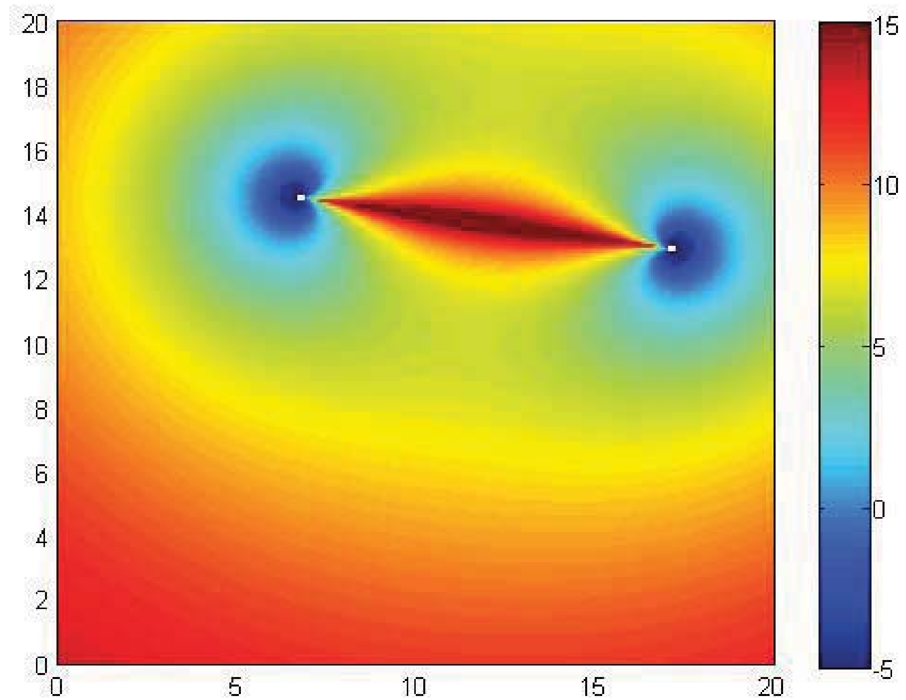

Figure 63-(b): Bistatic RCRLB of the target velocity [dBm/sec]. *Pair 19.* 2nd configuration

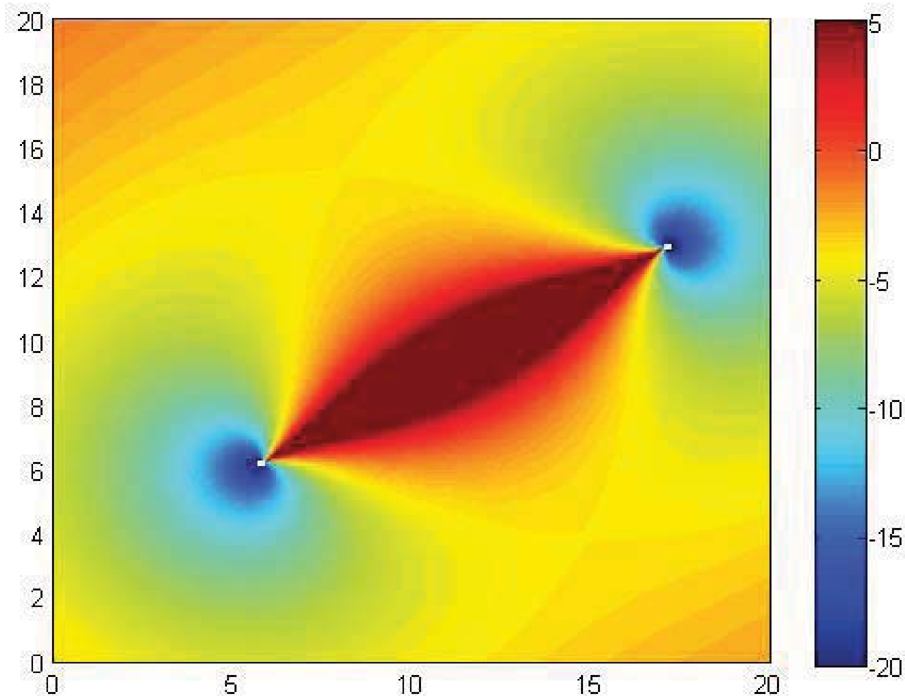

Figure 64-(a): Bistatic RCRLB of the target Range [dBm]. *Pair 20*. 2^{nd} configuration

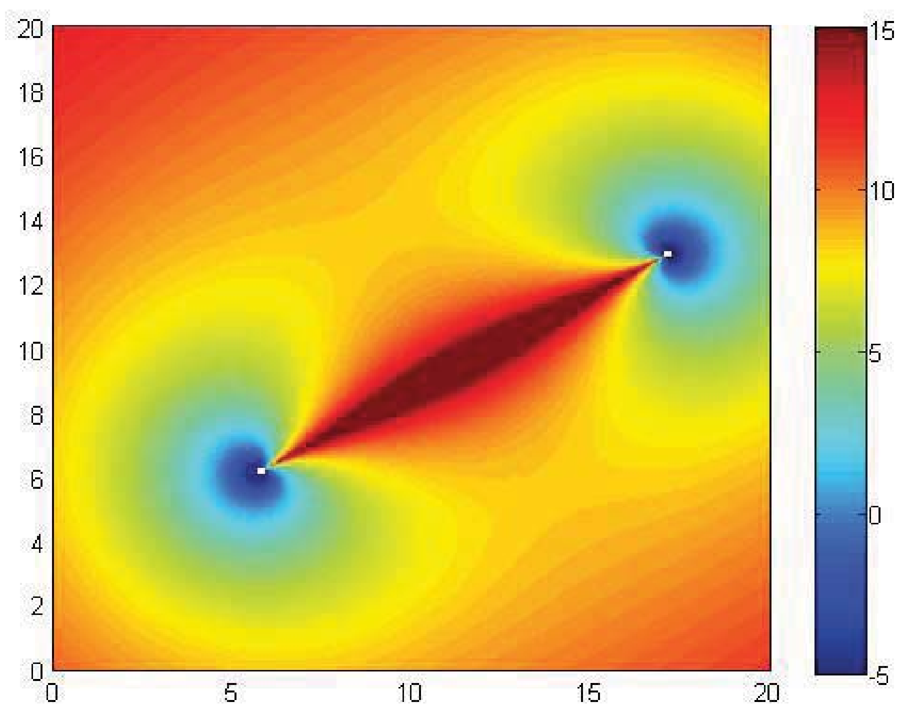

Figure 64-(b): Bistatic RCRLB of the target velocity [dBm/sec]. *Pair 20*. 2^{nd} configuration

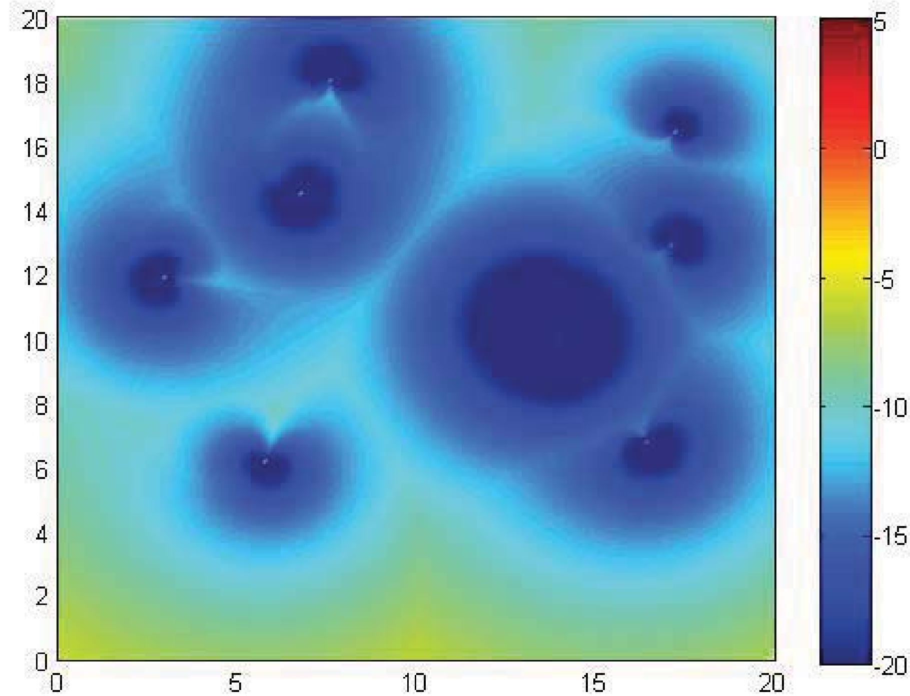

Figure 65-(a): Minimum RCRLB of the target Range [dBm], 2nd configuration

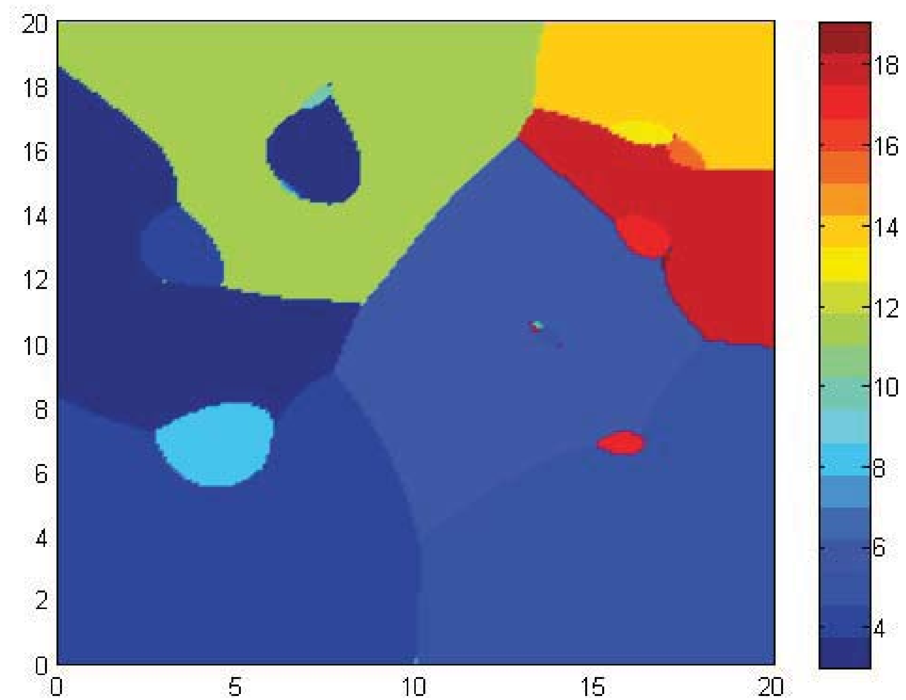

Figure 65-(b): Optimum pair map for target range estimation, 2nd configuration

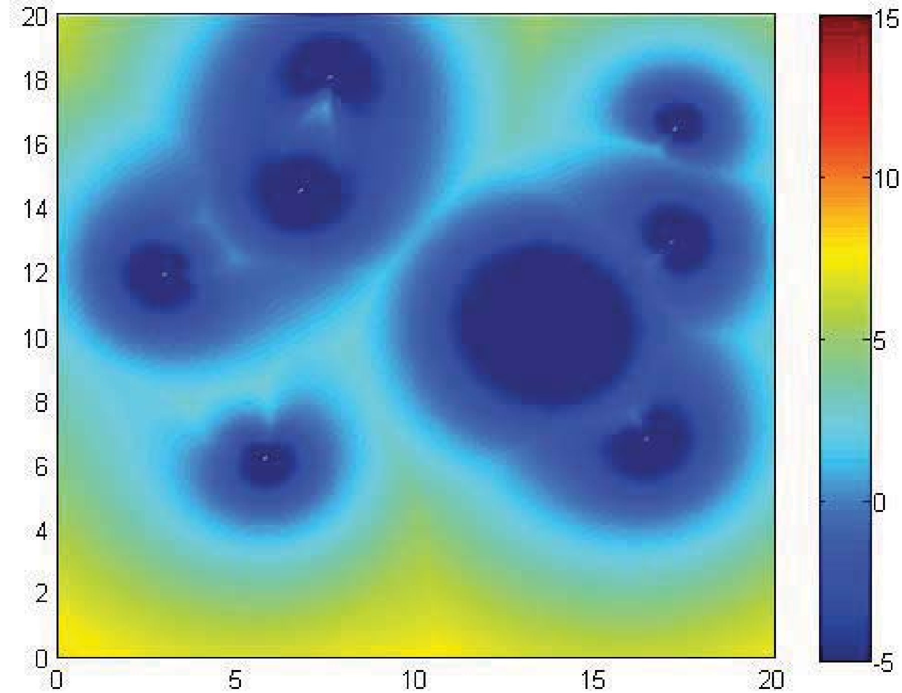

Figure 66-(a): Minimum RCRLB of the target velocity [dBm/sec], 2nd configuration

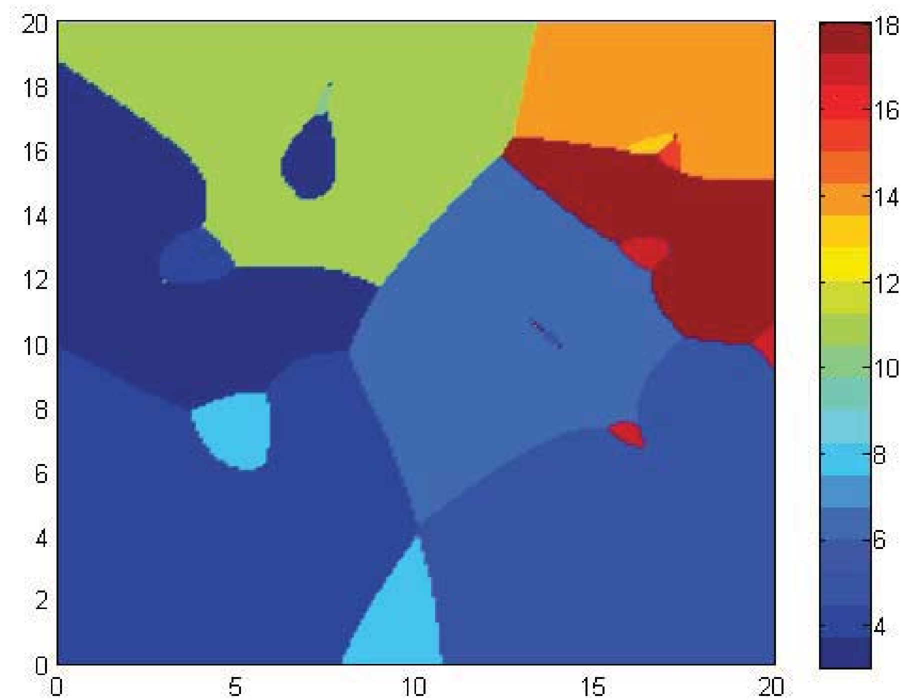

Figure 66-(b): Optimum pair map for target velocity estimation, 2nd configuration

6 FINAL REMARKS

In this technical report, we calculated the bistatic AF for a burst of LFM pulses. We exploited the relation between the AF and the CRLB to calculate the bistatic CRLBs of target range and velocity. The bistatic CRLBs provide a local measure of the estimation accuracy of these parameters. Then, we compared monostatic and bistatic CRLBs as a function of the number of integrated pulses, target direction of arrival (DOA), and bistatic baseline length. Subsequently, we used the information gained through the calculation of the bistatic CRLBs for the choice of the optimum transmit-receive pair in a multistatic radar system. The performance of each bistatic channel heavily depends upon the geometry of the scenario and the position of the target with respect to each receiver and transmitter. We approach the problem of optimally selecting the TX-RX pair based upon the CRLB for the bistatic geometry of each pair. The optimal pair was defined as that exhibiting the lowest bistatic CRLB for the target velocity or range. These results can be used for the dynamical selection of the TX-RX signals for the tracking of a radar target moving along a trajectory in a multistatic scenario.

In this work we assumed that only one couple of TX-RX is active, neglecting the interference among the other transmitters on the selected one. This ideal situation can be achieved selecting orthogonal waveforms for all the transmitters and matching dynamically the selected receivers to the waveform of the selected transmitter.

Ongoing research focuses on dynamic reconfiguration of selected TX-RX as a function of RCRLBs as well as tracking accuracy. In this phase we will take also into account the contemporaneous presence of all the transmitted signals.

APPENDIX A – Relation between CRLB and AF

In this appendix we report the proof of eq. (8). The complex signal received by the radar is

$$r(t) = s(t, \mathbf{A}) + w(t) \qquad 0 \le t \le T \tag{A.1}$$

where $w(t)$ is a zero mean complex Gaussian process and $s(t, \mathbf{A})$ is the received signal in absence of noise which depends on the vector $\mathbf{A} = \begin{bmatrix} A_1 & A_2 & \ldots & A_N \end{bmatrix}^T$ composed by the unknown, nonrandom parameters that we want to estimate. We let the observation interval $[0, T]$ be long enough to completely contain the pulse.

We approach the problem by making a *K*-coefficient approximation of $r(t)$. Assuming that

$$\varphi_i(t) \qquad i = 1, 2, \ldots, K \tag{A.2}$$

is a orthonormal basis, the *K*-coefficient approximation of $r(t)$ is given by

$$r_K(t) = \sum_{i=1}^{K} r_i \varphi_i(t) \tag{A.3}$$

where

$$r_i = \int_0^T r(t)\varphi_i(t)dt \tag{A.4}$$

Substituting Equation (A.1) into this expression, we obtain

$$r_i = s_i(\mathbf{A}) + w_i \tag{A.5}$$

where

$$s_i(\mathbf{A}) = \int_0^T s(t, \mathbf{A})\varphi_i(t)dt \tag{A.6}$$

and

$$w_i = \int_0^T w(t)\varphi_i(t)dt \tag{A.7}$$

Therefore, the samples r_i are independent, identically distributed (IID), complex Gaussian variables with variance σ_w^2 and mean $s_i(\mathbf{A})$, in short notation $r_i \sim CN\left(s_i(\mathbf{A}), \sigma_w^2\right)$. The probability density function of r_i is given by:

$$p_{r_i}(r_i, \mathbf{A}) = \frac{1}{\pi\sigma_w^2} e^{-\frac{|r_i - s_i(\mathbf{A})|^2}{\sigma_w^2}} \tag{A.8}$$

In order to find the CRLB of the non-random parameters A_n, where $n = 1, 2, ..., N$, the first step is to find the likelihood function. With obvious notation, the likelihood function can be written as

$$\Lambda_1\left[r_K(t), \mathbf{A}\right] = p_{r_K(t),\mathbf{A}}(r_K(t), \mathbf{A}) = \prod_{i=1}^{K} \frac{1}{\pi\sigma_w^2} e^{-\frac{|r_i - s_i(\mathbf{A})|^2}{\sigma_w^2}} \tag{A.9}$$

Now, if we let $K \to \infty$, $\Lambda_1\left[r_K(t), \mathbf{A}\right]$ is not well defined. In [Van71] it is shown that we can divide a likelihood function by anything that does not depend on $\mathbf{A}$ and still have a likelihood function. In order to avoid the convergence problem, we divide (A.9) by

$$p_{r_K(t)|H_0}(r_K(t)|H_0) = \prod_{i=1}^{K} \frac{1}{\pi\sigma_w^2} e^{-\frac{|r_i|^2}{\sigma_w^2}} \tag{A.10}$$

before letting $K \to \infty$. Because this function does not depends on $\mathbf{A}$, it is legitimate to divide by it here. Let define the likelihood function

$$\Lambda\left[r_K(t), \mathbf{A}\right] = \frac{\Lambda_1\left[r_K(t), \mathbf{A}\right]}{p_{r_K(t)|H_0}(r_K(t)|H_0)} \tag{A.11}$$

Substituting into this expression, cancelling common terms and taking the logarithm, we obtain

$$
\begin{aligned}
\ln\Lambda\left[r_K(t),\mathbf{A}\right] &= -\frac{1}{\sigma_w^2}\sum_{i=1}^{K}\left[\left|s_i(\mathbf{A})\right|^2 - 2\Re e\left\{r_i^* s_i(\mathbf{A})\right\}\right] = \\
&= -\frac{1}{\sigma_w^2}\sum_{i=1}^{K}\left[\left|s_i(\mathbf{A})\right|^2 - r_i^* s_i(\mathbf{A}) - r_i s_i^*(\mathbf{A})\right]
\end{aligned} \tag{A.12}
$$

Letting $K \to \infty$ we have

$$
\ln\Lambda\left[r(t),\mathbf{A}\right] = -\frac{1}{\sigma_w^2}\int_0^T \left|s(t,\mathbf{A})\right|^2 dt + \frac{1}{\sigma_w^2}\int_0^T r^*(t)s(t,\mathbf{A})dt + \frac{1}{\sigma_w^2}\int_0^T r(t)s^*(t,\mathbf{A})dt \tag{A.13}
$$

From [Kay93] the Fisher Information Matrix (FIM) is given by

$$
\mathbf{J} = \begin{bmatrix}
E\left\{\frac{\partial^2 \ln\Lambda\left[r(t),\mathbf{A}\right]}{\partial A_1^2}\right\} & E\left\{\frac{\partial^2 \ln\Lambda\left[r(t),\mathbf{A}\right]}{\partial A_1 \partial A_2}\right\} & \dots & E\left\{\frac{\partial^2 \ln\Lambda\left[r(t),\mathbf{A}\right]}{\partial A_1 \partial A_N}\right\} \\
E\left\{\frac{\partial^2 \ln\Lambda\left[r(t),\mathbf{A}\right]}{\partial A_2 \partial A_1}\right\} & E\left\{\frac{\partial^2 \ln\Lambda\left[r(t),\mathbf{A}\right]}{\partial A_2^2}\right\} & \dots & \dots \\
\dots & \dots & \dots & \dots \\
E\left\{\frac{\partial^2 \ln\Lambda\left[r(t),\mathbf{A}\right]}{\partial A_N \partial A_1}\right\} & \dots & \dots & E\left\{\frac{\partial^2 \ln\Lambda\left[r(t),\mathbf{A}\right]}{\partial A_N^2}\right\}
\end{bmatrix} \tag{A.14}
$$

where $E\{\cdot\}$ is the Expectation operator.

By differentiating Equation (A.13) with respect to A_n we obtain:

$$
\begin{aligned}
\frac{\partial \ln\Lambda\left[r(t),\mathbf{A}\right]}{\partial A_n} &= -\frac{1}{\sigma_w^2}\int_0^T \frac{\partial s(t,\mathbf{A})}{\partial A_n} s^*(t,\mathbf{A})dt - \frac{1}{\sigma_w^2}\int_0^T s(t,\mathbf{A})\frac{\partial s^*(t,\mathbf{A})}{\partial A_n} dt + \\
&+ \frac{1}{\sigma_w^2}\int_0^T r^*(t)\frac{\partial s(t,\mathbf{A})}{\partial A_n} dt + \frac{1}{\sigma_w^2}\int_0^T r(t)\frac{\partial s^*(t,\mathbf{A})}{\partial A_n} dt
\end{aligned} \tag{A.15}
$$

that can be wrote as

$$\frac{\partial \ln \Lambda\left[r(t),\mathbf{A}\right]}{\partial A_n} = \frac{1}{\sigma_w^2}\int_0^T \left[r(t)-s(t,\mathbf{A})\right]^* \frac{\partial s(t,\mathbf{A})}{\partial A_n}dt + \frac{1}{\sigma_w^2}\int_0^T \left[r(t)-s(t,\mathbf{A})\right]\frac{\partial s^*(t,\mathbf{A})}{\partial A_n}dt \tag{A.16}$$

Differentiating again with respect to A_m we obtain:

$$\begin{aligned}\frac{\partial^2 \ln \Lambda\left[r(t),\mathbf{A}\right]}{\partial A_n \partial A_m} &= \frac{1}{\sigma_w^2}\int_0^T \left\{-\frac{\partial s^*(t,\mathbf{A})}{\partial A_m}\frac{\partial s(t,\mathbf{A})}{\partial A_n} + \left[r(t)-s(t,\mathbf{A})\right]^* \frac{\partial^2 s(t,\mathbf{A})}{\partial A_n \partial A_m}\right\}dt + \\ &+ \frac{1}{\sigma_w^2}\int_0^T \left\{-\frac{\partial s(t,\mathbf{A})}{\partial A_m}\frac{\partial s^*(t,\mathbf{A})}{\partial A_n} + \left[r(t)-s(t,\mathbf{A})\right]\frac{\partial^2 s^*(t,\mathbf{A})}{\partial A_n \partial A_m}\right\}dt\end{aligned} \tag{A.17}$$

Taking the expectation, we obtain:

$$E\left\{\frac{\partial^2 \ln \Lambda\left[r(t),\mathbf{A}\right]}{\partial A_n \partial A_m}\right\} = -\frac{1}{\sigma_w^2}\int_0^T \frac{\partial s^*(t,\mathbf{A})}{\partial A_m}\frac{\partial s(t,\mathbf{A})}{\partial A_n}dt - \frac{1}{\sigma_w^2}\int_0^T \frac{\partial s(t,\mathbf{A})}{\partial A_m}\frac{\partial s^*(t,\mathbf{A})}{\partial A_n}dt \tag{A.18}$$

where we observed that

$$E\left\{r(t)-s(t,\mathbf{A})\right\} = E\left\{w(t)\right\} = 0 \tag{A.19}$$

Assuming that

$$s(t,\mathbf{A}) = \sqrt{E}u(t,\mathbf{A}) \tag{A.20}$$

where E is the energy of $s(t,\mathbf{A})$ and $u(t,\mathbf{A})$ is a unitary energy signal, Equation (A.18) can be written as

$$E\left\{\frac{\partial^2 \ln \Lambda\left[r(t),\mathbf{A}\right]}{\partial A_n \partial A_m}\right\} = -2SNR\frac{\partial^2}{\partial A_n \partial A_m}\int_0^T \left|u(t,\mathbf{A})\right|^2 dt \tag{A.18}$$

where $SNR = E/\sigma_w^2$ is the Signal to Noise Ratio.

It is interesting to observe that $\int_0^T |u(t,\mathbf{A})|^2\, dt$ is the Ambiguity Function of $u(t,\mathbf{A})$ evaluated around its maximum. Denoting $\chi(\mathbf{A}) = \int_0^T |u(t,\mathbf{A})|^2\, dt$, it is possible to write

$$CRLB_{A_n} = \left[\mathbf{J}^{-1}\right]_{n,n} \tag{A.19}$$

where

$$\mathbf{J}^{-1} = -\frac{1}{2SNR}\begin{bmatrix} \frac{\partial^2 \chi(\mathbf{A})}{\partial A_1^2} & \frac{\partial^2 \chi(\mathbf{A})}{\partial A_1 \partial A_2} & \cdots & \frac{\partial^2 \chi(\mathbf{A})}{\partial A_1 \partial A_N} \\ \frac{\partial^2 \chi(\mathbf{A})}{\partial A_2 \partial A_1} & \frac{\partial^2 \chi(\mathbf{A})}{\partial A_2^2} & \cdots & \cdots \\ \cdots & \cdots & \cdots & \cdots \\ \frac{\partial^2 \chi(\mathbf{A})}{\partial A_N \partial A_1} & \cdots & \cdots & \frac{\partial^2 \chi(\mathbf{A})}{\partial A_N^2} \end{bmatrix}^{-1} \tag{A.20}$$

APPENDIX B – CRLB derivation: Chain rule

Suppose we need to derive with respect to x and y the function $z = f(u,v)$ where $u = h(x,y)$ and $v = g(x,y)$. Then for the chain rule:

$$\frac{\partial z}{\partial x} = \frac{\partial f}{\partial u}\frac{\partial u}{\partial x} + \frac{\partial f}{\partial v}\frac{\partial v}{\partial x}, \quad \frac{\partial z}{\partial y} = \frac{\partial f}{\partial u}\frac{\partial u}{\partial y} + \frac{\partial f}{\partial v}\frac{\partial v}{\partial y}, \tag{B.1}$$

For the second derivatives the following relations hold

$$\frac{\partial^2 z}{\partial x^2} = \frac{\partial^2 f}{\partial u^2}\left(\frac{\partial u}{\partial x}\right)^2 + 2\frac{\partial^2 f}{\partial u \partial v}\frac{\partial v}{\partial x}\frac{\partial u}{\partial x} + \frac{\partial^2 f}{\partial v^2}\left(\frac{\partial v}{\partial x}\right)^2 + \frac{\partial f}{\partial u}\frac{\partial^2 u}{\partial x^2} + \frac{\partial^2 v}{\partial x^2}\frac{\partial f}{\partial v}, \tag{B.2}$$

$$\frac{\partial^2 z}{\partial y^2} = \frac{\partial^2 f}{\partial u^2}\left(\frac{\partial u}{\partial y}\right)^2 + 2\frac{\partial^2 f}{\partial u \partial v}\frac{\partial v}{\partial y}\frac{\partial u}{\partial y} + \frac{\partial^2 f}{\partial v^2}\left(\frac{\partial v}{\partial y}\right)^2 + \frac{\partial f}{\partial u}\frac{\partial^2 u}{\partial y^2} + \frac{\partial^2 v}{\partial y^2}\frac{\partial f}{\partial v}, \tag{B.3}$$

$$\begin{aligned} \frac{\partial^2 z}{\partial x \partial y} = \frac{\partial^2 z}{\partial y \partial x} &= \frac{\partial^2 f}{\partial u^2}\frac{\partial u}{\partial y}\frac{\partial u}{\partial x} + \frac{\partial^2 f}{\partial u \partial v}\frac{\partial v}{\partial y}\frac{\partial u}{\partial x} + \frac{\partial f}{\partial u}\frac{\partial^2 u}{\partial x \partial y} \\ &+ \frac{\partial^2 f}{\partial u \partial v}\frac{\partial v}{\partial x}\frac{\partial u}{\partial y} + \frac{\partial^2 f}{\partial v^2}\frac{\partial v}{\partial y}\frac{\partial v}{\partial x} + \frac{\partial f}{\partial v}\frac{\partial^2 v}{\partial x \partial y} \end{aligned}, \tag{B.4}$$

REFERENCES

[Dog01] A. Dogandzic, A. Nehorai, "Cramér-Rao Bounds for estimating Range, Velocity, and Direction with and Active Array", *IEEE Trans. on Signal Processing*, Vol. 49, No. 6, June 2001, pp. 1122-1137.

[Kay93] S. M. Kay, *Fundamentals of Statistical Signal Processing, Estimation Theory*. Englewood Cliffs, NJ: Prentice-Hall, 1993.

[Lev04] N. Levanon, E. Mozeson, *Radar Signals*, New York: Wiley, 2004.

[Sko01] M. Skolnik, *Introduction to Radar systems*, Third Edition, McGraw-Hill, New York, NY, 2001.

[Tsa97] T. Tsao, M. Slamani, P. Varshney, D. Weiner, H. Schwarzlander, "Ambiguity Function for a Bistatic Radar", *IEEE Trans. on Aerospace and Electronic Systems*, Vol. 33, No. 3, July 1997, pp. 1041-1051.

[Van71] H. L. Van Trees, *Detection, Estimation and Modulation Theory*. New York: Wiley, 1971, Vol. III.